Mechanosensing modulates dendritic cell function and metabolism

by

Kevin Chu

A thesis submitted in partial fulfillment of the requirements for the degree of

Master of Science

in

Immunology

Department of Medical Microbiology and Immunology

University of Alberta

Abstract

Dendritic cells (DCs) are antigen presenting cells critical for the initiation of the adaptive immune response. As such, DCs continually circulate the body to survey for foreign antigen in the periphery. DCs encounter a milieu of environmental cues within the traversed microenvironment that can modulate their metabolism and function during inflammation or infection. DC signaling in response to cytokine and pattern recognition receptor stimulation have been extensively characterized. However, DCs also encounter non-immunological cues from the microenvironment that may contribute to the collective regulation of the immune response. A less well studied non-immunological cue is tension exerted by substrate stiffness. In early experiments, our collaborators observed substrate tension could modulate DC cytokine production and activation. In response to tension, DCs also upregulated the expression of TAZ, a transcription co-activator. TAZ is involved in mechanosensing in non-immune cell types and has a homolog known as YAP with similar functionality, hinting that DC mechanosensing may involve YAP/TAZ signaling. In addition, through enrichment analysis, we found that respiratory diseases were strongly predicted to be associated with tensional changes to DC biology.

My research aims to expand on these observations using an in vitro culturing protocol whereby bone-marrow derived DCs (BMDCs) are grown on substrates engineered to a stiffness of 2 or 50 kPa, or on plastic only conditions. In my study, I examined whether substrate stiffness could modulate DC antigen presentation and metabolism, as DC maturation and function are intimately connected with metabolic changes. To study the involvement of YAP/TAZ on DC mechanosensing in a respiratory context, we adopted an influenza model. In this model, I examined the day 9 antiviral response in mice with DC specific deletion of YAP/TAZ after immunization with mouse adapted H1N1 influenza. Overall, I found that BMDCs grown on

plastic were better at activating T cells, and the effects of substrate stiffness on DC maturation may be a reversible process. Furthermore, DCs conditioned on stiff substrates displayed increased glycolysis and oxidative phosphorylation, suggesting DC metabolism could be modulated by substrate stiffness. As YAP/TAZ translocate into the nucleus upon activation, I incorporated image flow cytometry to probe for the translocation of YAP/TAZ in DCs in response to tension. BMDCs conditioned on 50 kPa and plastic demonstrate a trend of increasing nuclear YAP/TAZ translocation, hinting at the involvement of YAP/TAZ in DC mechanosensing. Interestingly, despite this observation and tension induced upregulation of TAZ in BMDCs, the deletion of YAP/TAZ in DCs did not impair day 9 antiviral response.

Preface

This thesis is composed of original work by Kevin Chu. Throughout, contains co-authored work by collaborators published in Chakraborty, M. *et al*. Mechanical Stiffness Controls Dendritic Cell Metabolism and Function. *Cell Rep*. 34, (2021). More information can be found in the contribution subsection at the beginning of chapter 3 and 4.

The research project, of which this thesis is a part, received research ethics approval from the University of Alberta Research Ethics Board, Project Name “The impact of obesity and insulin resistance on immune function”, No. AUP00003251, approved August 6, 2019.

Acknowledgements

I would like to take this opportunity to thank the people whom supported me throughout my Master degree. This is and was an important transitional period in my life. I am eternally thankful for my supervisor Dr. Sue Tsai for having me as her first graduate student, and her patience despite the multiple challenges when working with me. None of this would had been possible without her support. Wayward though I may be, I have learned tremendously through Dr. Tsai's continued guidance and encouragement to think scientifically. Words cannot express truly how grateful I am for her kindness and guidance.

Special thanks to Dr. Xavier Clemente-Casares and Dr. Masoud Akbari for their outstanding technical support. I would like to thank my committee Dr. Kevin Kane and Dr. Matthew Macauley for their input and suggestion on the direction of my project. In addition, thank you to the Baldwin, Kane, and Ostegaard lab for the joint lab meetings that provided me an opportunity to learn and disseminate scientific data.

I remember a period when I was the only student in our lab alongside Dr. Akbari whom was also a new member at the time. I am thankful to the wonderful personalities I had the fortune to later meet: Megan Lee, Kasia Dzierlega, Erin Strachan, Mengyi Zhu, and Aklima Akter. Your support and friendship enriched the vibracy of our lab and made my Master degree more memorable despite the ongoing COVID-19 pandemic. An additional thank you to the undergraduates Felicia Kanji and Camille Huang, I enjoyed teaching and learning alongside you.

Last but not least, thank you to my family and friends for their unconditional love and encouragement, in particular thank you to my parents Huyen Chu and Anh Ta, and my brother Lucky for his unconventional support.

Table of Contents

List of tables

List of figures

List of abbreviations

Abbreviations	Full description
2-DG	2-deoxyglucose
2-NBDG	2-(N-(7-Nitrobenz-2-oxa-1,3-diazol4-yl)Amino)-2-Deoxyglucose
AKT	Ak strain transforming (Also known as PKB)
APCs	Antigen presenting cells
ATP	Adenosine trisphosphate
BATF3	Basic leucine zipper ATF-like transcription factor 3
BCR	B cell receptor
BM	Bone marrow
BMDCs	Bone marrow-derived dendritic cells
CCL	C-C ligand
CCR	C-C chemokine receptor
cDCs	Conventional dendritic cells
CFSE	Carboxyfluorescein succinimidyl ester
CLRs	C-type lectin receptors
DCs	Dendritic cells
DC-SIGN	Dendritic-cell specific intercellular adhesion molecule-3-grabbing non-integrin
ECAR	Extracellular acidification rate
ECM	Extracellular matrix
ELISA	Enzyme-linked immunosorbent assay
ER	Endoplasmic reticulum
FAD	Flavin adenine dinucleotide
FCCP	Carbonyl cyanide-*p*-trifluoromethoxyphenylhydrazone
FLT3	FMS-like tyrosine kinase 3, also known as CD135
FLT3L	FMS-like tyrosine kinase 3 ligand
G6P	Glucose 6-phosphate
GLUT	Glucose transpoter
GM-CSF	Granulocyte-macrophage colony-stimulating factor
HEV	High endothelial venules
HIF-1α	Hypoxia-inducible factor 1-alpha
HK	Hexokinase

IAV	Influenza A virus
IFN-I	Type 1 interferon
IFN-γ	Interferon-gamma
IL	Interleukin
iNOS	Inducible nitric oxide
IRF4	Interferon regulator factor 4
KO	Knockout
kPa	Kilopascal
LATS1/2	Large tumor suppressor kinases 1 & 2
LDH	Lactate dehydrogenase
LNs	Lymph nodes
LPS	Lipopolysaccharide
MCP-1	Monocyte chemoattractant protein-1
MHC	Major histocompatibility complexes
MIP-2	Macrophage-inflammatory protein-2
MLN	Mediastinal lymph node
MMR	Macrophage mannose receptor
MOB1a1/b	Mps one binder kinase activator-like 1A and 1B
moDCs	Monocyte derived dendritic cells
MST1/2	Mammlian Ste20-like 1 & 2
mTOR	Mechanistic target of rapamycin
NAD	Nicotinamide adenine dinucleotide
NFAT	Nuclear factor of activated T cells
NF-κB	Nuclear factor kappa B
OCR	Oxygen consumption rate
OT-I	Ovalbumin-specific CD8+ T cells
OVA	Ovalbumin
OXPHOS	Oxidative phosphorylation
pDCS	Plasmacytoid dendritic cells
PDMS	Polydimethylsiloxane
PGC1α	PPARγ co-activator 1α
PI3K	Phosphoinositide 3-kinase
PKB	Protein kinase B, also known as AKT
PPARγ	Peroxisome proliferator-activated receptor-γ
PPP	Pentose phosphate pathway
PR8 IAV	Puerto Rico strain H1N1 influenza A virus

PRR	Pattern recognition receptors
PTEN	Phosphatase and tensin homolog
RhoA	Ras homolog family member A
Rot/Anti-A	Rotenone/Antimycin A
RTK	Receptor
S6RP	S6-ribosomal protein
SAV1	Salvador family WW-domain-containing protein 1
STAT	Signal transducer and activator of transcription
TAZ	Transcriptional coactivator with PDZ-binding motif
TCA cycle	Tricarboxylic acid cycle
TCR	T cell receptor
TEAD	Transcriptional enhancer factor domain
Th1	Type 1 helper T cells
TLR	Toll-like receptor
TNF	Tumor necrosis factor
TSC	Tuberous schlerosis
WASP	Wiskott-Aldrich syndrome protein
WT	Wildtype
WWTR1	WW domain containing transcription regulator 1
YAP	Yes-associated protein

Chapter 1: Introduction

1.1. Dendritic cells

Dendritic cells (DCs) are professional antigen present cells (APCs) that bridge the innate with the adaptive immune response through processing and presenting antigens to T cells. DCs encounter a variety of microenvironments with unique physical properties such as topography, stiffness, and fluidity throughout their life cycle. The physiological stiffness of tissues acutely transitions from a soft to hard stiffness during inflammation due to extracellular matrix (ECM) remodeling and lymphocyte infiltration[1–4]. In certain disease states such as fibrosis or tumors, tissues can stiffen beyond the range typically encountered. Thus, tension generated from substrate stiffness could conceivably function as an environmental cue for DCs to distinguish healthy and diseased tissues. While studies have shown that substrate stiffness can modulate metabolic flux and immunological functions of some immune cells, to date it is still unclear whether and how different forms of mechanical forces can affect DC biology[5–8]. Activated DCs are matured DCs that have received immunological stimulation, whereas mature DCs refer to DCs that have yet to encounter antigen but have undergone the hematopoietic differentiation process. During development and following activation, DCs undergo extensive metabolic reprogramming - a process of rewiring metabolic pathways used to synthesize metabolites and energy required for development and function, such as secretion of cytokines and antigen presentation.

1.1.1. Dendritic cell development

DCs are a heterogenous group of APCs derived from the bone marrow (BM)[9]. DC subsets are regulated by differential expression of multiple linage restricted transcription factors including basic leucine zipper ATF-like transcription factor 3 (BATF3), interferon regulatory

factor 8 (IRF8), interferon regulatory factor 4 (IRF4), and E2-2[10–12]. DC subsets are also characterized by distinct surface marker expression, localization patterns and cytokine profiles, and all DCs are capable of antigen presentation[13]. Critically, hematopoietic precursor cells with the capacity to differentiate into DCS are characterized by the surface expression of the FMS-like tyrosine kinase 3 (FLT3 or CD135) receptor[13–15]. DCs can develop from both lymphoid and myeloid progenitors. In the lymphoid and non-lymphoid tissues of healthy mice and humans, plasmacytoid (pDCs) and conventional DCs (cDCs) comprise the two major populations of DCs. cDCs are generally categorized into two subgroups, $CD8a^+$ or $CD103^+$ expressing cDC1 and $CD11b^+$ expressing cDC2[16]. Both subtypes of cDCs are further subdivided depending on their anatomical localization, which include organ specific-DCs such as Langerhans's cells, lymphoid tissue associated DCs, and thymic DCs[16]. In comparison to a steady state, monocyte derived DCs (moDCs), and tumor necrosis factor (TNF) and inducible nitric oxide (iNOS) producing DCs only develop and appear following immunologic challenge[13,16,17].

The phosphoinositide 3-kinase (PI3K) and mechanistic target of rapamycin (mTOR) signaling induced by FTL3 activation was recently identified to have an important role in the regulation of DC homeostasis[18]. The development of all DC subsets are severely impaired when murine BM precursors were cultured together with FLT3 ligand (FLT3L) and rapamycin, an inhibitor of mTOR[18]. Alternatively, when mice were injected with FLT3L, an increased phosphorylation of S6-ribosomal protein (S6RP), a component downstream of mTOR signaling, was observed in splenic DCs[18]. Interestingly, systemic or DC-specific deletion of phosphatase and tensin homolog (PTEN), a phosphatase involved in the inhibition of protein kinase B (PKB or AKT), led to the increased expansion of mainly $CD8a^+$ cDCs in lymphoid tissues – under physiological conditions PI3K activates PKB, which initiate a downstream cascade to activate

mTOR[18]. The expansion of $CD103^+$ cDCs, the functionally equivalent subset of $CD8^+$ DCs in non-lymphoid tissues, was also observed in PTEN deficient mice[19]. The deletion of PTEN partially ameliorated the inhibitory effects of rapamycin on DC development, and the enhanced effects of PTEN deletion on $CD8^+$ cDCs development was attenuated when treated with rapamycin[18]. Studies downstream of the PI3K/mTOR signaling axis suggests FLT3 signaling supports development of all DC subsets through the activation of signal transducer and activator of transcription 3 (STAT3)[20,21]. Collectively these results suggest FLT3 signaling occurs via PI3K/AKT/mTOR signaling but is most critical in the development of $CD8^+$ cDCs.

DCs can also develop from BM precursors when cultured with the growth factor granulocyte-macrophage colony-stimulating factor (GM-CSF)[22]. However, unlike the FLT3L generated DCs that resemble DCs at a steady state, DCs generated with only GM-CSF are more akin to subsets present during an inflammatory state[17,23]. Namely, GM-CSF stimulates the development of moDCs and TNF/iNOS producing DCs. An abundance of GM-CSF is produced by early responding innate cells such as mast cells and macrophages and by fibroblast and endothelial cells during inflammation[24,25]. This propensity may therefore be a representation of the advantage these subsets of DCs confer during early immune response[26]. Indeed, the absence of TNF/iNOS producing DCs severely impair clearance of primary bacterial infection in mice[26]. Furthermore, moDCs are important to prime the development of memory $CD8^+$ T cells during acute infection[27]. Compared to the significant reduction of all DC subsets in lymphoid and peripheral tissues of FLT3 deficient mice, GM-CSF deficient mice have mildly reduced DC development in lymphoid organs, but a significant loss in non-lymphoid organs[28]. The loss of GM-CSF signaling does not affect the pDC development[29]. The variable effects of GM-CSF and FLT3L on DC development can be explained by the signaling pathways utilized. Common to

both cytokines is the activation of PI3K/mTOR and STAT3, whereas only GM-CSF can activate nuclear factor kappa B (NF-κB) and STAT5[20,21,30]. The effects of STAT5 activation appears to supersede STAT3 signaling, leading to the generation of inflammatory DCs[30].

1.2 Dendritic cell subsets & biology

DCs are distributed throughout the body, serving as the interface between the innate and adaptive immune system. The capacity for DCs to function as APCs represents one of the major defenses against respiratory viral infections. At a steady state, the lung is comprised of cDCs and pDCs. cDCs all express class II major histocompatibility complexes (MHC II) and CD11c. The cDCs subset are comprised of two main population characterized by the expression of cell surface markers - the CD103+ expressing cDC1 (CD8α+ in lymphoid tissues) and the CD11b+ expressing cDC2. The expression of X-C motif chemokine receptor 1 unifies both CD103 and CD8α expressing cDC1s[31]. pDCs on the other hand have a lower expression of MHC II and CD11c and is differentiated from cDCs based on the expression of B220, Siglec-H, CD317[12,32]. During infection and inflammation, a 4th subset of DCs, the moDCs are generated[13,16]. Critically, although all DCs can uptake and process antigens (Ag), different subset of DCs have evolved with specialized functions.

1.2.1 Conventional Dendritic Cells 1 (cDC1)

cDC1s are one of the two main subsets of cDCs found in lymphoid and non-lymphoid tissues. cDC1s in non-lymphoid organs are predominantly characterized by the expression of the integrin CD103, and an equivalent population expressing CD8α are found in lymphoid organs[16]. The expression of the transcription factors BATF3 and IRF8 are absolutely required for the generation and survival of cDC1s[33,34]. Relative to cDC2s, cDC1s are more proliferative in response to FLT3L stimulation due to a higher expression of FLT3 receptor[35]. Generally, cDC1s

are connective tissue resident cells but within the lung, $CD103^+$ DCs can localize in the respiratory airway within the mucosa and in close proximity to endothelial cells[36]. Comparable to the intestines, the lung is an organ vulnerable to frequent pathogenic insult, as the respiratory epithelium is the first site of contact to inhaled agents[37]. Upon activation, the migration of peripheral cDCs to draining lymph nodes (LNs) is predominantly dependent on the upregulated surface expression of the C-C chemokine receptor 7 (CCR7)[38]. This process is facilitated by the affinity of CCR7 to the cytokines C-C ligand 19 and 21 (CCL19 & CCL21), both of which are abundantly produced by stromal cells within the T cell zone in the LNs[39]. The strategic localization of cDC1s in the lung therefore poise cDC1s to efficiently sample and respond to the surrounding environment.

As initiators of the adaptive immune system, cDC1s are unrivaled APCs, a property ascribed to their ability for cross presentation, a process involving the uptake, processing, and presentation of exogenous antigens on MHC I molecules to naive cytotoxic $CD8^+$ T cells[40]. cDC1s are integral to the clearance of intracellular pathogens, especially influenza A virus (IAV) by activating $CD8^+$ T cells via presentation of exogenous peptides on MHC-I molecules[41]. Overall, cDC1s have a higher constitutive basal expression of transporter associated with antigen processing 1 & 2 than cDC2s and thus can more efficiently process and load viral Ags onto MHC I complexes[42]. Although not exclusive to cDC1s, IAV has been shown to favor infecting cells with high MHC II expression in mice[43]. As such, cDC1s and cDC2s are susceptible to IAV infection due to their high expression of MHC II, whereas pDCs were not[43]. The transit of IAV using lung cDCs as vectors function as an important method of presenting viral antigen to T cells, as IAV normally will not freely reach the draining LNs[44].

Moreover, the clearance of intracellular pathogens is enhanced by potent production of interleukin-12 (IL)-12 by cDC1s, a cytokine that promotes differentiation of naïve T cells into type I helper T cells (Th1) and production of interferon-gamma (IFN-γ) from T cells[37,45]. Consequently, depletion of $CD103^+$ cDC1s severely compromised clearance of IAV due to impaired $CD8^+$ T cell priming[46]. Similar results are recapitulated in BATF3 knockout mice, a deficiency that affects only the development of cDC1s[34]. In these mice, defective cross presentation, virus specific $CD8^+$ T cell cytotoxicity, and rejection of syngeneic tumors are observed[34]. Given that the specific ablation of cDC1s impairs anti-viral response, this suggests that the role of cDC1 cannot be compensated by other APCs to induce a robust immune response.

1.2.2 Conventional Dendritic cells 2 (cDC2)

cDC2s are characterized by the expression of $CD11b^+$ and the absence of the integrin $CD103^+$[47,48.] In the lungs, cDC2s are predominantly localized in the lamina propria[47]. Compared to cDC1s, cDC2s are not a homogenous subset as they variably express pattern recognition receptors (PRR) and the dependence of developmental transcription factors can differ[48]. Numerous transcription factors, such as Notch2, IRF2, and IRF4, have been identified to regulate cDC2 development[48]. Hierarchical importance of each transcription factor remain poorly understood given the heterogeneity of the subset[48]. For instance, reflective of their heterogeneity, IRF4 deficiency have variable tissue penetrance and does not completely abrogate the development of cDC2s[49].

cDC2s are most adept at presenting antigen to $CD4^+$ lymphocytes but can cross present at a reduced efficiency[50]. The affinity to prime $CD4^+$ T cells is attributed to a higher intrinsic expression of MHC II machinery[50]. Specifically, it was identified that IRF4 regulates MHC II

antigen presentation, whereby conditional deletion of IRF4 in cDC2s severely impaired antigen presentation but is restored by retroviral transduction of IRF4[51]. cDC2 support the development and retention of memory $CD8^+$ T cells within draining LNs whilst cDC1 are functionally important in the generation of CD8+ T effector cells in a CD24 mediated process[52]. Moreover, during viral infection, migrating cDC2 have also been shown to transfer antigens to cDC1 within draining LNs that then directly prime $CD8^+$ T cells[53,54]. Given the specialization of cDC2s and the fact cDC2s cannot compensate for the anti-viral function of cDC1s in BATF3 deficient mice, it appears that cDC1s are the most critical subset for the presentation of pulmonary antigens.

Findings against the cDC paradigm have been reported by a study whereby early T cell responses were primed by both cDC1 and cDC2, but is later dominated by cDC2 antigen presentation during peak infection[55]. In this study, $CD103^-$ $CD11b^+$ DCs directly cross primed $CD8^+$ T cells following exogenous antigen capture, and did not transfer antigen to lymphoid $CD8a^+$ DCs[55]. This anti-viral response was identified to be contingent on the expression of the costimulatory molecule CD70, a ligand for CD27 which facilitates primary and secondary $CD8^+$ T cell responses[56]. The viral dosage and the differential effects of IAV directly infecting DCs subsets have been suggested as potential mechanisms[57]. It is thought that during mild influenza infection, directly infected cDC2 can migrate to the draining LNs to induce $CD8^+$ activation[57]. In contrast, cDC2 succumb to direct viral infection during severe infection, serving as a means for cDC1s to acquire viral antigens for cross presentation. Indeed, it has been demonstrated that pulmonary cDC1s preferentially acquire and transport apoptotic cells draining LNs for cross presentation[58].

1.2.3 Plasmacytoid Dendritic Cells (pDCs)

pDCs comprise a small population of DCs within the lung[59]. Similar to cDCs, the development of pDCs requires FLT3 signaling, but lineage commitment requires the expression of the transcription factor E2-2[18]. Functionally, pDCs are best characterized by their contribution to the innate anti-viral response through potent production of type 1 IFN (IFN-I) - a result of constitutive IRF7 expression[60,61]. pDCs are additionally recognized for their capacity to modulate the adaptive response, functioning as cross presenting APCs and as polarizers of Th_1 cells via secretion of IL-12[61–63]. pDCs mature and upregulate CCR7 expression post-influenza challenge, and the trafficking of pDCs bearing influenza antigen to the lung and draining LNs have been observed, however their overall role in anti-viral responses is unclear[46,62]. Despite pDCs being more resistant to influenza virus infection and IFN-I as a major contributor to effective antiviral responses, antibody mediated depletion of pDCs does not exacerbate influenza severity nor impact viral clearance in mice[46,62,64]. Instead, it appears pDCs are involved in regulating long term immune responses, as pDC depletion led to a decreased production of viral specific antibodies following influenza clearance[46]. This phenotype is recapitulated in a separate study conducted by genetic depletion of pDCs, in which case T cell recruitment to the lung was delayed but did not affect the activation or function of $CD8^+$ T cells[65]. The function of pDCs in viral clearance perhaps vary depending on the pathogen, since pDCs are indispensable for limiting persistent respiratory syncytial virus infection but does not affect influenza clearance[66].

1.2.4 BM-derived DCs (BMDCs)

Studying DCs directly from blood and tissue is complicated by the low frequency and time-consuming extraction process[22]. To circumvent this, DC biology is studied *in vitro* using murine BM hematopoietic precursors or blood monocytes cultured with growth factors to

generate a substantial number of immature BMDCs. Two established DC culturing protocols involves the usage of GM-CSF or FLT3L to generate GM-DCs or FL-DCs, respectively[22]. While these in vitro culturing protocols have contributed to expand our understanding of DC biology, there are limitations to both models with notable controversy concerning the heterogeneity and whether bona fide in vivo counterparts exist for the generated BMDCs.

One caveat of the GM-CSF culturing model, as the name of the growth factor GM-CSF suggest, is the generation of a heterogenous population of cells that includes macrophages and neutrophils[22]. The GM-DCs generated by this model display a small degree of heterogeneity and are distinguished from macrophages and neutrophils by the expression of CD11c and high expression of MHC II[22]. GM-DCs has been established to be enriched by CD11c selection[22]. On the contrary, the culturing of murine BM precursors with FLT3L yields a heterogenous FL-DC population comprised of pDCs, cDC2s, and cDC1-like cells that would require cell sorting with potentially low yield for studying individual subsets[67]. Moreover, the separation and identification of these subsets is hindered by the occasional expression of CD11b on all conventional subsets and cDC1-like cells having an abnormal phenotype lacking the expression of key cDC1 markers, CD8 and CD103[67].

A critical disadvantage of the GM-CSF model is that although a substantial number of DCs are produced, the GM-DCs generated are only distantly related to *in vivo* steady-state DC subsets[68]. As discussed previously, the development of steady-state DCs is comprised of cDCs and pDCs that are dependent on FLT3L signaling[69]. GM-DCs however can undergo development that is FLT3L independent and are generally less tolerogenic[68,69]. Significant differences in gene expression between developing GM-DCs and *ex vivo* cDC1s and cDC2s has been identified by transcriptomic analysis[68]. By gene expression, the closest *in vivo* counterpart

of GM-DCs are only cDC2s given both of their dependence on IRF4 for development. Furthermore, GM-CSF can inhibit the development of pDCs[30].

At steady state conditions, a low concentration of GM-CSF is found in circulation in mice but is elevated during inflammation[30]. Overall, the GM-DCs produced in this model are more representative of inflammatory DCs than steady-state DCs. Increased GM-CSF concentration has a role in inducing the differentiation of moDCS from inflammatory monocytes[30,70,71]. It is thought that GM-CSF cultured DCs may better reflect moDCs in tissues driven by GM-CSF during inflammation[69]. Functionally, moDCs are more pro-inflammatory than FLT3L differentiated DCs, although the ability of moDCs to activate T cells is comparable[70]. Unfortunately, it is unclear how closely GM-DCs resemble moDCs as comparative gene expression was not examined between moDCs and GM-DCs[68]. While this model can generate a substantial number of mostly homogenous DCs, it also yields a population of contaminating cells of macrophages and neutrophils[68]. The contaminating cells could partially be addressed by CD11c purification but the inherent inflammatory nature of the GM-DCs remain unavoidable in this model[68].

1.3 Dendritic cell metabolism

The immune system is an important regulator of whole-body metabolism[72]. However, cellular metabolic reprogramming is also pivotal for the proper functioning of the immune system. Immune cells undergo dynamic metabolic reprogramming at various stages of its life cycle, and the integration of different metabolic pathways has been shown to coincide with immune cell gene expression, differentiation, and effector function at stages of development, during migration and recirculation, and following activation[73–76]. Effective host immune responses are therefore interwoven with the capacity for the immune system to meet imposed

metabolic demands. In addition to physiological requirements, immune cells must compete for limited nutrients within the microenvironment among other immune cells and against pathogens during infection. Subsequently, this confers immune cells with distinct metabolic profiles respective to their function and environment. In situations of metabolic dysregulation, the immune system is adversely affected, rendering improper immune activation and resolution, leading to increased risk of developing chronic diseases and autoimmunity.

Unlike non-immune cells, immune cells do not have large deposits of nutrient storage, making the uptake of nutrients an important response following activation to support metabolic remodeling[73]. Among the major conserved metabolic pathways, glycolysis, and oxidative phosphorylation (OXPHOS) are central pathways commonly utilized by immune cells. Of the two pathways, OXPHOS is a slower and oxygen dependent pathway restricted to the mitochondria but is the most efficient approach to generate adenosine trisphosphate (ATP) - yielding up to 36 ATP per glucose molecule, whereas glycolysis is anaerobic, occurring in the cytoplasm and generates 2 ATP per glucose molecule (**Figure 1.1)**. For cells that primarily derive energy through OXPHOS, the tricarboxylic acid cycle (TCA cycle) constitutes a key intermediary pathway as the electron transporters generated via the oxidation of acetyl-CoA is used to fuel OXPHOS. The electron transporters are used to sustain the mitochondrial membrane potential to drive ATP synthesis by OXPHOS. Importantly, while acetyl-CoA can be synthesized via carbohydrates such as glucose in the presence of oxygen, acetyl-CoA can also be derived through the slower processes of lipid and amino acid catabolism. The breakdown of fatty acids can produce the most energy, yielding over a hundred ATP at the cost of higher oxygen consumption[77]. The catabolism of glucose per mole of oxygen is 53% more efficient at

generating ATP than catabolism of fatty acids. This flexibility permits a greater yield of ATP by complete metabolism depending on the origin of the acetyl-CoA used to fuel the TCA cycle.

1.3.1 Biosynthetic pathways in DCs

Glycolytic and TCA cycle intermediates are used in several biosynthesis pathways such as the pentose phosphate pathway (PPP) and fatty acid synthesis (**Figure 1.1**). In the first step of glycolysis, glucose enters the cell through the glucose transporter 1 (GLUT1) and converted into glucose 6-phosphate (G6P) by the enzyme hexokinase (HK). The synthesis of G6P ensures the continuation of glycolysis by preventing the glucose molecule from leaving the cell. Alternatively, G6P can be shuttled through the PPP to synthesize nucleotides and electron carriers to support fatty acid synthesis. Under anaerobic and aerobic conditions, G6P is catabolized through glycolysis to terminally produce two pyruvate molecules. In the absence of oxygen, pyruvate is used for lactic acid fermentation to yield lactate. The lactate dehydrogenase (LDH) mediated conversion of pyruvate is necessary to regenerate electron carriers for sustained glycolysis. Under normoxic conditions, pyruvate is transformed into acetyl-CoA and directed through the TCA cycle. The newly generated acetyl-CoA is subsequently catabolized into citrate. At this stage, citrate can be funneled for fatty acid synthesis or complete the TCA cycle to produce electron precursors for OXPHOS. Thus, metabolic flux enable immune cells to function efficiently by satiating energetic demands needed for the synthesis of macromolecules necessary in response to physiological demands[78].

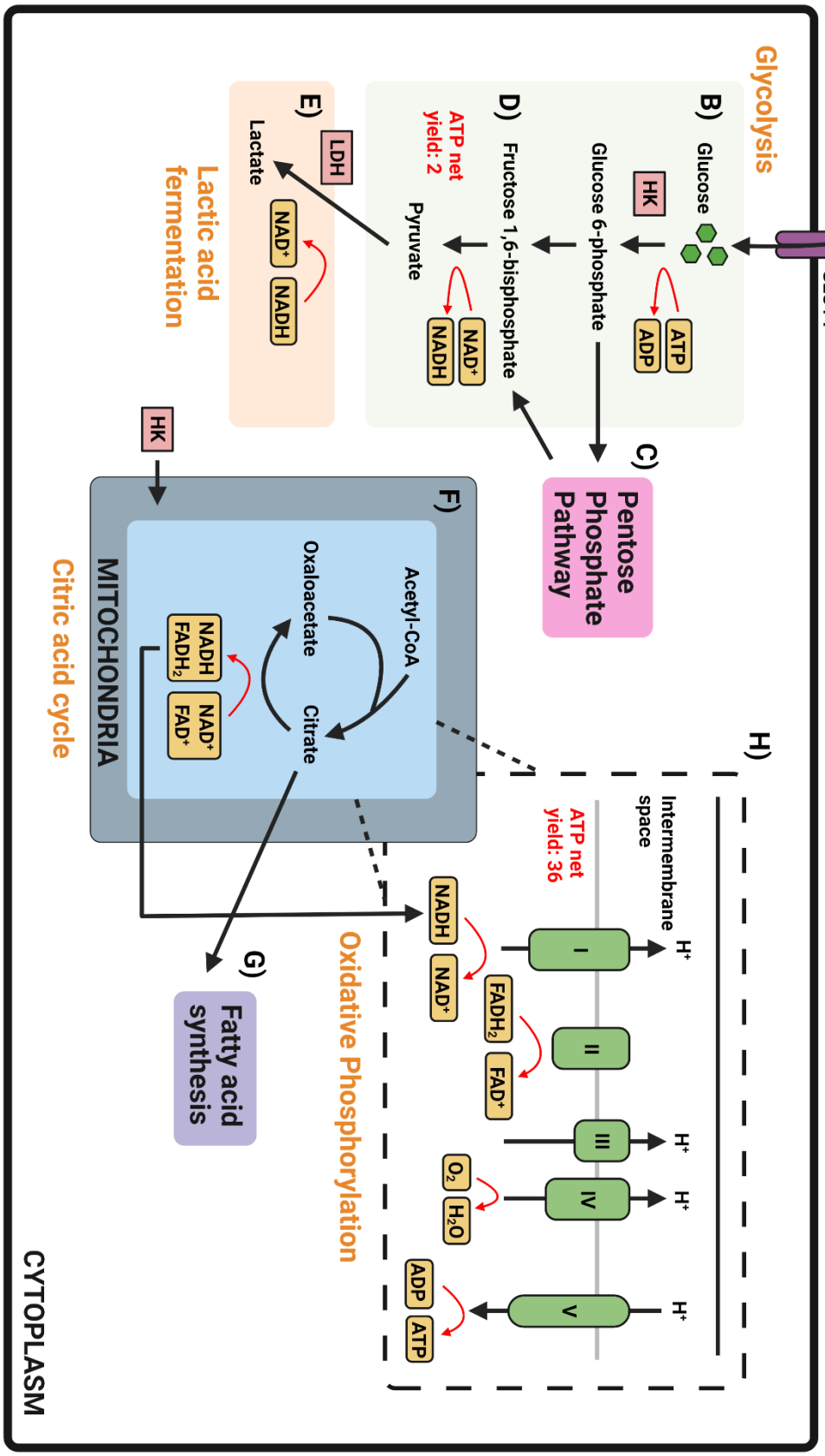
A) Glucose
GLUT1
Glycolysis
B) Glucose
HK
ATP
ADP
Glucose 6-phosphate
C) Pentose Phosphate Pathway
D) Fructose 1,6-bisphosphate
ATP net yield: 2
NADH
NAD+
Pyruvate
E) Lactic acid fermentation
LDH
Lactate
NAD+
NADH
HK
F) MITOCHONDRIA
Citric acid cycle
Acetyl-CoA
Oxaloacetate
Citrate
NADH
FADH2
NAD+
FAD+
G) Fatty acid synthesis
H) Oxidative Phosphorylation
Intermembrane space
ATP net yield: 36
NADH
NAD+
FADH2
FAD+
I
II
III
IV
V
H+
O2
H2O
ADP
ATP
CYTOPLASM

Figure 1.1. Simplified view of the interconnected relationship between metabolic pathways. Glycolysis is catabolic process **(A)** Glucose is transported into the cytoplasm via glucose transporter 1 (GLUT1). **(B)** In an energy dependent process, glycolysis is initiated by the conversion of glucose into glucose 6-phosphate (G6P) by the enzyme hexokinase (HK). **(C)** In parallel, G6P can be used for the synthesis of nucleotide precursors via the pentose phosphate pathway. **(D)** The complete catabolism of glucose into pyruvate requires the reduction of the electron acceptor nicotinamide adenine dinucleotide (NAD^+) into NADH – yielding a net of 2 ATP. Glycolysis cannot run indefinitely under anaerobic conditions due to the depletion of NAD^+. **(E)** To compensate, pyruvate is used for lactic acid fermentation mediated by lactate dehydrogenase (LDH) to regenerate NAD^+ via the oxidation of NADH. **(F)** HK can also translocate to the outer mitochondrial membrane for direct access to ATP. In the presence of oxygen, pyruvate is converted into acetyl-CoA and shuttled into the mitochondria. Acetyl-CoA is catabolized through the citric acid cycle (CAC) to generate metabolic intermediates and maximize ATP production. A key intermediate produced by the CAC is citrate, a metabolite that can be used in a complete cycle of CAC, mediated by the reduction of electron acceptors flavin adenine dinucleotide (FAD^+) and NAD^+ into $FADH_2$ and NADH, respectively. Additionally, the metabolite oxaloacetate is generated at the end of the CAC that is used with acetyl-CoA to synthesize citrate. **(G)** Alternatively, citrate is a precursor for fatty acid synthesis. **(H)** To maximize ATP generation, $FADH_2$ and NADH produced during the CAC is used for OXPHOS, a process in which ATP (complex V) is formed through the transfer of electrons from $FADH_2$ and NADH to O_2 by a series of electron carriers (complex I to IV) within the inner mitochondrial membrane. NAD^+ and FAD^+ are regenerated in OXPHOS, and a yield of approximately 36 ATP is produced starting at glycolysis and ending at OXPHOS. Drawn on BioRender.com.

1.3.2. Metabolic pathways supporting in vitro BMDC development

Respiring quiescent or sessile cell types are generally faced with minimal energic demands and utilize slower metabolic pathways, deriving substrates for the TCA cycle via catabolism of carbohydrates, proteins and lipids[73]. On the contrary, activated or proliferative cell types significantly upregulate glycolysis, a metabolic process quicker than OXPHOS[79]. Strikingly, the preference for glycolysis is observed even under normoxic conditions - a process referred to as aerobic glycolysis or the Walburg effect[73]. Enhanced aerobic glycolysis is beneficial to rapidly generate ATP and glycolytic intermediates used to biosynthesize macromolecules such as nucleic acids, proteins, and lipids, all of which are necessary for biomass[79]. Whilst it is advantageous for proliferating cells to utilize aerobic glycolysis, elevated glycolysis is not always for the purpose of growth or proliferation. Neutrophils for example, increase glucose uptake and undergo substantial aerobic glycolysis following PRR activation to produce reactive oxygen species required for the respiratory burst. As such, bacterial infections are exacerbated in neutrophils that are deficient for hypoxia-inducible factor 1-alpha (HIF-1α), a transcription factor that regulate the expression of GLUTs[80].

At a steady state, DCs are predominately catabolic and metabolic reprogramming is critical for early development[73,78,81,82]. Elevated glucose uptake and oxygen consumption is seen *in vitro* in both human moDCs differentiated from monocytes by GM-CSF and IL-4 treatment, and in mouse GM-DCs[81]. This metabolic flux coincides with increased mitochondrial membrane potential and ATP levels in human moDCs and mouse GM-DCs, suggesting glucose is used to fuel OXPHOS. Consistent with these observations, the inhibition of the OXPHOS with rotenone impairs human moDC development[82]. Under hypoxic conditions, the differentiation of GM-DCs is dampened and worsened by HIF-1α deficiency[83]. GM-DC development is also impaired

following lipid metabolism inhibition[84]. In this study, GM-DC differentiation is reduced when acetyl-CoA carboxylase, an enzyme that generate the precursor for fatty acid synthesis, is inhibited. Similar observations are recapitulated in the same study when fatty acid synthase is inhibited. Importantly, the singular inhibition of a particular metabolic pathway did not completely abrogate DC development. These observations therefore highlight the metabolic flexibility of DCs and the significance of metabolic reprogramming on DC development.

GM-CSF induced differentiation of monocyte derived human moDCs mechanistically depend on PI3K mediated activation of mTOR signaling – which is comprised of two complexes mTORC1 and mTORC2[81]. The activation of mTORC1 regulates the expression of various transcription factors involved in metabolic activation (**Figure 1.2)**. A major downstream target of mTOR signaling is the transcription of peroxisome proliferator-activated receptor-γ (PPARγ), a transcription factor regulating lipid metabolism, and PPARγ coactivator 1α (PGC1α), a regulator of mitochondrial biogenesis[85]. The expression of glycolytic genes is concomitantly induced by mTORC1 via the activation of MYC, a family of transcription factors regulating metabolism and proliferation, of which there are 3 paralogues: MYC, MYCN, and MYCL[86]. From a metabolic viewpoint, the previously discussed impaired FL-DC development when co-treated with rapamycin and FLT3L is therefore partly explained by the regulatory function of mTOR on metabolism[18]. Moreover, this is consistent with *in vitro* FLT3L treatment skewing the differentiation of murine BM precursors towards cDC1 in mice with CD11c-specific deletion of PTEN, a phosphatase that regulates lipid and glycolytic metabolism[84]. Specifically, PTEN functions as a negative regulator of mTORC1 signaling through upstream inhibition of AKT[84]. Although the importance of metabolic reprogramming for physiological process is established, the precise mechanisms involved in regulating the process is still unclear due to the redundancy

and crosstalk between metabolic and non-metabolic pathways. The tuberous sclerosis 1 & 2 (TSC1/2) heterodimeric complex is a negative regulator of mTORC1 with a mode of action different than PTEN that exhibit contrasting effects on DC development depending on ontogeny[87,88]. When TSC1 is deleted in mice, the development of GM-DCs is enhanced - an effect associated with increased mTORC1 expression[88]. On the contrary, regardless of elevated glycolysis and lipid synthesis, the development of FLT3L-DCs from TSC1 single deletion mice was unexpectedly impaired[87]. This developmental effect is attenuated in TSC1 and MYC double knockout mice. Confoundingly, FLT3L-DCs generated from double deletion or MYC single deletion mice showed relatively normal metabolic profiles. Together, the contrasting results from these studies suggest that the metabolic requirements of DCs within two culturing systems may be variable and/or the Myc paralogues differentially regulate DC metabolism.

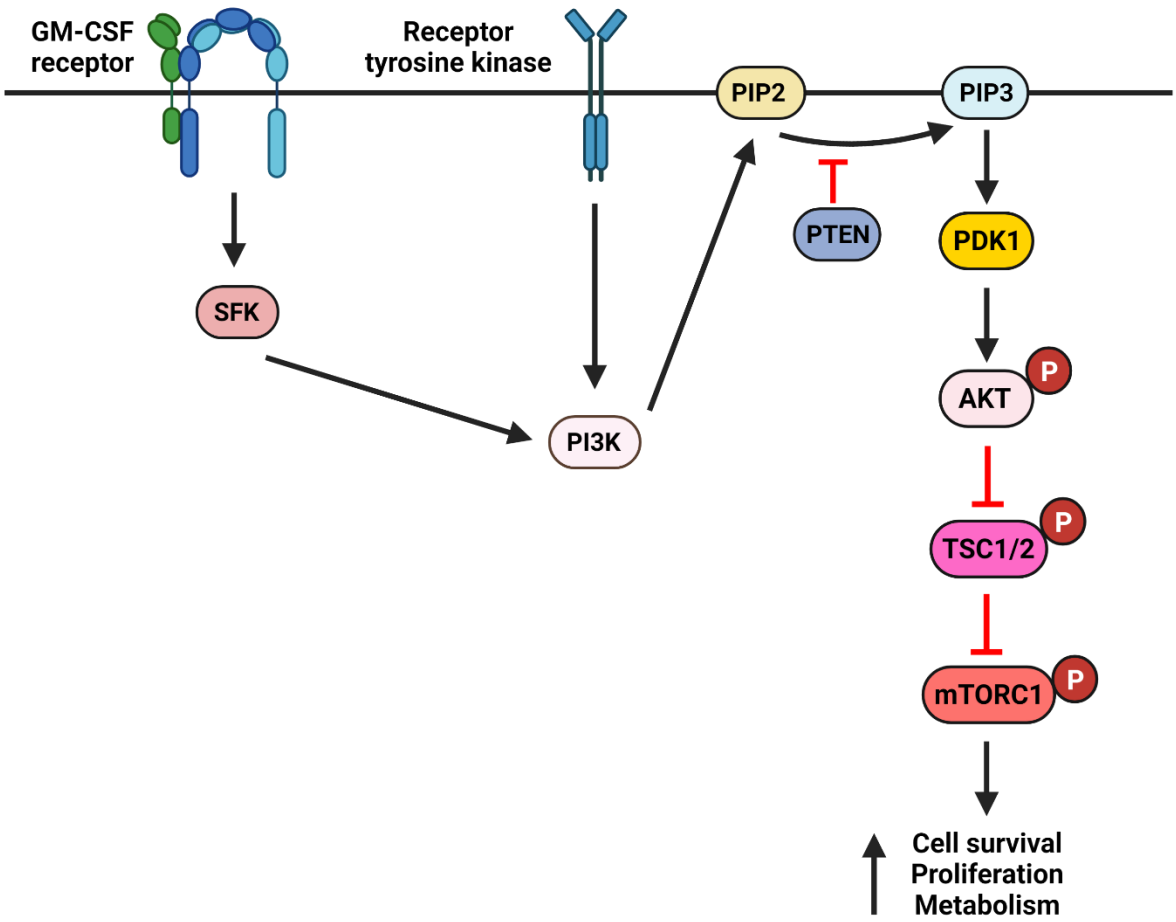

Figure 1.2. Condensed schematic of PI3K/AKT signaling. The PI3K/AKT signaling cascade is initiated upon activation of the GM-CSF and receptor tyrosine kinase cell surface receptors. Downstream signaling promote the expression of genes for cell survival, proliferation, and metabolism. Notable upregulated metabolic genes include regulator of glycolysis, MYC, and genes encoding for proteins involved in lipid metabolism and mitochondrial biogenesis such as PPARγ and PGC1α, respectively. PDK1: phosphoinositide-dependent kinase-1; PIP2 & 3: phosphatidylinositol (4,5)-bisphosphate & phosphatidylinositol (3,4,5)-trisphosphate; SFK: Src family kinase. Drawn on BioRender.com.

1.3.3 Metabolism of resting and activated GM-DCs

DCs upon activation undergo anabolic metabolic flux[81,82]. Activated GM-DCs stimulated by lipopolysaccharide (LPS) substantially increase glycolysis, lactate fermentation, fatty acid synthesis, and PPP activity[81,82]. The strength of stimulants on DCs is correlated with the degree of glycolysis upregulation and duration. The production of lactate via LDH-mediated conversion of pyruvate is a necessary to recycle the constituents required for continued glycolysis. Unlike cancer cells that upregulate aerobic glycolysis for the purpose of rapid ATP generation, the upregulation of glycolysis in DCs does not reflect the need to synthesize ATP as OXPHOS is sufficient to meet energic demands[84,89]. Upregulated glycolysis is indispensable, as inhibition of glycolysis by 2-deoxyglucose (2-DG) which inhibits the production of G6P, effectively impairs GM-DC activation[84] (**Figure 1.3)**. The respiratory capacity of early activated DCs is concurrently elevated with glycolysis, indicating the abundance of pyruvate generated from glycolysis is shuttled through the TCA cycle and oxygen dependent pathways. OXPHOS is not absolutely required during early DC activation as mitochondrial inhibition by oligomycin has a minimal effect on DC activation[84]. Instead, the TCA cycle is rewired, and the TCA cycle intermediates produced are preferentially used to support fatty acid synthesis – a process that synthesizes fatty acids from citrate, most of which are derived from pyruvate produced in glycolysis[84,90] (**Figure 1.4)**. The synthesized fatty acids are necessary for the expansion of the endoplasmic reticulum and Golgi apparatus[84]. The onset of glycolytic and fatty acid synthesis correlates with upregulation of co-stimulatory and secretion of cytokines such as CD40, CD80, CD86, MHC II, and IL-6 and TNFα[84]. Citrate is produced during the early steps of the TCA cycle and is proceeded by generation of isocitrate. As a major source of carbon for fatty acid synthesis, the intracellular levels of citrate and isocitrate decline while downstream intermediates

are unaffected after LPS stimulation[84,91]. Analysis by carbon tracing reveals the percentage of glucose-derived carbon is greater in citrate than in downstream TCA intermediates, indicating the flux of glucose is used to support fatty acid synthesis[84]. Lastly, to balance the redox reactions of fatty acid synthesis, the PPP is driven by glycolysis to generate NADPH. Unifying these observations, LPS stimulated GM-DCs have diminished lipid accumulation when glycolysis or fatty acid synthesis is pharmacologically inhibited[84].

In summary, resting DCs are metabolically quiescent. At a resting state, the ER is constrained and less active. DCs undergo metabolic reprogramming following toll-like receptor (TLR) stimulation to meet energy and biosynthetic demands. Notably, glycolysis is upregulated along with fatty acid synthesis, PPP, and OXPHOS activity. The early glycolytic intermediate, G6P, can undergo complete glycolysis to yield pyruvate, or shuttled through the PPP to regenerate the NADPH used in fatty acid synthesis and to produce nucleotides for transcription. The conversion of pyruvate into citrate during the TCA cycle can have two outcomes. In the first outcome, citrate undergoes complete catabolism to drive ATP synthesis via OXPHOS. Alternatively, citrate can be exported for fatty acid synthesis. The synthesis of lipids is integral to reducing ER stress and is used toward the expansion of the Golgi apparatus - a process necessary for efficient protein production and transport[84].

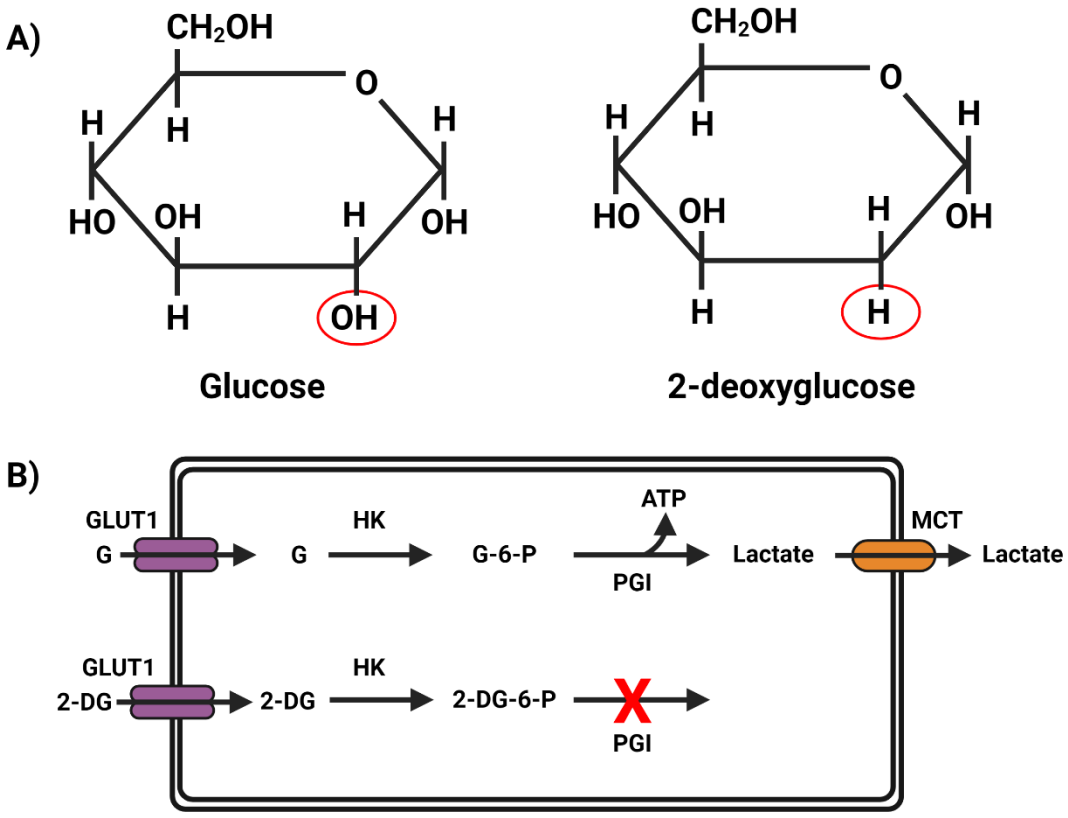

Figure 1.3. Inhibition of glycolysis by 2-deoxyglucose. (A) The molecular structure of glucose (G) (left) and 2-deoxyglucose (2-DG) (right). 2-DG is an analog of glucose, differing at the second carbon by substitution of hydrogen for the hydroxyl group (circled red). Lactic acid fermentation can occur at the end of glycolysis to produce lactate, which is then transported outside the cell via monocarboxylic transporters (MCT) **(B)** Glucose and 2-DG enter cells through glucose transporter 1 located in the plasma membrane. The first step of glycolysis is mediated by hexokinase (HK) synthesizing glucose 6-phosphate (G6P) and 2-deoxyglucose 6-phosphate (2-DG-6-P) from glucose and 2-DG, respectively. Due to the missing 2-hydroxyl group in 2-DG, the synthesized 2-DG-6P cannot be catalyzed by phosphoglucoisomerase (PGI) to proceed further through glycolysis. Image is adapted from Zhang et al[92] and drawn on BioRender.com.

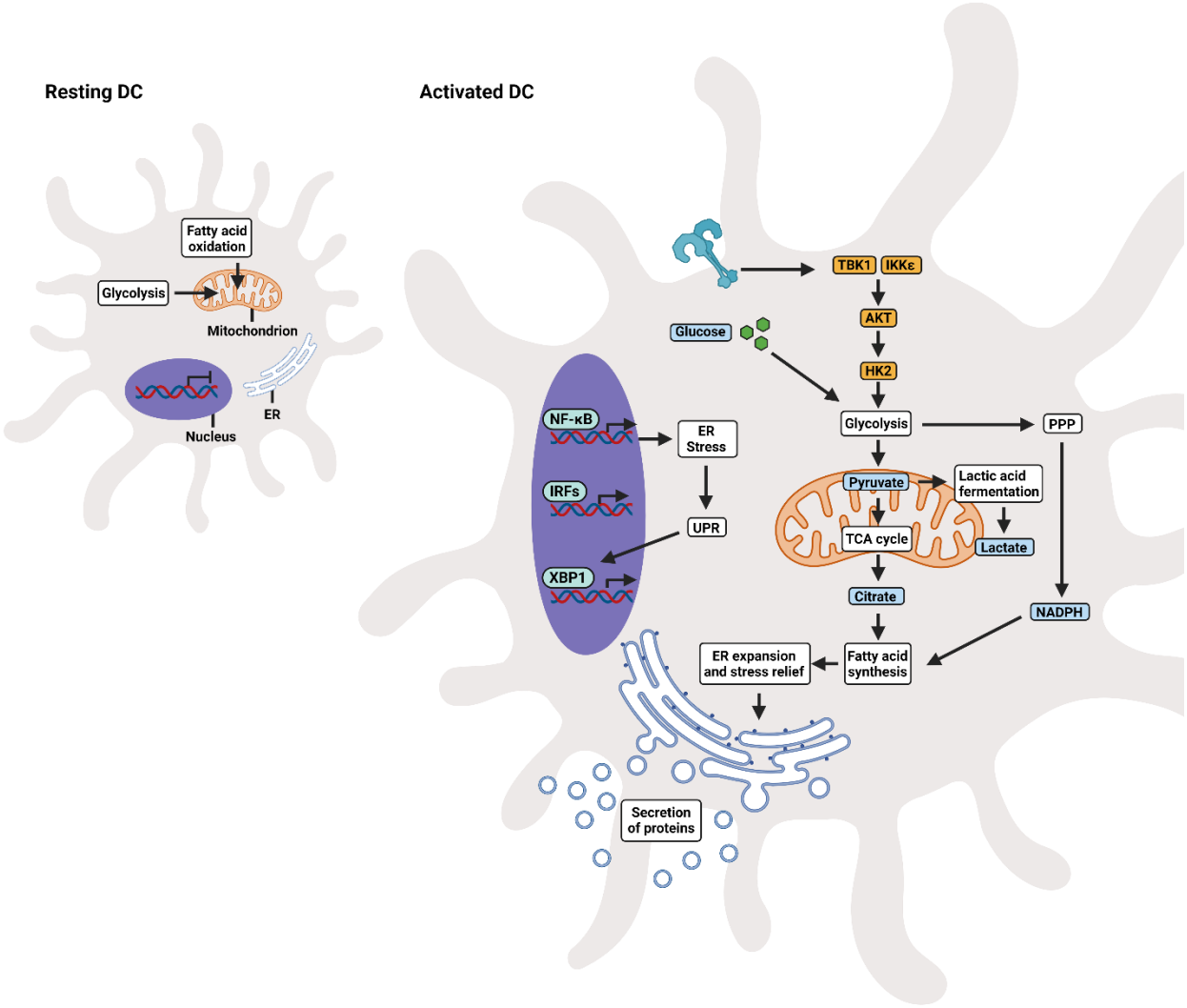

Figure 1.4. Dendritic cells undergo metabolic reprogramming following TLR stimulation. Resting DCs are metabolically inactive, deriving ATP through glycolysis and fatty acid oxidation. At this stage, the ER is relatively compact. DCs are activated following TLR stimulation leading to upregulated expression of maturation genes and increased protein synthesis. The accumulation of synthesized proteins stresses the ER, promoting the expression of enzymes for fatty acid synthesis. Synthesized fatty acids are used for the expansion of the Golgi apparatus and ER to accommodate for the abundance of newly synthesized proteins destined for secretion. Concurrently, TLR stimulation is transduced through AKT signaling, leading to the

upregulation of glycolysis. The pyruvate generated via glycolysis are used in the TCA cycle to synthesize citrate, a precursor for fatty acid synthesis. Complete citrate catabolism in the TCA cycle generates electron carriers for OXPHOS (not shown). PPP activity, fueled by early glycolytic intermediates, is increased to facilitate the production of NADPH used in fatty acid synthesis. IRFs: Interferon regulator factors; NF-κB: nuclear factor kappa B; UPR: Unfolded protein response; XBP1: X-box binding protein 1. Image is adapted from Pearce & Everts[82] and drawn on BioRender.com.

1.4. Mechanotransduction in immune cells

1.4.1. Mechanosensing

Environmental cues can modulate immunological function and metabolism. The impact of cytokine and PRR signaling on immunity in response to danger or pathogen associated molecular patterns have been extensively studied. However, the impact of non-immunological cues from the microenvironment that may also contribute to the collective regulation of the immune response during inflammation or infection is not well understood. These cues are context dependent and may include pH, temperature, oxygen, salt/ion balance, and nutrient availability. Mechanical forces represent another important environmental cue encountered within the microenvironment.

Immune cells naturally encounter environments with diverse physical properties. The mechanical forces exerted on resident or migratory immune cells arise through a multitude of physical means within the microenvironment that are influenced by features such the stiffness of the extracellular matrix, topography, and fluidity[2]. Some examples of mechanical stimuli are muscle contractions and shear stress from blood flow within blood vessels[93]. In general, mechanical forces are comprised of three major types: compression, tension, and shear. Compressional and tensional forces are mechanical stimuli that push or pull perpendicular to the surface of an object, whereas shear forces act parallel on the surface[2,93]. Young's elastic modulus is a parameter used to describe the amount of tension exerted by tissue or substrate stiffness and is expressed as units of pascal (Pa)[93]. In this model, tensile elasticity is defined as an object's resistance to deformation and is quantified by the linear relationship between stress and strain – where stress refers to compression or elongation forces, and strain is described by the deformation induced[2].

At a steady state, the stiffness of most soft tissues, including lymphoid organs, are between 2 to 5 kPa[2,93]. Muscles and bones on the other hand have a physiological stiffness of 10 to 20 kPa and 100 kPa, respectively[2,93–96]. The sustained stiffness of healthy tissues can change during inflammation or by diseases such as fibrosis[2,93]. For instance, lymph nodes stiffen during inflammation due to acute tissue remodeling and increased leukocyte trafficking and localized proliferation[1,4,6,95–97]. Another example is a healthy lung which has a physiological stiffness of about 2 kPa, whereas a fibrotic lung can reach a stiffness upwards of 50 kPa in rare cases[2,98]. In a tissue culture setting, plastic or glass substrates exhibit a stiffness that range magnitudes higher than physiological stiffness, at 10^6-10^8 kPa[93]. Thus, careful consideration is necessary when using these substrates, as supraphysiological effects may be exerted by the plastic or glass moduli.

1.4.2. The impact of mechanical signals on immune responses

Mechanical forces are critical for the migration of T cells. Prior to activation, T cells circulate peripheral and secondary lymphoid tissues via high endothelial venules (HEV) in search of cognate antigen. Selectins and integrins expressed by T cells function as mechanosensors that are sensitive to the shear flow[99,100]. T cell adhesion to endothelial cells within HEV is enhanced by low shear forces that promote the formation of catch bonds, a non-covalent bond that normally becomes stronger when a pulling force is applied[99–101]. In this context, low shear force allows integrins to adopt a high affinity, open confirmation that is conducive for T cell arrest and extravasation during transmigration. In shear-free conditions, T cell motility is sustained despite the activation of integrins by CCL21[99]. Furthermore, tensional forces can affect T cell function, as activated T cells migrate faster on stiffer substrates[7].

For adaptive immune cells, immunoreceptors have a dual function as mechanosensors regulating activation. Mechanical signals are required for the activation of T cells following the recognition of cognate antigens. Generation of cytoskeletal tension is necessary to stabilize the synaptic contact of migratory T-cells with APCs[102,103]. Specifically, the Wiskott-Aldrich syndrome protein (WASP) is rapidly activated after T cell receptor (TCR) engagement to mediate focal nucleation of actin and contraction of actin filaments[102]. The synapse is broken late in the activation process by internalization and degradation of WASP[102]. Patients with WASP deficiency have impaired TCR-mediated activation of T cells as a result of defective actin reorganization[103]. Interestingly, antigen-coated beads smaller than 4μm poorly stimulated T cells relative to larger. Furthermore, the TCR is an anisotropic mechanosensor that is topographically sensitive, whereby non-agonist anti-CD3 monoclonal antibodies could activate T cells only when force is applied by optical tweezers[104].

For B cells, mechanical signals also serve as a regulator of activation. To mount an effective antibody response, B cells must extract cognate antigens from the surface of APCs. Therefore, selective B cells that express high affinity B cell receptors (BCR) can more proficiently acquire antigen and subsequently obtain better T cell help. Recently, a study demonstrated the mechanism by which B cells discriminate antigen affinity is tension dependent. In this study, antigens were immobilized on surfaces of varying stiffness made from plasma membrane of adherent cells that are then suspended on a cover slip[5]. Using this experimental approach, it was demonstrated that B cells apply tension to the BCR-antigen bond[5]. In the case of weak antigen-bond, the tension applied will break the synapse between the BCR and antigen-presenting surface, preventing antigen extraction[5]. This process is further regulated by the flexibility of the antigen presenting substrate, namely antigen extraction is inhibited by rigid

surfaces because they prevent B cells from invaginating and pinching off the antigen from the surface[5]. As such, the physical properties of APCs are a critical factor regulating B cell activation. However, there appears to be a surface stiffness threshold for optimal B cell antigen acquisition. Follicular dendritic cells which are stiffer cells adapted for B cell responses promote stringent antigen affinity discrimination and accumulation of BCR microclusters, whereas DCs that are softer and more critical for T cell responses promote B cell acquisition of low affinity antigens[105].

1.4.3. Mechanotransduction in DCs

Despite DCs being potent orchestrators of the adaptive immune response, our understanding of how mechanical cues affects DC biology and function is limited. Only recently has research into this topic began to bloom. Mennen et al., using human DCs conditioned on polyacrylamide substrates with stiffness of 2, 12, and 50 kPa, demonstrated substrate stiffness affect DC function and phenotype[106]. Substrate stiffness did not affect DCs viability in this study but did impact the expression of C-type lectin receptors (CLRs), a family of PRRs – specifically macrophage mannose receptor (MMR) and dendritic-cell specific intercellular adhesion molecule-3-grabbing non-integrin (DC-SIGN)[106]. In this study, the intermediate stiffness of 12 kPa has an inhibitory effect on DC function[106]. The expression of MMR and DC-SIGN was the most upregulated for mature DCs conditioned on 2 kPa, followed by 50 kPa, whereas mature DCs conditioned on the intermediate tension of 12 kPa exhibited the lowest expression of MMR and DC-SIGN[106]. Consistent with a lower expression of C-type lectin receptors by DCs conditioned at 12 kPa, these cells had a lower uptake of ovalbumin (OVA), an antigen internalized by MMR[106]. Furthermore, chemokine directed migration of activated DCs is affected by substrate stiffness[106]. The expression of CCR7 was significantly higher in mature

DCs conditioned on 2 and 50 kPa compared to DCs conditioned on 12 kPa, suggesting substrate stiffness may affect DC migration to lymph nodes[106]. Substrate stiffness however did not affect the expression of most co-stimulatory molecules nor the capacity to activate T cells[106].

In our recent work we further investigated the impact substrate stiffness on DC function using BMDCs conditioned on polydimethylsiloxane (PDMS) hydrogel-coated plates of 2 kPa, 50 kPa, or plastic only[107]. However, unlike the observations of Mennen et al., we demonstrated that BMDCs function was enhanced by higher tension. BMDCs were more proliferative on 50 kPa compared to the physiological stiffness of 2 kPa, and BMDCs conditioned on higher stiffness acquired a more pro-inflammatory phenotype when stimulated with LPS[106,107]. Contrary to Mennens et al., who reported no change to CD80 expression in response to substrate stiffness, we found the heightened pro-inflammatory phenotype we observed corresponded with a higher expression of CD80 and CD86[106,107]. In addition, we found BMDCs conditioned on higher stiffness could better prime T cells[107].

Substrate stiffness affected DC function in both studies discussed, although in our study we did not observe 2 kPa enhancing DC biology. The differences in reported observations may be due to the physical properties of the substrates utilized, for instance hydrophobicity, which can impact other mechanical forces such as fluidity. Only the effects of tension were examined in these studies, thus, the impact of other mechanical forces in these studies remain unknown. Another area unexplored is the mechanisms and signaling pathways in DCs regulating the mechanotransduction of tension. Our novel finding of DCs conditioned on higher stiffness upregulating the expression of WW domain containing transcription regulator 1 (WWTR1), a gene encoding for TAZ, suggests this protein may be important for DC mechanosensing.

Investigating the function of TAZ in DCs is particularly intriguing, as TAZ is known to be involved in mediating cell adhesion and mechanical signaling in non-immune cells[108].

1.4.4. The role of YAP & TAZ

TAZ is a transcriptional coactivator sharing 46% amino acid identity with a homolog known as Yes-associated protein 1 (YAP), that are encoded by paralogous genes (**Figure 1.5**). Together both proteins serve as a nexus for a spectrum of physiological processes and is best understood as the penultimate effectors of the Hippo signaling pathway[109,110]. Unlike traditional signaling pathways, YAP/TAZ are not regulated by a singular dedicated pathway but is instead regulated by input from a diverse network and mechanisms (**Figure 1.6)**. A non-exhaustive list of established YAP/TAZ downstream functions include regulation of cell proliferation, cell fate decisions, organ overgrowth, wound healing and regeneration, mechanosensing, and functioning as metabolic and nutrient sensors[109–111]. Significant efforts have been directed at understanding and manipulating YAZ/TAZ in the context of cell differentiation and tumor immunity[111]. Beyond this little is known about the function of YAP/TAZ in immunology.

As transcription coactivators, YAP/TAZ shuttles from the cytoplasm into the nucleus in response to upstream signaling[111–114]. Although YAP/TAZ can interact with numerous transcription factors, the best characterized interaction of YAP/TAZ is with the transcription factor family, transcriptional enhancer factor (TEA)-domain (TEAD), due to its role as the transcriptional output of Hippo signaling - a pathway regulating cell proliferation and apoptosis[114]. At an inactive state, phosphorylated YAP/TAZ is retained in the cytoplasm by 14-3-3 protein binding, a group of phosphoserine/phosphothreonine binding proteins[110,112]. Conversely, YAP/TAZ is activated when dephosphorylated, allowing entry into the nucleus[110,112]. As transducers of Hippo signaling, YAP/TAZ is regulated by a series of core

Hippo kinases in response to various upstream stimulation, such as substrate stiffness[113]. YAP/TAZ is dephosphorylated when cells are exposed to high tension, whereas low tension induce YAP/TAZ inhibition[113]. Indeed, activated YAP/TAZ is prominently observed in adherent cells[112]. The first step of YAP/TAZ inhibition in the Hippo signaling pathways involves activation of large tumor suppressor kinases 1 and 2 (LATS1/2) by a complex of serine/threonine kinases, also known as mammalian Ste20-like 1 and 2 (MST1/2) and the scaffolding protein salvador family WW-domain-containing protein 1 (SAV1)[110,112,113] (**Figure 1.6**). In turn, activated LATS1/2 forms a complex with Mps one binder kinase activator-like 1A and 1B (MOB1a/b), which then directly inhibit YAP/TAZ by phosphorylation[110,112,113]. Thus, YAP/TAZ phosphorylation and translocation is one method to examine activity.

The function of YAP/TAZ in non-immune cells are mostly interchangeable and they are not known to interact with each other[110]. Interestingly, YAP/TAZ is dispensable depending on the biological function[110]. Maintenance of tissue homeostasis is unaffected by the loss of YAP/TAZ but is required for organ development and rapidly proliferating cells[110]. To date, 8 isoforms of YAP and 3 isoforms of TAZ have been identified in mammals[115–118]. The characterization of YAP/TAZ isoforms are limited and have focused primarily on the impact on embryonic stem cell differentiation[116,118]. From these limited studies, YAP/TAZ isoforms were shown to have overlapping, yet variable function and half-life[116,117,119]. For instance, in a study on two YAP isoforms, Wang et al. reported deletion of one isoform but not the other significantly impaired nervous system development[116]. Therefore, the differential function of YAP/TAZ in non-immune cell is potentially ascribed to the variable expression of YAP/TAZ isoforms. In the context of immunology, mRNA transcripts of 8 YAP isoforms were barely detectable in leukocytes compared to a relatively higher expression in tissues, suggesting

immune cells may differentially express YAP/TAZ isoforms[117]. YAP/TAZ have been reported to have immunoinhibitory and pro-inflammatory functions in immune cells[6,120–123]. YAP in T cells is a mechanosensor with immunoinhibitory effects[6,120,124]. YAP expression is upregulated following activation and functions as a suppressor, dampening function and tumor infiltration[120,124]. On high stiffness conditions, YAP suppresses T cell proliferation by preventing the translocation of the transcription factor, nuclear factor of activated T-cells (NFAT)[6]. This function of YAP is distinct from the conventional mechanism of YAP nuclear translocation to promote transcription[6]. On the other hand, T cell specific cre-mediated deletion of YAP improves activation, function, and differentiation without affecting T cell development or thymic egression[6,120,124]. Furthermore, YAP has been reported to suppress the metabolic reprogramming of activated T cells[6]. The impact of YAP/TAZ signaling on B cell biology and function is currently unknown.

For innate immune cells, persistent macrophage inflammation is observed with fibrotic and scar tissues, suggesting macrophages are sensitive to substrate stiffness[125]. Recently Meli et al. demonstrated YAP mediated mechanotransduction underlie macrophage pro-inflammatory response to tissue stiffness[8]. Macrophages conditioned on soft substrates were less inflammatory and is associated with a reduction in YAP expression and activity[8]. Inflammation was heightened when macrophage overexpressed YAP, compared to the depletion of YAP inhibiting macrophage mediated inflammation[8]. Altogether, it appears YAP deficiency confers macrophage a reparative phenotype. Congruently, YAP/TAZ deficiency in macrophages is associated with improved infarct healing post myocardial infarction[121].

To date, only one study has examined the role of YAP/TAZ in DCs but not the impact on DC mechanosensing[123]. The significance of MST1/2 deficiency have also been investigated in

DCs[122,123]. Du et al. reported MST1/2 signaling orchestrate the metabolic reprogramming and function of $CD8^+$ DCs. Specific deletion of MST1/2, but not LATS1/2 or YAP/TAZ impaired the antigen presenting ability of $CD8^+$ DCs while $CD8^-$ DCs were unaffected[123]. The impaired functionality of MST1/2 deficient $CD8^+$ DCs was associated with significantly lower OXPHOS and glycolytic flux than wildtype $CD8^+$ DCs[123]. On the contrary, Cho et al. reported MST1/2 deficiency hyperactivated DCs[122]. MST1/2 deficient DCs in this study were better T cell activators than wildtype counterparts[122]. Curiously, MST1/2 deficiency led to increased AKT1 phosphorylation and expression of MYC suggesting an active metabolism but was not further investigated[122]. Altogether, the current understanding of YAP/TAZ signaling in DCs is limited.

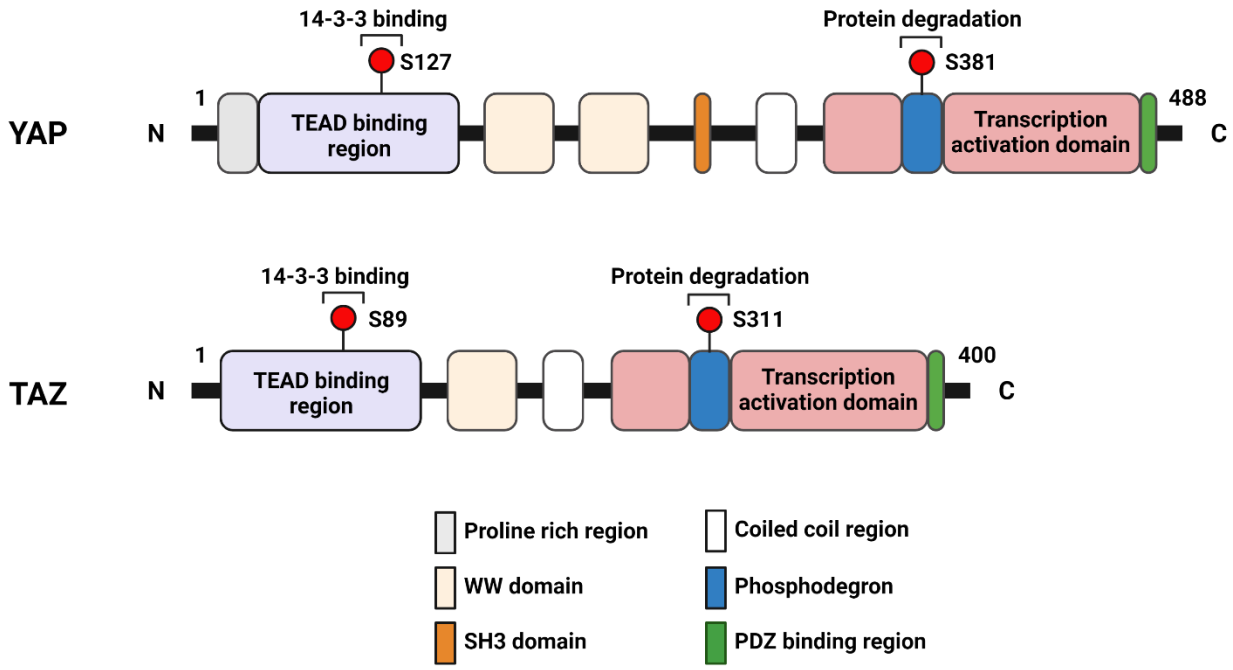

Figure 1.5. A schematic representation of Yes-associated protein (YAP) and transcriptional coactivator with PDZ-binding motif (TAZ) protein domains. (Top) YAP is comprised of a N-terminal proline rich region, transcriptional enhanced associate domain (TEAD) binding region, two WW domains, a Src homology domain 3 (SH3) binding motif, coiled-coil (CC) domain, a phosphodegredon motif, a transcription activation domain, and a C terminal PDZ-binding motif. 14-3-3 proteins sequester YAP in the cytoplasm when YAP is phosphorylated at S127. YAP is marked for proteasomal degradation when S381 is also phosphorylated. (Bottom) TAZ is a smaller protein comprised of similar protein domains as YAP. TAZ does not have a proline rich domain, a single WW domain and the SH3 binding domain. TAZ is sequestered by 14-3-3 proteins when phosphorylated at S89. Phosphorylation at S311 targets TAZ for proteasomal degradation. The TEAD binding domain allow YAP/TAZ to interact with the transcription factors TEAD to initiate transcription. Drawn on BioRender.com.

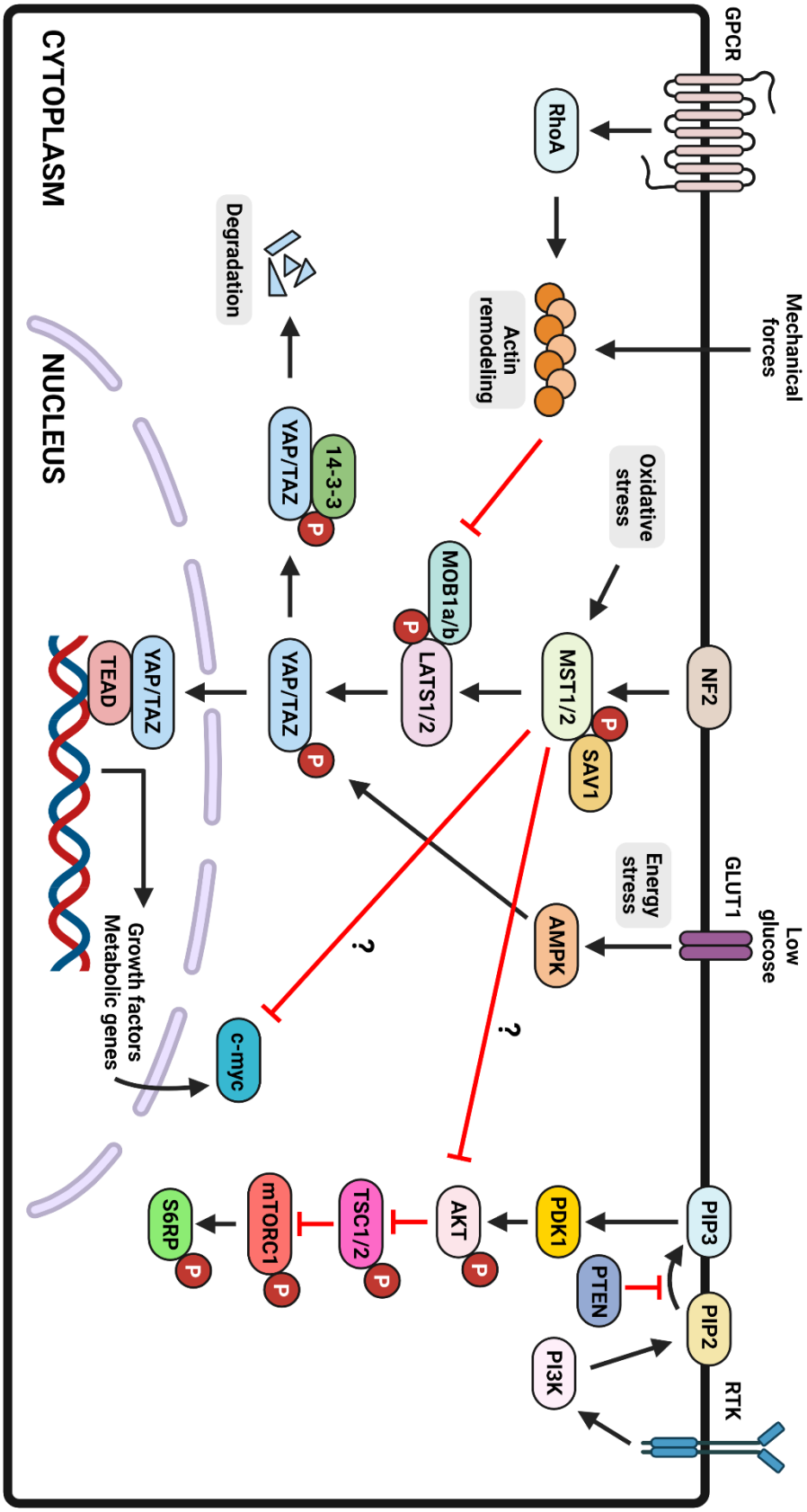
CYTOPLASM
NUCLEUS
GPCR
RhoA
Actin remodeling
Mechanical forces
Degradation
14-3-3
YAP/TAZ
P
MOB1a/b
LATS1/2
Oxidative stress
MST1/2
SAV1
NF2
YAP/TAZ
TEAD
Growth factors
Metabolic genes
c-myc
?
?
Energy stress
AMPK
Low glucose
GLUT1
PIP3
PIP2
PTEN
PI3K
RTK
PDK1
AKT
TSC1/2
mTORC1
S6RP

Figure 1.6. YAP/TAZ is involved in crosstalk with various signaling pathways. YAP/TAZ activity is regulated by a diverse repertoire of upstream input through the Hippo signaling pathway[109,110,112]. The core Hippo signaling pathway consists of NF2, MST1/2, SAV1, MOB1, and LATS1/2 that initiates a phosphorylation cascade, leading to the phosphorylation of YAP/TAZ. YAP/TAZ are sequestered in the cytoplasm and targeted for proteasomal degradation when phosphorylated. YAP/TAZ function as mechanosensors via G-protein coupled receptor signaling, a large family of cell surface receptors can activate or inhibit YAP/TAZ in a Ras homolog family member A (RhoA) mediated manner by inducing actin cytoskeletal reorganization - RhoA is a small GTPase. Alternatively, mechanical forces such as substrate stiffness and shear force can regulate YAP/TAZ by inducing cytoskeletal stress Furthermore, YAP/TAZ are metabolic sensors, whose function is inhibited when under energy stress. Receptor tyrosine kinases, a family of high affinity surface receptors for growth factors can regulate YAP/TAZ activity. When dephosphorylated, YAP/TAZ translocate into the nucleus, initiating the transcription of genes involved in cell proliferation, cell fate decisions, organogenesis, wound healing and regeneration, mechanosensing, and metabolism[109–111]. AMPK: AMP-activated protein kinase; NF2: Neurofibromatosis type 2. Drawn on BioRender.com.

1.5. Hypothesis and Objectives of Study

In our recent work, we found that DC function is intertwined with mechanical cues. The purpose of this current study is to understand how mechanical signals are translated into biochemical signals by probing for the mechanisms controlling DC mechanosensing – an area that is unexplored. Investigating the role of YAP/TAZ is particularly captivating as we saw upregulated expression of TAZ, a transcription co-activator known to be involved in mechanosensing. Taking into consideration of prior studies on YAP/TAZ, we hypothesize that the loss of YAP/TAZ will impair the mechanosensory capacity of DCs, thus altering metabolic programming to attenuate the substrate stiffness mediated enhancement of DC function. The knowledge gained in this study will provide valuable insight that is applicable to the development of novel DC mediated therapy, such as boosting vaccination effectiveness or dampening/bolstering immune responses through the manipulation of DC mechanosensing.

The experimental setup encompasses an *in vitro* and *in vivo* component. For *in vitro* studies, GM-DCs are used. GM-DCs are cultured on plastic culturing plates and plates coated with polydimethylsiloxane gels with a stiffness of 2 and 50 kPa. GM-DCs are purified at the end of the culturing for downstream analysis. The BM precursors are from wildtype and KO mice that have CD11c specific single knockout of YAP and TAZ or double knockout using the Cre-lox system. For *in vivo* studies, the YAP/TAZ KO mice are infected with mouse adapted H1N1 influenza virus. Using this experimental setup, we will address three questions:

1. How does substrate stiffness regulate DC metabolism?
2. Does the loss of YAP/TAZ affect the homeostasis & function of DCs?
3. Is the anti-viral response of mice with CD11c-specific YAP/TAZ deficiency impaired?

Chapter 2: Methods & Materials

2.1. Mice

6-12 weeks old commercially available mice were used for experiments (Jackson Laboratory). OT-1 transgenic mice (003831) were used for $CD8^+$ T cell activation assays. Dendritic cell-specific Yap/Taz conditional knock out mice (CD11c-Cre^+ $YAP^{fl/fl}$ and CD11c-Cre^+ $TAZ^{fl/fl}$) via a CD11c promoter-driven Cre recombinase transgene (CD11c-Cre) were generated using CD11c-Cre (008068), TAZ^{fl} (032669), and YAP^{fl} (027929) mice[126–128]. All mice are bred and housed in a pathogen-free, temperature-controlled, and 12 hr light and dark cycle environment at the University of Alberta Health Sciences Laboratory Animal Services mouse barrier facility. All the experimental procedures were approved by the Animal Care committee at the University of Alberta. Mice genotypes were confirmed by PCR and gel electrophoresis.

2.2. Flow cytometry

Single cell suspension from various organs were used for flow cytometry. Cell viability was determined by LIVE/DEAD Near-IR staining (ThermoFisher). Fluorophore conjugated antibodies were diluted 1/200 unless otherwise recommended by the supplier prior to surface and intracellular staining at 4°C for 30 min. Intracellular staining was done after fixation and permeabilization with FOXP3 staining buffer set (eBioscience). For intracellular cytokine assays, cell suspensions were first stimulated with phorbol myristate acetate in the presence of Golgi Stop (PMA+, eBioscience) for 4 hr. Viral specificity of T cells from H1N1 infected organs were stained with tetramers (NIH). Permeabilized/fixed samples and viral infected samples were resuspended in permeability buffer or 1% paraformaldehyde, while unfixed samples were resuspended in FACs buffer for flow cytometric analysis on a BD LSR Fortessa-SORP and BD

Fortessa X-20 at the Flow Cytometry Facility (University of Alberta). FACS plots were generated using FlowJo software.

2.2.1. ImageStream flow cytometry

Nuclear translocation of YAP and TAZ in purified $CD11c^+$ BMDCs were quantified by image flow cytometry. Surface staining were done as described. Intracellular staining for nuclei (DAPI, BioLegend), YAP, and TAZ were done following fixation and permeabilization with FOXP3 staining buffer set (eBioscience). Fluorophore conjugated (Santa Cruz Biotechnology) and unconjugated (Cell Signaling) TAZ specific antibodies were used. ImageStream flow cytometry was carried out on an Amnis ImageStream Flow Cytometer at the Flow Cytometry Facility (University of Alberta). The IDEAS application was used to analyze ImageStream data, and the translocation scores were calculated using the program's translocation similarity score algorithm.

2.3. Polydimethylsiloxane (PDMS) hydrogels

Cell culturing plates with a tension of 2 kPa and 50 kPa were made using Dow Corning Sylgard 527 silicone dielectric gel (Part A and B, Ellsworth). To obtain the appropriate tensions, part A and B were mixed at the following ratio - for 2 kPa gel, the ratio of A:B was 1.2 and for 50 kPa the ratio of A:B was 0.3. 6-well plates were coated with 2 mL of gel/well then incubated overnight at 60°C to polymerize. After 24 hrs, the coated plates are sterilized by UV irradiation for 15 minutes. Prior to use, plates are coated with fibronectin (1µg/ml in PBS, Sigma) for 6 to 24 hr followed with 2 times washing with PBS. The elastic tension of the gels using the described ratios were confirmed by our collaborators at the University of Toronto on a JPK NanoWizard II (JPK Instruments) atomic force microscope.

2.4. Culturing of BMDCs

BMDCs were cultured using a protocol by Inba et al.[22]. BM progenitor cells are harvested from the femur and tibia of mice. The BM is flushed with PBS followed with hemolysis. Cells are hemolyzed at room temperature for 5 minutes then washed with PBS. Cells are resuspended and grown at a density of 4 x 10^6 /3mL in GM-CSF (20ng/ml) in cell culturing medium (RPMI-1640 (Wisent) supplemented with Penicillin (100 U/ml, Sigma), Streptomycin (100µg/ml, Sigma), L –glutamine (2 mM, Sigma), 2-mercaptoethanol (50 µM, Sigma), and 10% heat-inactivated and FBS (Wisent)). At day 3 and 6, cells are supplemented with 2 mL of GM-CSF (20 ng/mL). Cultured cells are harvested on day 7 and purified using a CD11c positive selection kit (Stemcell) following manufacturer's instructions.

2.5. Carboxyfluorescein succinimidyl ester (CFSE) antigen presentation assay

OT-1 T cell proliferation was examined using a 2-day CFSE assay. OT-I T cells are harvested from the bone marrow of OT-1 transgenic mice and purified with an EasySep™ mouse $CD8^+$ negative selection kit (STEMCELL technologies) according to manufacturer's protocol. Purified $CD8^+$ cells are labelled with CellTrace™ CFSE (ThermoFisher). Each well of a 96-well plate were seeded with 500000 OT-1 T cells and 5000 purified $CD11c^+$ DCs and treated with 0 µg/ml, 0.01 µg/ml, or 0.1µg/ml of $OVA^{257-264+}$ peptide (GenScript). Proliferation was measured by flow cytometric analysis for the dilution of CFSE.

2.6. Dendritic cell activation assay

DC response to LPS stimulation *in vitro* was evaluated by measuring the expression of DC activation marker and cytokine production. Purified $CD11c^+$ DCs were treated with 0.1 µg/ml LPS with or without the addition of 125 nM of verteporfin. Cells were harvested after 1 day and the expression of CD80, CD86, CD40, and Ki67 were examined by flow cytometry.

2.7. Metabolic assays

Glycolysis and mitochondrial respiration of purified $CD11c^+$ GM-DCs were quantified on an Agilent Seahorse XFe24 metabolic flux analyzer (provided by Dr. Evangelos Michelakis, University of Alberta) using a glycolytic and mitochondrial stress test kit (Agilent Technologies). On the day before the assay, 24-well Seahorse XF24 V7 PS cell culture microplates (Agilent Technologies) are pre-coated with Corning™ Cell-Tak Cell and Tissue Adhesive (Fisher Scientific) overnight to promote the formation of a monolayer. On the day of the assay, cells are plated at a final density of 1.0×10^5 cells/mL.

The metabolic assays were performed following manufacturer's instructions. Rate of glycolysis and glycolytic capacity was calculated using the readout from the instrument programmed to take three repeated-measurements at baseline and following injection of glucose (measurements 3 - 6), oligomycin (measurements 7 - 9), and 2-deoxyglucose (measurements 10 −12), respectively (**Figure 2.2)**. Rates of glycolysis and glycolytic capacity were calculated by subtracting glucose-induced extracellular acidification (ECAR) (6^{th} measurement) or oligomycin induced ECAR (9^{th} measurement) from the baseline after 2-DG treatment (12^{th} measurement), respectively. To quantify oxidative metabolic flux, the instrument provides three repeated measurements at baseline and following injection of oligomycin (measurements 3-6), carbonyl cyanide-*p*-trifluoromethoxyphenylhydrazone (FCCP) (measurements 7-9), and rotenone & antimycin A (measurements 9-12). Mitochondrial respiration and maximal respiratory capacity were calculated by subtracting the basal (3^{rd} measurement) or maximal (9^{th} measurement) from baseline (12^{th} measurement). Glucose uptake was measured by allowing DCs to uptake the fluorescent glucose analog, 2-(N-(7-Nitrobenz-2-oxa-1,3-diazol4-yl)Amino)-2-Deoxyglucose (2-NBDG, Cayman Chemical), followed by flow cytometric analysis.

A)

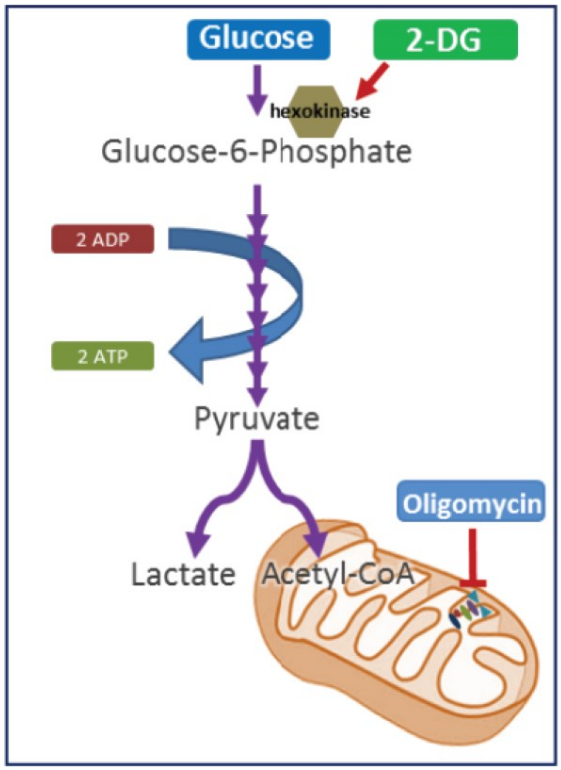
Glucose
2-DG
hexokinase
Glucose-6-Phosphate
2 ADP
2 ATP
Pyruvate
Oligomycin
Lactate
Acetyl-CoA

B)

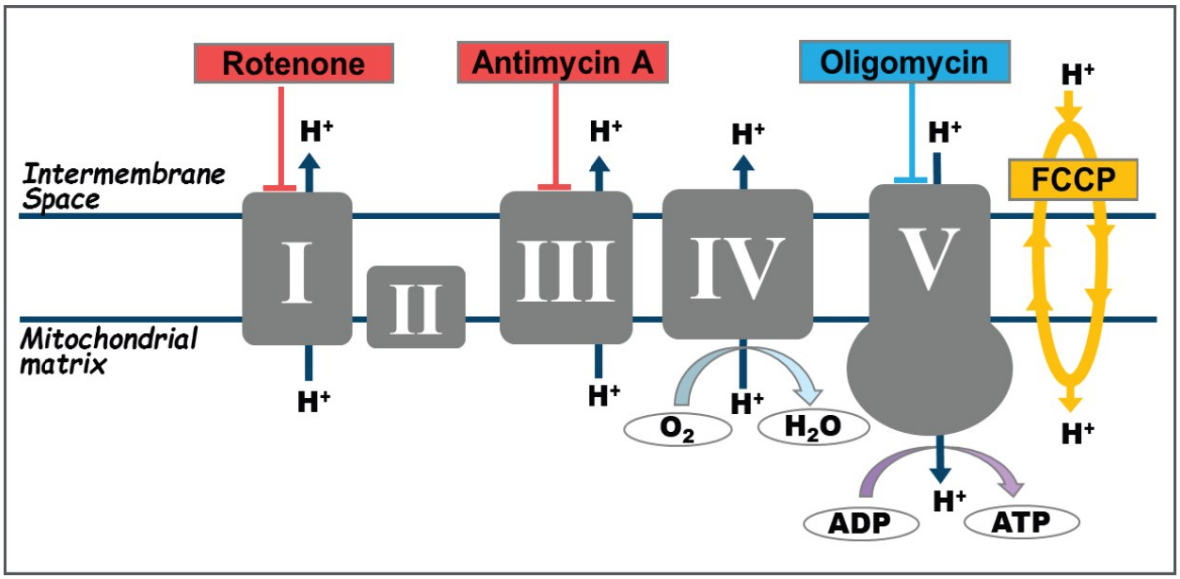
Rotenone
Antimycin A
Oligomycin
H+
FCCP
Intermembrane Space
Mitochondrial matrix
I
II
III
IV
V
O2
H2O
ADP
ATP

Figure 2.1. Outline of drug targets used in Seahorse glycolysis and mitochondria stress assays. (A) Glycolytic flux is measured by the acidification of media mainly due to the production of lactate by lactic acid fermentation. The first treatment is the addition of glucose to drive glycolysis in a process mediated by HK phosphorylating glucose into G6P. The second treatment is oligomycin to shut down mitochondrial respiration via ATP synthase inhibition – this forces the cell to upregulate glycolysis and undergo lactic acid fermentation to recycle metabolites needed to sustain glycolysis for ATP generation. The third and last treatment is with 2-DG, an analog of glucose that cannot be metabolized by phosphoglucose isomerase, thereby shutting down glycolysis. **(B)** Figure depicting the mitochondrial electron transport chain involved in aerobic respiration. As this is an oxygen dependent pathway, mitochondrial respiration is measured based on changes to oxygen consumption. The first treatment in this assay is the addition of oligomycin to disrupt electron flow through at complex V, thereby reducing oxygen consumption. The second treatment is FCCP, a proton gradient uncoupler that disrupts the mitochondrial membrane potential, allowing electrons to flow through the ETC uninhibited and increases oxygen consumption when the protons reach complex IV. Lastly, to shutdown mitochondrial respiration entirely, rotenone/antimycin-A is added to block electron flow. Images were taken from the Seahorse product manuals.

A)

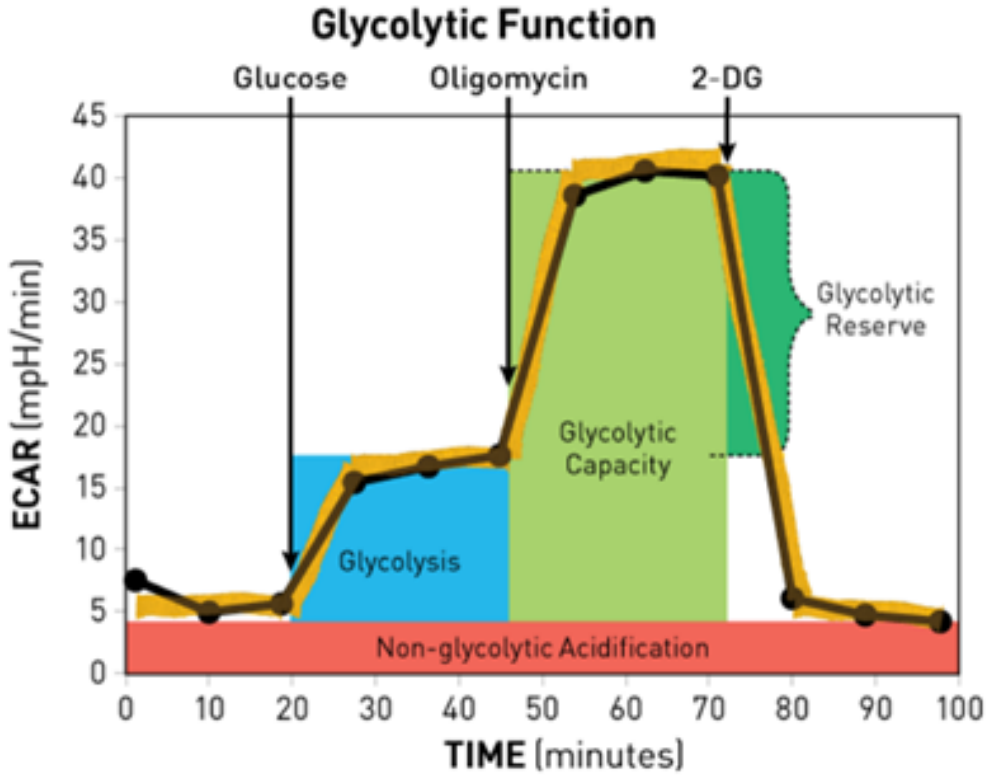
Glycolytic Function
Glucose
Oligomycin
2-DG
ECAR (mpH/min)
45
40
35
30
25
20
15
10
5
0
Glycolytic Reserve
Glycolytic Capacity
Glycolysis
Non-glycolytic Acidification
0
10
20
30
40
50
60
70
80
90
100
TIME (minutes)

B)

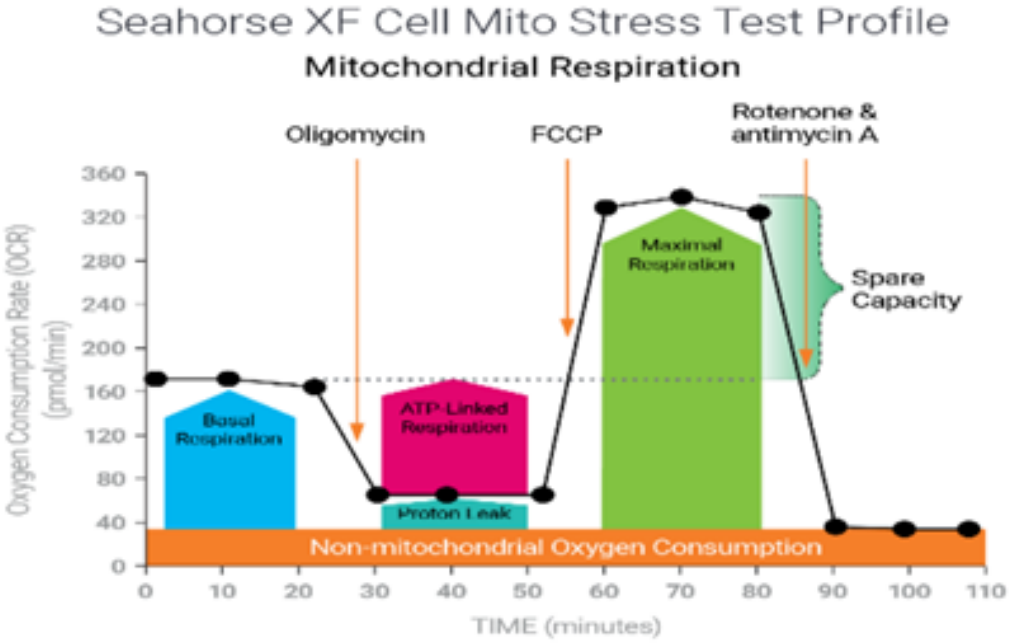
Seahorse XF Cell Mito Stress Test Profile
Mitochondrial Respiration
Oligomycin
FCCP
Rotenone & antimycin A
Oxygen Consumption Rate (OCR) (pmol/min)
360
320
280
240
200
160
120
80
40
0
Basal Respiration
ATP-Linked Respiration
Proton Leak
Maximal Respiration
Spare Capacity
Non-mitochondrial Oxygen Consumption
0
10
20
30
40
50
60
70
80
90
100
110
TIME (minutes)

Figure 2.2. Sample curves generated from the Seahorse glycolysis and mitochondria stress test assays. The Agilent Seahorse XFe24 metabolic flux analyzer makes triplicate recording during the assays before and after treatment with specific drugs. **(A)** Glycolysis is measured by extracellular acidification (ECAR). Glucose, oligomycin, and 2-DG are administered at different time points to promote or inhibit glycolysis. Rates of glycolysis and glycolytic capacity were calculated by subtracting glucose-induced ECAR (6^{th} measurement) or oligomycin induced ECAR (9^{th} measurement) from the baseline after 2-DG treatment (12^{th} measurement), respectively. **(B)** OXPHOS activity is measured by changes to oxygen consumption rate (OCR). The cells are administered oligomycin, FCCP, and rotenone/Antimycin-A at different time points to stress the mitochondria. Mitochondrial respiration and maximal respiratory capacity were calculated by subtracting the basal (3^{rd} measurement) or maximal (9^{th} measurement) from baseline (12^{th} measurement). Images were taken from the Seahorse product manuals.

2.8. H1N1 influenza infection model

Mice were infected intranasally with 0.175 HAU of Puerto Rico strain H1N1 influenza A virus (PR8) (provided by Dr. Kevin Kane, University of Alberta) and euthanized 9 days post-infection. The immunization protocol was kindly provided and demonstrated by Gang Zhou from the Kane lab. Body weight was recorded prior to infection and monitored daily at similar times. The lung, spleen, and mediastinal lymph node were obtained from H1N1 infected mice for quantification. H1N1 infected mice were housed in a pathogen-free, temperature-controlled, and 12 hr light and dark cycle environment at the University of Alberta Health Sciences Laboratory Animal Services level 2 biocontainment facility.

2.9. Tissue isolation & digestion

The mediastinal lymph node, lung, and spleen were retrieved from healthy or infected mice after euthanasia for processing. Lungs were flushed with PBS - a single lobe is weighed then digested for downstream applications. Lung tissue is minced and digested with gentle shaking for 1 hr. Spleens and digested lungs were passed through a 40 μL cell strainer prior to hemolysis. Mediastinal lymph nodes were processed by passing through a cell strainer without hemolysis.

2.10. Western Blotting

The expression and phosphorylation of YAP, TAZ, AKT, and S6 ribosomal protein were quantified by western blotting using standard protocol. Cell lysates from purified $CD11c^+$ DCs were prepared using commercial cell lysis buffer (Cell signaling) and protease/phosphatase inhibitor (Cell Signaling) according to manufacturer instructions. Protein concentration was determined using a Pierce™ BCA Protein Assay Kit (ThermoFisher). 25 to 50 μg of protein were loaded with 1x Laemmli Sample Buffer (BIO-RAD) and resolved on 8% Tris-Glycine gel

then transferred onto a polyvinylidene difluoride membrane (Millipore). After transfer, the membrane was blocked with Intercept™ TBS blocking buffer (Li-Cor) for 1 hr. Antibodies used for western blots were diluted in Intercept™ antibody diluent T20 TBS buffer (Li-Cor). Primary antibodies were diluted as follow: actin 1/2000, phospho-AKT and phospho-S6RP 1/500, total AKT & S6RP 1/1000. Secondary antibodies were diluted 1/1000. Membrane development proceeded with 1° antibody incubation overnight at 4°C then with detection antibody (Li-Cor) at room temperature for 1 hr. The developed membrane was scanned using an Odyssey Fc Imaging System. Protein bands were quantified using the Li-Cor Image Studio Acquisition Software.

2.11. Statistical analysis

All statistical analyses were performed using the GraphPad Prism 9 software. The number of biological replicates is listed as the n value in figure legends. Statistical significance was assessed using Mann-Whitney U- test or students T-test set at $p < 0.05$.

2.12. Tables of reagents and software

Table 1. List of antibodies used for flow cytometry or Western Blotting. All listed antibodies are available commercially.

Reagents	Clone	Source	Catalog number
Antibodies			
TAZ (E8E9G) Rabbit mAb	E8E9G	Cell Signaling	83669
TAZ Antibody (D-8) PE	D-8	Santa Cruz Biotechnology	sc-518026 PE
YAP1 Antibody (G-6) Alexa Fluor 647	G-6	Santa Cruz Biotechnology	sc-376830 AF647
PE anti-mouse TNF-a antibody	MP6-XT22	BioLegend	506306

APC/Cyanine7 anti-mouse CD4 antibody	GK1.5	BioLegend	100414
Brilliant Violet 711 anti-mouse CD45 antibody	30-F11	BioLegend	103147
PE/Dazzle 594 anti-mouse CD86 antibody	GL-1	BioLegend	105042
Brilliant Violet 421 anti-mouse IFN-γ antibody	XMG1.2	BioLegend	505830
Pacific Blue anti-mouse I-Ab antibody	AF6-120.1	BioLegend	116422
Alexa Fluor 488 anti-mouse CD80 antibody	16-10A1	BioLegend	104716
FITC anti-mouse CD40 antibody	HM40-3	BioLegend	102906
FITC anti-mouse/human CD11b antibody	M1/70	BioLegend	101206
Alexa Fluor 647 anti-mouse CD11c antibody	N418	BioLegend	117312
PE/Cyanine7 anti-mouse CD3ε antibody	145-2C11	BioLegend	100320
PerCP/Cyanine5.5 anti-mouse I-Ab antibody	AF6-120.1	BioLegend	116416
eFluor 450 anti-mouse CD11b antibody	M1/70	ThermoFisher	48-0112-82
PE/Dazzle 594 anti-mouse Ki-67 antibody	16A8	BioLegend	652428
PerCP/Cyanine5.5 anti-mouse CD4 antibody	GK1.5	BioLegend	100434
APC anti-mouse CD103 antibody	2E7	BioLegend	121414
APC anti-mouse CD64 antibody	X54-5/7.1	BioLegend	139305

PE/Dazzle 594 anti-mouse Ki-67 antibody	16A8	BioLegend	652428
Brilliant Violet 510 anti-mouse CD62L antibody	MEL-14	BioLegend	104441
Purified anti-β-actin Antibody	2F1-1	BioLegend	643801
Phospho-AKT (Ser473) XP Rabbit mAB	D9E	Cell Signaling	4060
Phospho-AKT (Thr308) XP Rabbit mAb	D25E6	Cell Signaling	13038
Phospho-S6 Ribosomal Protein (Ser235/236) Rabbit mAb	91B2	Cell Signaling	4857
IRDye 680RD Goat anti-Mouse	N/A	Li-Cor	926-68170
IRDye 680RD Goat anti-Rabbit	N/A	Li-Cor	926-68171

Table 2. List of reagents used for cell culturing, digestion of lung tissues, or Western Blotting.

Chemicals & Peptides		
DAPI	BioLegend	422801
Fibronectin	Millipore-Sigma	F1141
2-NBDG	Cayman Chemical	11046
$OVA^{257-264+}$ peptide	GenScript	RP10611
LIVE/DEAD Near-IR staining	ThermoFisher	L34973
Sodium Pyruvate	ThermoFisher	11-360-070
DNase	Sigma	D5025
Collagenase	Sigma	C0130

CellTrace™ CFSE	ThermoFisher	C34554
4x Laemmli Sample Buffer	BIO-RAD	1610747
Protease/Phosphtase Inhibitor (100x)	Cell Signaling	5872
Cell Lysis Buffer (10x)	Cell Signaling	9803
Recombinant Mouse GM-CSF (carrier-free)	BioLegend	576304
Murine (PR8) H1N1/H-2D^{b} Tetramer	NIH	N/A
Intercept™ Antibody Diluent T20 TBS	Li-Cor	927-65001
Intercept™ Blocking Buffer TBS	Li-Cor	927-60001

Table 3. List of commercial assays and kits used.

Commercial Assays/Kits		
EasySep™ Mouse CD8^{+} T Cell Isolation Kit	Stemcell	19853A
EasySep™ Mouse CD11c Positive Selection Kit II	Stemcell	18780
FOXP3/Transcription Factor Staining Buffer Set	eBioscience	00-5523-00
Pierce™ BCA Protein Assay Kit	ThermoFisher	23227
Immobilon-FL PVDF membrane	Millipore-Sigma	N/A
Corning® Cell-Tak™ Cell and Tissue Adhesive	Corning	354240

Table 4. List of software used for data analysis.

Software		
FlowJo	FlowJo, LLC	N/A
GraphPad Prism 9	GraphPad Softwares	N/A
IDEAS Application	Amnis	N/A
Image Studio Software	Li-Cor	N/A

Chapter 3: Mechanosensing Modulates DC Metabolism and Function

3.1 Contributions

The work characterizing the effects of substate tension on DC cytokine production and maturation presented in this chapter were conducted by the Tsai lab and our collaborators, of which contributed to data analysis - a complete list of authors could be found here[107]. This study on substrate stiffness modulating DC biology is an important foundation from which I expanded on with the help and guidance of Dr. Sue Tsai by investigating whether DC metabolism is also affected by substrate stiffness. Undergraduate student Camille Huang assisted in the preparation of metabolic assays. Seahorse glycolysis and mitochondria stress kits were used to examine substrate associated metabolic alterations in DCs. These assays are performed using a key piece of instrument, the Seahorse XFe24 metabolic flux analyzer. Access to a Seahorse XFe24 metabolic flux analyzer was kindly provided by Dr. Evangelos Michelakis (University of Alberta). The work characterizing the nuclear translocation of YAP and TAZ in BMDCS with ImageStream flow cytometry was performed by me with assistance from undergraduate student Felicia Kanji.

3.2 Introduction

Lymphocytes undergo substantial metabolic reprograming following activation to support biosynthesis and functionality[81,82]. In the case of mature DCs, both glycolysis and OXPHOS are active at a low rate relative to activated DCs. Rapid glycolytic flux is observed following PRR ligation, such as TLR stimulation, to support the production of metabolic intermediates necessary to synthesize ATP, development, and function. AKT1 is activated downstream of LPS stimulated DCs, that goes on to critically activate HK by phosphorylation[84] (**Figure 1.1 & 1.4**). HK mediated conversion of glucose to G6P initiates glycolysis and prevents glucose molecules from

leaving the cytoplasm. This critical step promotes the upregulation of glycolysis and metabolic pathways required for endoplasmic reticulum (ER) and Golgi biogenesis[84]. These metabolic pathways in turn support the expression of proteins required for DC function – namely, MHC, co-stimulatory ligands, and cytokines[84]. Thus, metabolic reprogramming constitutes an indispensable process for DC biology and functionality. In addition to PRR ligation, non-classical immunological sensing mechanisms from the environment can also activate DCs[106].

As discussed previously, mechanical signals modulate the functionality and maturation of macrophages, T cells, and B cells. Given the role of DCs as APCs, the study on the impact of mechanical signals on DCs can provide insights into a novel parameter for consideration in the understating the development of disease and its treatment. Through our work and the efforts of Mennen et al., substrate stiffness has recently been identified as a stimulus regulating DC biology[106,107]. The mechanism regulating this process is currently unknown but given that metabolism is closely intertwined with physiological processes, I postulate that DC metabolic flux is regulated by mechanosensing, which in turn shapes DC function. Of the multiple metabolic pathways, I have chosen to focus on glycolysis and OXPHOS flux due to their prominence as two major energy generating pathways.

Glycolysis is a metabolic pathway that is upregulated in active DCs, and the products of glycolysis feeds into multiple pathways that eventually intersect in the OXPHOS pathway in respiring cells. The availability of assays designed to measure glycolysis and OXPHOS permits in depth and accurate characterization, thus making investigation of these pathways more feasible. The DCs used in my study are generated *in vitro*, as isolation of primary DCs from digested animal tissues is an inefficient process often resulting in low yield. To address this issue, BMDCs are the primary DC subtype used - generated using an established protocol by

culturing precursor BM cells with GM-CSF for 7 days on plastic culturing plates or house-made plates coated with hydrogels with a stiffness of 2 and 50 kPa.

In this chapter, my primary focus is to investigate substrate stiffness associated metabolic changes in BMDCs conditioned on different substrate tension. Using Seahorse glycolysis and mitochondria stress test kits, I demonstrate for the first time the substrate stiffness enhancement on DC function is associated with a metabolically active state. Using an antigen presentation assay, I saw that the substrate stiffness associated effects are lost when BMDCs are pre-treated with the glycolysis inhibitor 2-DG. In this experiment, T cell proliferation were reduced when co-culture with pre-treated BMDC. Furthermore, consistent with substrate stiffness affecting BMDC metabolism, I observed changes to the AKT signaling pathway that regulate metabolic reprogramming.

3.3 Results

3.3.1 Substrate stiffness modulates BMDC maturation

When DCs are activated, new proteins are synthesized and expressed on the cell surface to support their ability to activate T cells. Upon PRR activation, the surface expression of the co-stimulatory receptors CD80, CD86, and MHC II are normally upregulated. The expression of these surface markers was used to determine if substrate stiffness could modulate BMDC maturation. Our study was performed by LPS stimulation of BMDCs that were conditioned on hydrogel with stiffnesses of 2 and 50 kPa for 7 days. The expression of CD80, CD86, and MHC II was determined by mean fluorescence intensity (MFI) using flow cytometry (**Figure 3.1a-c**). We saw that LPS activated BMDCs grown on 2 kPa had a lower activation marker expression than BMDCs conditioned on 50 kPa. Substrate stiffness was associated with a significant 2-fold higher expression of CD80 and CD86 on 50 kPa than 2 kPa (**Figure 3.1a-b**). Consistent with

stiffness promoting DC maturation, there is a trending increase of MHC II expression (**Figure 3.1c)**.

Given that DCs traverse different microenvironments during recirculation and may encounter tissues with altered mechanical properties during inflammation and disease, we next asked whether the effects of substrate stiffness on DC maturation was reversible[129]. To address this, I cultured BMDCs on plastic substrate for 7 days then an additional 2 days on either plastic or 2 kPa hydrogel. BMDCs were purified by positive selection on the 9th day and an equal number of BMDCs were stimulated with LPS overnight. The reversibility of substrate stiffness on BMDC maturation was examined based on the MFI of CD40, CD80, CD86, and MHC II (**Figure 3.1d-g**) **–** CD40, which was not examined in the earlier experiments, is another co-stimulatory molecule expressed by DCs. A longer culturing duration after substrate transfer was not considered for the experiment given the short life span of DCs. The LPS stimulated BMDCs that were conditioned only on plastic had a significantly higher MFI for CD40, CD80, CD86, and MHC II compared to BMDCs that were initially conditioned on plastic then transferred to 2 kPa. Altogether, this data suggests substrate stiffness is a non-classical immunological parameter that can regulate DC maturation, with the effects being partially transient.

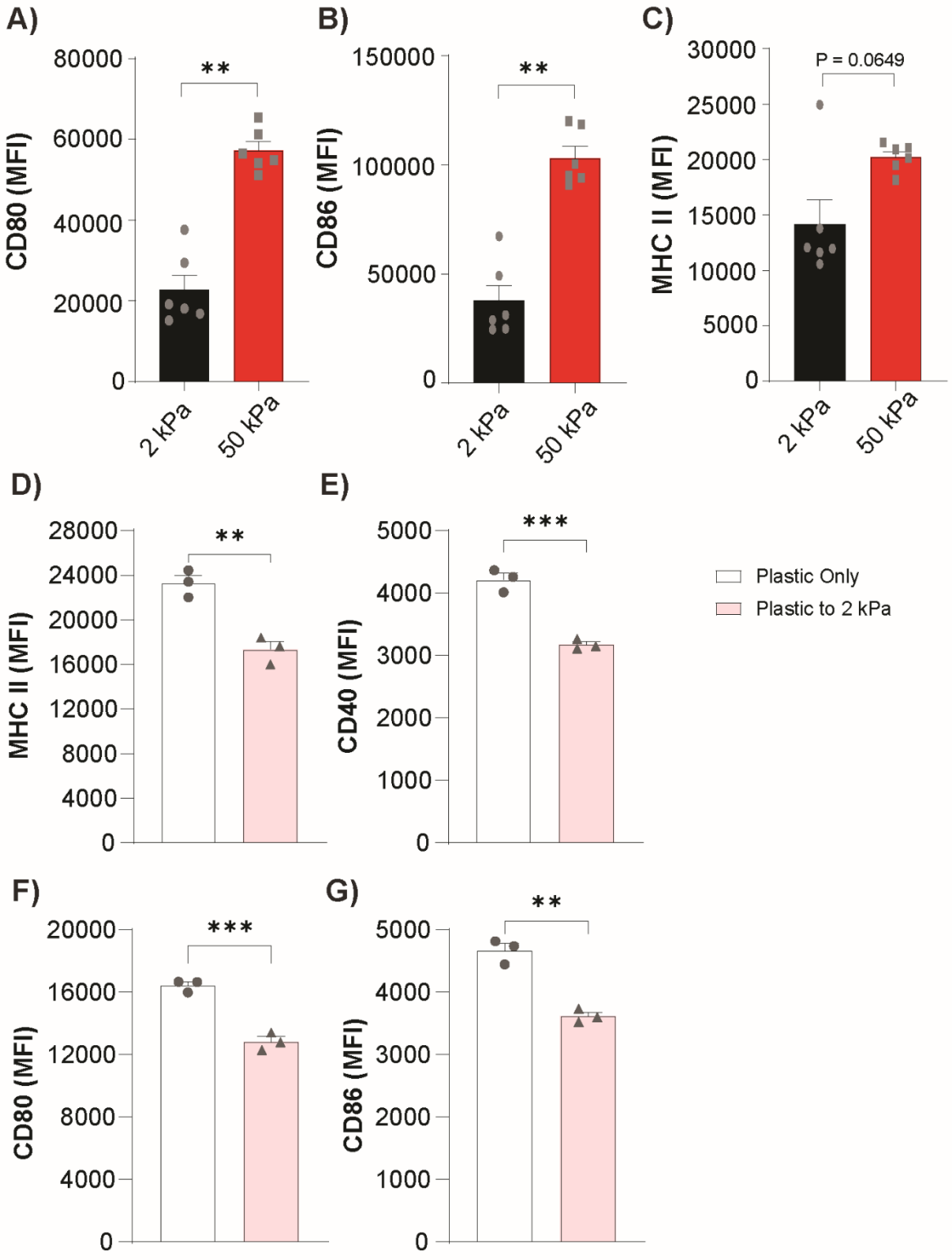
A)
CD80 (MFI)
80000
60000
40000
20000
0
**
2 kPa
50 kPa
B)
CD86 (MFI)
150000
100000
50000
0
**
2 kPa
50 kPa
C)
MHC II (MFI)
30000
25000
20000
15000
10000
5000
0
P = 0.0649
2 kPa
50 kPa
D)
MHC II (MFI)
28000
24000
20000
16000
12000
8000
4000
0
**
E)
CD40 (MFI)
5000
4000
3000
2000
1000
0
***
Plastic Only
Plastic to 2 kPa
F)
CD80 (MFI)
20000
16000
12000
8000
4000
0
***
G)
CD86 (MFI)
5000
4000
3000
2000
1000
0
**

Figure 3.1. Substrate stiffness modulates BMDC maturation in a reversible process. (A-C) The surface expression of CD80, CD86, and MHC II after LPS stimulation by BMDCS conditioned on 2 kPa and 50 kPa was evaluated by flow cytometry using antibodies specific for the molecules of interest (n=6). **(A)** Surface expression of CD80. **(B)** Surface expression of CD86. **(C)** Surface expression of MHC II. (D-E) Bar graphs showing the surface expression of MHC II, CD40, CD80, and CD86 after overnight LPS stimulation of purified BMDCs conditioned on plastic for 7 days that were then transferred to 2 kPa or remained on plastic substrates for an additional 2 days to examine the reversibility of tension **(D)** Surface expression of MHC II. **(E)** Surface expression of CD40. **(F)** Surface expression of CD80. **(G)** Surface expression of CD86. An equal number of purified BMDCs was stimulated to examine the reversibility of tension (100000 cells) (n=3). The mean fluorescence intensity (MFI) was examined in the live $CD11c^+$ $MHC\ II^+$ high population in Flowjo. Data are presented as mean +/- SEM. $^{**}p < 0.01$, $^{***}p < 0.001$ as determined by Mann-Whitney U test or unpaired T test.

3.3.2 Substrate stiffness modulates DC proinflammatory cytokine production

Since substrate stiffness could affect DC maturation, and stiffness is known to modulate the expression of some PRRs without immunogenic stimulation[106], this led us to consider if substrate stiffness could additionally impact DC effector function. One approach to address this question was by examining DC production of pro-inflammatory cytokines TNFα and IL-6 using Luminex assay and enzyme-linked immunosorbent assay (ELISA), and by intracellular flow cytometry after LPS stimulation **(Figure 3.2**). This was performed by stimulating BMDCs cultured on 2 and 50 kPa hydrogels with LPS for 24 hours. Using multiplex assay to study a diverse number of cytokines known to be produced by DCs, we found that 50 kPa conditioned BMDCs upregulated IL-1α, IL-1β, IL-6, IL-12, monocyte chemoattractant protein-1 (MCP-1), macrophage-inflammatory protein-2 (MIP-2), and TNF-α (**Figure 3.2a**). Congruent with this, a higher percentage of IL-6 and TNF-α positive BMDCs was observed by intracellular cytokine staining (**Figure 3.2b**). We next performed an ELISA to examine the effects of substrate stiffness alone on TNFα production. In the absence of LPS stimulation, we observed decreased TNF-α production by BMDCs cultured on pliant stiffness versus 50 kPa (**Figure 3.2c**). In tandem with LPS stimulation, BMDCs of 50 kPa significantly upregulated production of TNF-α compared to 2 kPa (**Figure 3.2d**). Taken together with our observations from the multiplex assay and intracellular cytokine staining experiment, it appears that substrate stiffness alone is a non-classical parameter regulating pro-inflammatory cytokine production but can additionally strengthen DC cytokine production in tandem with LPS as an immunological stimulus.

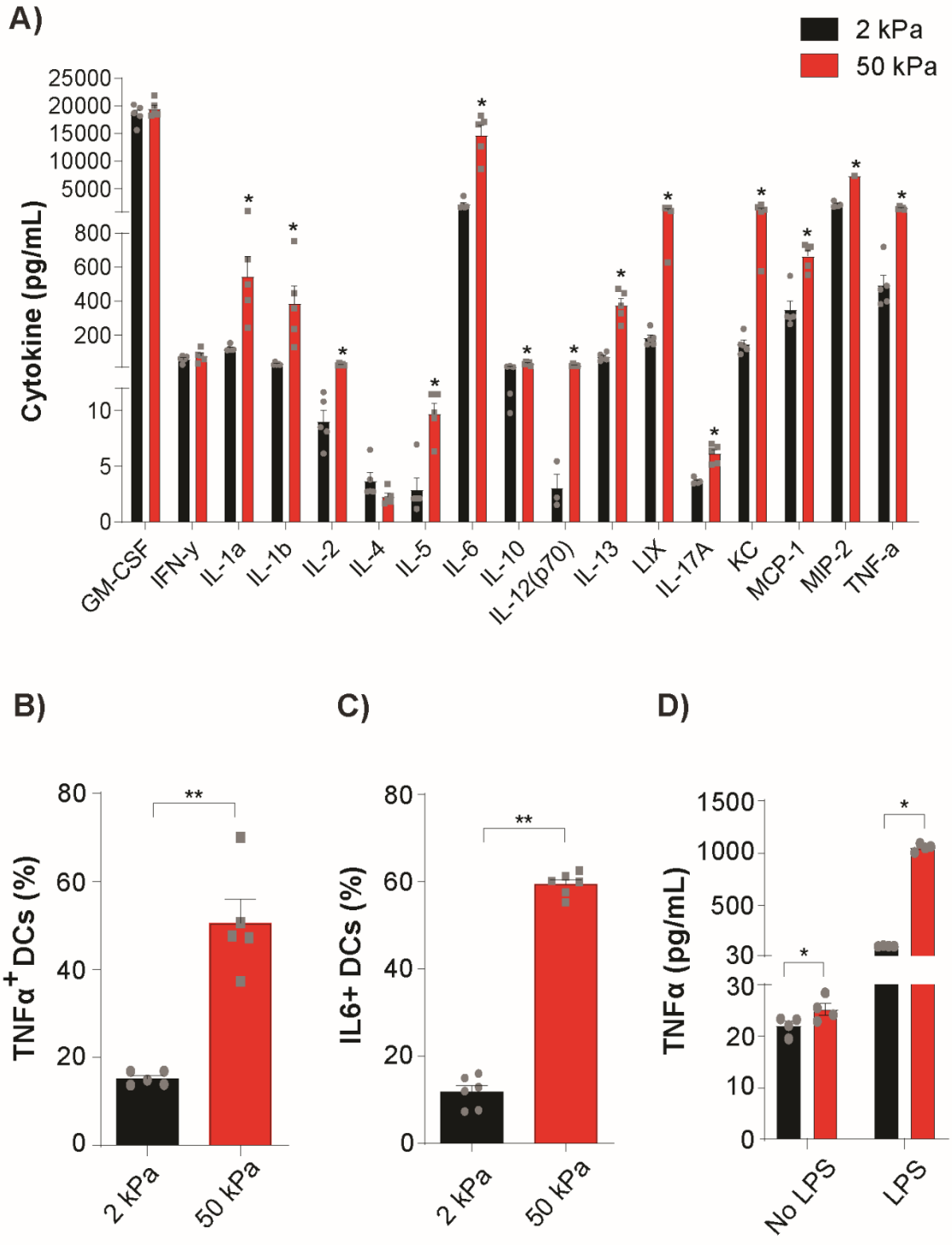
A)
2 kPa
50 kPa
Cytokine (pg/mL)
25000
20000
15000
10000
5000
800
600
400
200
10
5
0
GM-CSF
IFN-γ
IL-1a
IL-1b
IL-2
IL-4
IL-5
IL-6
IL-10
IL-12(p70)
IL-13
LIX
IL-17A
KC
MCP-1
MIP-2
TNF-a
B)
TNFα+ DCs (%)
80
60
40
20
0
**
2 kPa
50 kPa
C)
IL6+ DCs (%)
80
60
40
20
0
**
2 kPa
50 kPa
D)
TNFα (pg/mL)
1500
1000
500
30
30
20
10
0
*
*
No LPS
LPS

Figure 3.2. Substrate stiffness modulates DC proinflammatory cytokine production. Production of pro-inflammatory cytokines after LPS stimulation produced by BMDCs conditioned on 2 or 50 kPa substrates for 7 days was examined by Luminex assay and ELISA in addition to intracellular flow cytometry. **(A)** Concentration of various cytokines and chemokines produced by BMDCs after LPS stimulation quantified by multiplex (Luminex) assay (n=5). **(B)** Percentage of $TNF\alpha^+$ DCs (n=5). **(C)** Percentage of IL-6^+ DCs (n=6). **(D)** Concentration of TNFα produced with or without LPS stimulation quantified by ELISA (n=4). Data are presented as mean ± SEM. $*p < 0.05$, $**p < 0.01$ as determined by Mann-Whitney U test.

3.3.3 Substrate stiffness alters DCs' ability to present antigen and activate T cells

A major function of DCs is the activation of T cells by providing encountered cognate antigens and co-stimulatory signals for activation. In response to substrate stiffness, DCs upregulated expression of MHC II, CD80, and CD86, all of which are important cell surface proteins involved in T cell activation and survival (**Figure 3.1**). This unique phenotype acquired from conditioning on stiff substrate suggests that these DCs may be more proficient at activating T cells. To address this, an *in vitro* proliferation assay was performed to measure the ability of DCs to activate T cells by co-culturing with BMDCs (**Figure 3.3a**). The ability of DCs to present antigen was quantified by T cell proliferation. This assay was performed by first pulsing BMDCs with OVA peptide. The BMDCs used were previously cultured on 2 kPa, 50 kPa or plastic conditions as described. After pulsing, the BMDCs are co-cultured with carboxyfluorescein succinimidyl ester (CFSE) labelled $CD8^+$ OT-I T cells. These T cells have a transgenic TCR specific for the OVA peptide, allowing us to measure the ability of DCs to activate T cells using OVA peptide. CFSE covalently stain cells by crossing the plasma membrane, allowing T cell proliferation to be visualized by CFSE dilution after each cycle of division (**Figure 3.3b**). T cells were most proliferative when co-cultured with BMDCs that were previously conditioned on plastic. In contrast, 2 kPa conditioned BMDCs were poor activators of T cells (**Figure 3.3**). Altogether, DCs grown on higher stiffness were better antigen presenters than BMDCs of pliant stiffness, and this propensity for BMDCs of higher stiffness to better activate T cells is consistent with substrate stiffness-associated upregulation of co-stimulatory molecules seen prior. T cells proliferated more when cultured with BMDCs grown on stiffer substrates versus pliant stiffness.

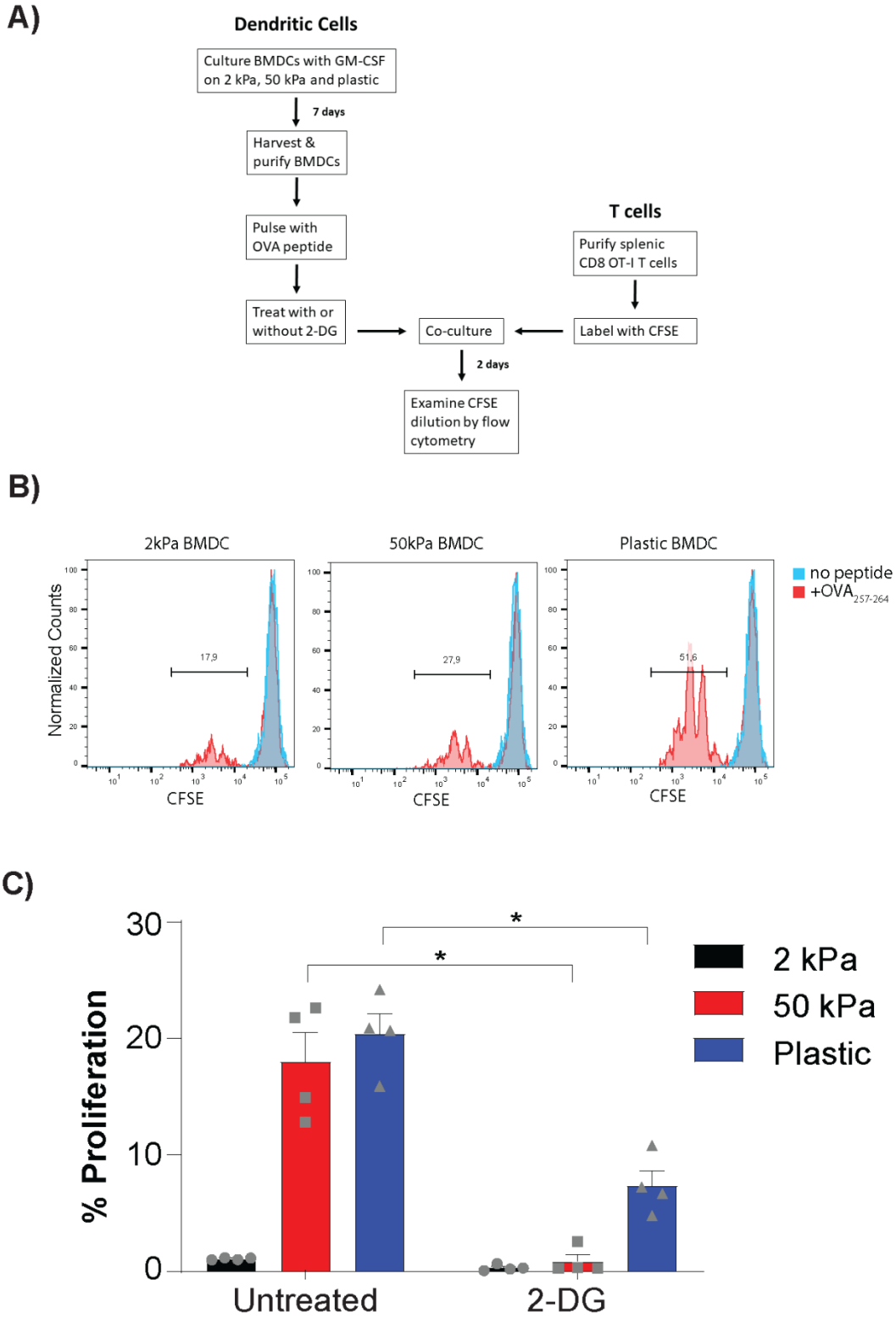
A)
Dendritic Cells
Culture BMDCs with GM-CSF on 2 kPa, 50 kPa and plastic
7 days
Harvest & purify BMDCs
Pulse with OVA peptide
Treat with or without 2-DG
T cells
Purify splenic CD8 OT-I T cells
Label with CFSE
Co-culture
2 days
Examine CFSE dilution by flow cytometry
B)
2kPa BMDC
50kPa BMDC
Plastic BMDC
Normalized Counts
CFSE
17,9
27,9
51,6
no peptide
+OVA257-264
C)
% Proliferation
30
20
10
0
Untreated
2-DG
2 kPa
50 kPa
Plastic
*
*

Figure 3.3. Substrate stiffness alters DCs' ability to present antigen and activate T cells. OVA pulsed BMDCs grown on 2 kPa, 50 kPa, or plastic substrates were co-cultured with CFSE stained transgenic OT-I T cells, with or without BMDCs being pre-treated with 2-DG. **(A)** Experimental outline of antigen presentation assay. **(B)** Representative FACs plot of OT-I T cell proliferation. Proliferation was determined based on CFSE dilution by flow cytometry. **(C)** (Left side) Percentage of OT-I proliferation without BMDC pre-treatment (n=4). (Right side) Percentage of OT-I proliferation with BMDCs that were pre-treated with an inhibitor of glycolysis, 2-DG (n=4). Living cells were distinguished by cell viability staining. Data are presented as mean ± SEM. $*p < 0.05$ as determined by Mann-Whitney U test.

3.3.4 Links between DC metabolism and function

Consistent with a higher expression of co-stimulatory receptors, BMDCs were also better APCs when conditioned on higher stiffness. However, the question as to what physiological processes connect the relationship between mechanosensing and function is unclear. Since DCs are known to have distinct metabolic patterns when activated, one element we sought to explore was the possibility that substrate stiffness could modulate DC metabolism and in turn affect downstream function. To explore this, I used the same *in vitro* antigen presentation assay as described, but prior to culturing BMDCs with OT-I T cells, I pre-treated the differentially conditioned BMDCs with 2-DG, an inhibitor of glycolysis. As a reminder, 2-DG is catalyzed by HK into a form of G6P that cannot undergo glycolysis (**Figure 1.3)**. The percentage of proliferating OT-I T cells substantially decreased compared to the untreated condition, suggesting the capacity for BMDCs to activate T cells had become impaired and is metabolically linked. Interestingly, despite inhibition of glycolysis, the plastic conditioned BMDCs was associated with the greatest degree of T cell proliferation, perhaps indicative of substrate stiffness also modulating metabolism **(Figure 3.3)**.

Using Seahorse assays that are designed to measure glycolysis and OXPHOS, I was able to investigate the possibility of substrate stiffness modulating metabolic reprogramming (**Figure 2.1)**. Changes to metabolism are detected by a Seahorse XFe24 metabolic flux analyzer. For these experiments BMDCs were grown on 2 kPa, 50 kPa, and plastic for 7 days, after which they are harvested and purified using a $CD11c^+$ isolation kit. To quantify glycolysis, the ECAR of media is measured as an indirect means to determine glycolytic flux. The drugs used to quantify glycolysis are designed to favor glycolysis by shutting down OXPHOS. Glycolysis, however, cannot run indefinitely as the electron transporter NAD required to fuel the pathway will deplete,

resulting in an accumulation of NADH. To recycle the necessary metabolic intermediates for prolonged glycolysis, lactic acid fermentation is concurrently upregulated to convert the end-product of glycolysis into lactic acid. NADH is oxidized from this conversion, thereby regenerating NAD (**Figure 1.1**). Overtime, the media will acidify from carbon dioxide and lactic acid production – thus glycolysis is indirectly quantified by measuring ECAR. The principle for measuring OXPHOS is similar. In this case, OCR is measured by stressing the mitochondria by disrupting the electron transport chain and proton gradient. As OXPHOS is an oxygen dependent process, cells will increase oxygen consumption in response to compensate for mitochondrial stress.

Using the glycolysis assay, I found that BMDCs acquired distinct glycolytic profiles contingent on the substrate stiffness they were conditioned on (**Figure 3.5**). Overall, BMDCs conditioned on stiffer substrates were more glycolytic. Strikingly at baseline, the plastic conditioned DCs have a higher ECAR than cells of 2 and 50 kPa due to non-glycolytic acidification (**Figure 3.5a**). Glycolysis is upregulated at around 20 minutes in all 3 conditions after glucose is added into the assay as fuel, with BMDCs conditioned on supraphysiological stiffness showing the most significant increase. This glycolytic flux is further increased at 50 minutes when OXPHOS is shutdown with oligomycin treatment. Between 50 minutes and 75 minutes into the assay, plastic conditioned BMDCs maintain the greatest degree of glycolytic flux, while 50 kPa conditioned BMDCs show a moderate increase in glycolysis relative to 2 kPa. At 75 minutes, ECAR declined upon treatment with 2-DG, confirming the ECAR increase seen throughout is due to glycolysis. Using the data generated from the assay, I calculated the glycolytic rate and glycolytic capacity (**Figure 3.5b-c**). The glycolytic rate considers acidification due to non-glycolytic processes, whereas the glycolytic capacity is a measurement

of how well cells switch to glycolysis at the maximum capacity based on peak ECAR rate following OXPHOS inhibition. For both measurements, I found that it was consistent with ECAR being higher on stiffer substrates after glucose addition. Specifically, BMDCs of 2 kPa had the lowest glycolytic rate and capacity while plastic is associated with the highest.

Next, I investigated whether OXPHOS in BMDCs also changed in response to substrate stiffness by measuring for oxygen consumption flux using the Seahorse mitochondria stress test kit. I found that cellular respiration indeed could be modulated by substrate stiffness (**Figure 3.5d-f**). At baseline, plastic conditioned BMDCs were the most respiratory. Oxygen consumption declined after the addition of oligomycin at 20 minutes, but plastic conditioned BMDCs retained the highest OCR. At 50 minutes FCCP, an uncoupling agent that disrupts mitochondrial membrane potential by collapsing the proton gradient is added. As a result of FCCP treatment, electron flow through the electron transport chain is now uninhibited. In a sense, FCCP artificially generates a demand for energy leading to maximal oxygen usage. Here, I saw a drastic increase in OCR by plastic conditioned BMDCs and a moderate increase in 50 kPa BMDC, while 2 kPa cells responded minimally. Concluding the assay is the addition of rotenone and antimycin-A (Rot/Anti-A) to effectively shut down OXPHOS, decreasing OCR for all 3 substrate conditions (**Figure 3.5d**). Rot/Anti-A treatment is a critical step that enables the calculation of nonmitochondrial respiration driven by respiratory processes outside of the mitochondria. When I examined basal respiration, a measure of oxygen consumed to meet energy demands at baseline, I found that plastic conditioned BMDCs had a significantly higher OCR than cells of 2 kPa and 50 kPa (**Figure 3.5e**). Furthermore, plastic conditioned BMDCs also had the highest maximal consumption rate after the addition of FCCP (**Figure 3.5f**).

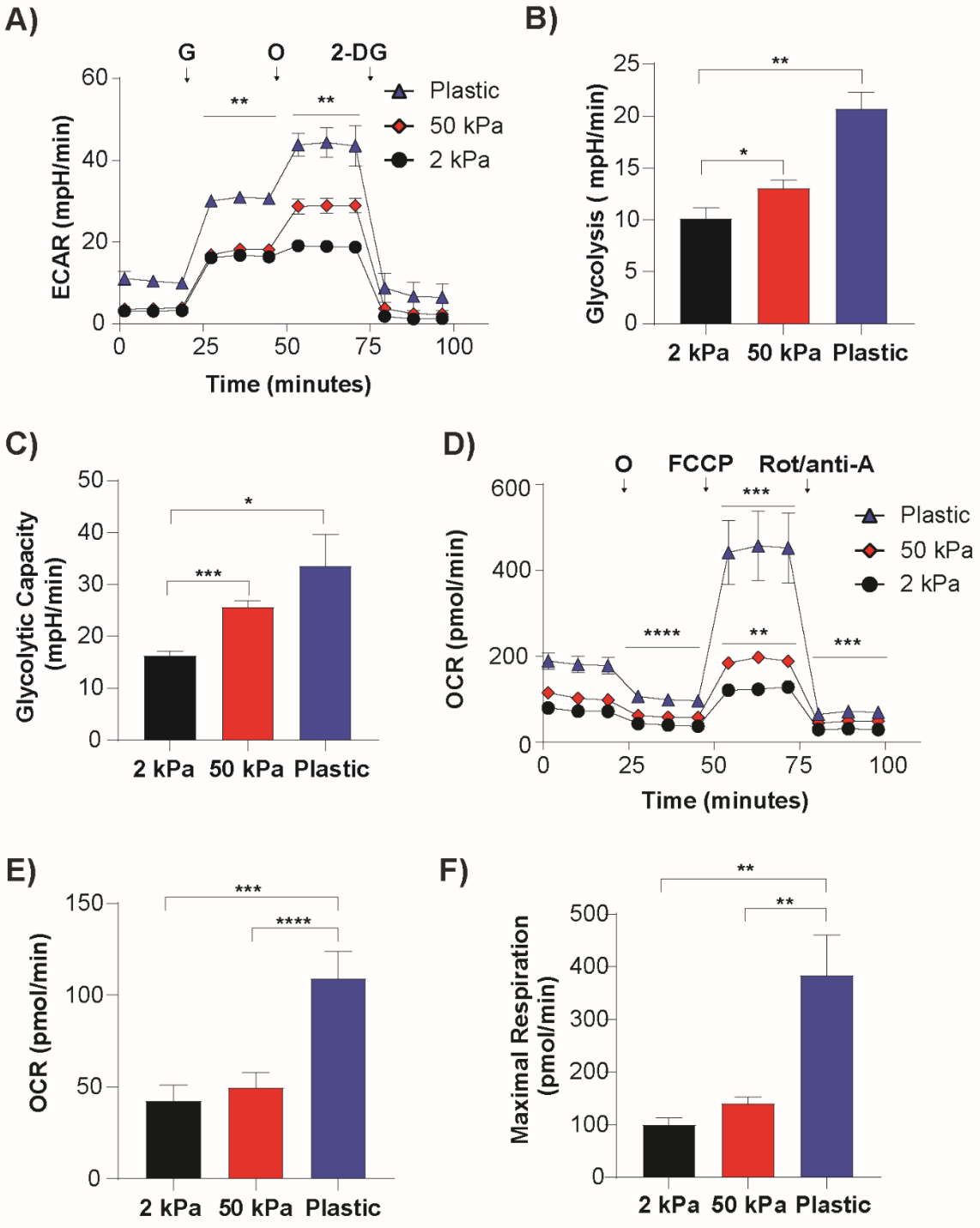
A)
G
O
2-DG
ECAR (mpH/min)
Time (minutes)
Plastic
50 kPa
2 kPa
B)
Glycolysis (mpH/min)
2 kPa
50 kPa
Plastic
C)
Glycolytic Capacity (mpH/min)
2 kPa
50 kPa
Plastic
D)
O
FCCP
Rot/anti-A
OCR (pmol/min)
Time (minutes)
Plastic
50 kPa
2 kPa
E)
OCR (pmol/min)
2 kPa
50 kPa
Plastic
F)
Maximal Respiration (pmol/min)
2 kPa
50 kPa
Plastic

Figure 3.5. Substrate stiffness modulates DC metabolism. Analysis of glycolytic (A-C) and OXPHOS (D-F) flux in purified BMDCs grown on 2 kPa, 50 kPa, or plastic for 7 days by Seahorse assays. Glycolysis is measured in units of extracellular acidification rate (ECAR) and OXPHOS by oxygen consumption rate (OCR). **(A)** Overall curve of ECAR in response to drug treatment. **(B)** Rate of glycolysis **(C)** The maximum capacity by which cells derive energy through glycolysis measured as glycolytic capacity. **(D)** Overall curve of OCR in response to drug treatment. **(E)** Rate of OCR. **(F)** The maximum rate of respiration in response to energy demands induced by FCCP. 24-well microplates were pre-treated with Corning™ Cell-Tak Cell and Tissue Adhesive to ensure a monolayer of cells were formed. BMDCs were plated at a density of 1.0×10^5 cells/mL. Formulae used to derive rate of glycolysis, glycolytic capacity, rate of oxygen consumption, and maximal respiration can be found in methods. Data are presented as mean ± SEM. $*p < 0.05$, $**p < 0.01$, $***p < 0.001$ as determined by Mann-Whitney U test. 2-DG, 2-deoxyglucose; G, glucose; FCCP, carbonyl cyanide-4 (trifluoromethoxy) phenylhydrazone; O, oligomycin; Rot/anti-A, rotenone/antimycin-A.

3.3.5 Tension induces phospho-AKT1 & phosphor-S6RP signaling in BMDCs

mTOR is a major pathway that regulates metabolism[130]. The activation of mTOR signaling is controlled by the conserved AKT signaling pathway (**Figure 1.6)**[130]. mTOR is indirectly activated by AKT following a cascade of downstream phosphorylation events[130]. The activity of AKT is regulated by phosphorylation at Ser473 in response to growth factors. As nutrient sensors, a central function of AKT/mTOR signaling is to coordinate anabolic and catabolic processes according to nutrient availability[130,131]. For innate immune cells, AKT/mTOR mediated metabolic reprogramming sustains homeostasis and function[131]. For example, AKT is a regulator of hexokinase, and the gene expression of hexokinase is regulated by mTOR[130].

So far, we have observed supraphysiological stiffness led to DCs acquiring a metabolic phenotype that is reminiscent of immunologically active DCs. To better understand the mechanism linking tension to an active metabolic state, I sought to determine if AKT signaling is involved. The activation of AKT is particularly enticing to study in the context of substrate stiffness since a recent study by Cho et al. reported a core component of Hippo signaling, MST-1 is a potential upstream regulator of AKT activity in DCs[122]. In the study, Cho et al. demonstrated MST1 deficiency led to the hyperactivation of moDCs via AKT signaling. Furthermore, a separate study reported Mst1 was indispensable for $CD8^+$ T cells metabolic reprogramming and function[123]. However, the focus of both studies was not on mechanosensing, but their metabolic discoveries involving Mst1 is relevant here because Mst-1 in non-immune cells is known to be involved in mechanosensing as a key member of the Hippo signaling pathway[108,112].

Given that activated AKT is phosphorylated, a promising starting point to study the mechano-metabolic relationship is to investigate the phosphorylation state of AKT from DCs that have been cultured on different stiffness conditions. To achieve this, I used Western blotting.

This was performed by blotting for phospho-proteins in lysate made from purified BMDCs cultured as described. By doing so, I found that increasing substrate stiffness correlated with an increasing phosphorylation of AKT at Ser473 (**Figure 3.6a-b**). AKT phosphorylation was the lowest in the 2 kPa condition but the highest on supraphysiological tension. To further investigate the involvement of AKT/mTOR signaling, I also probed for the phosphorylation of S6RP (**Figure 3.6c-d)**. S6RP is indirectly activated by AKT through the activation of mTOR (**Figure 1.2)**. Congruent with increasing AKT phosphorylation, I saw more S6RP phosphorylation as substrate stiffness increased. Curiously, the expression of total S6RP in BMDCs also increased in response to substrate stiffness. Altogether my Western blot results suggest substrate tension associated metabolic reprogramming of DCs could potentially involve AKT/mTOR/S6RP signaling and altered protein expression of S6RP.

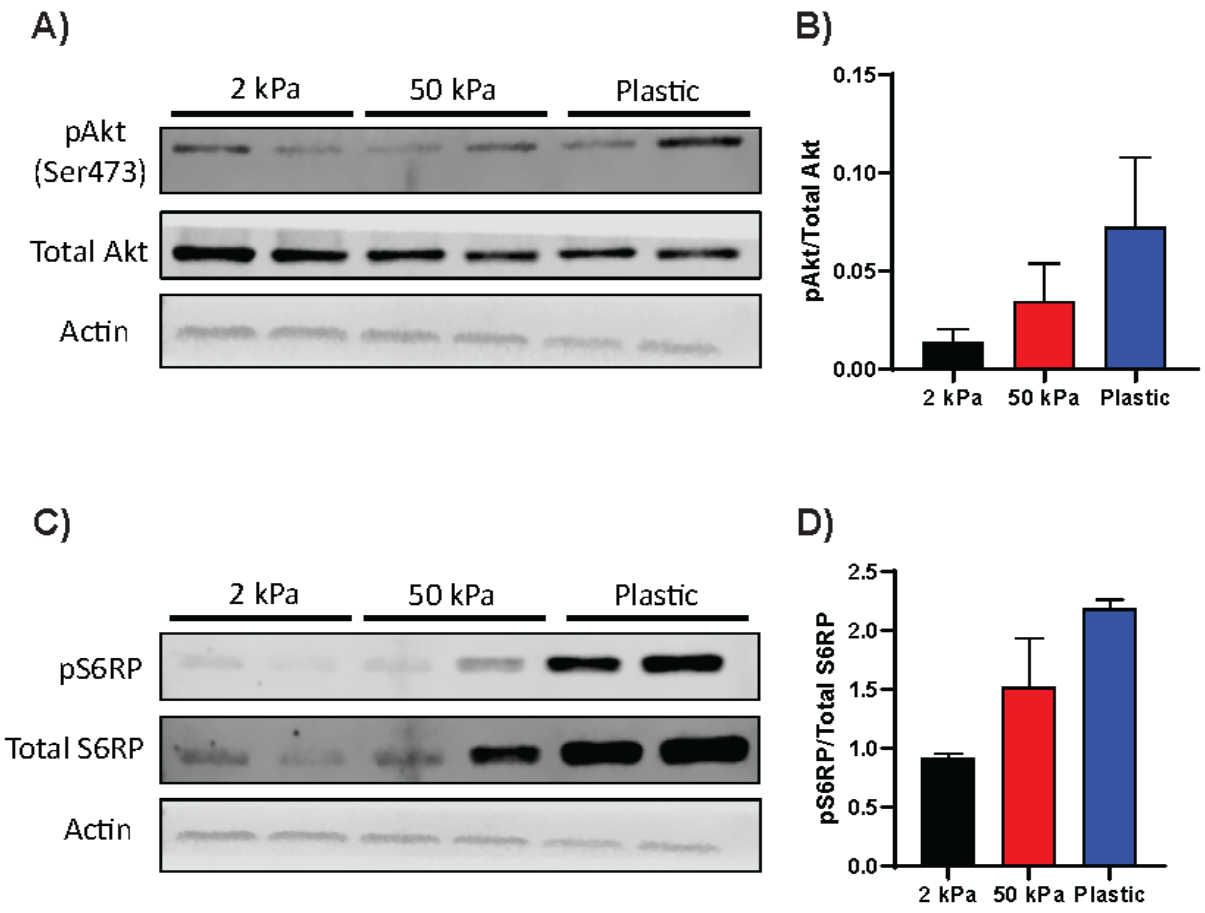

Figure 3.6. Substrate tension induces the phosphorylation of AKT1 and S6RP. Western blotting for phosphorylated AKT1 (Ser473) and S6RP from whole cell lysates made from BMDCs conditioned on 2 kPa, 50 kPa, and plastic. **(A)** Western blot of phospho-AKT1 (Ser473) (n=2). **(B)** Quantified phospho-AKT1 (Ser473) bands from blot normalized to total AKT. **(C)** Western blot of phospho-S6RP. **(D)** Quantified phospho-S6RP bands from blot normalized to total S6RP (n=2). 20 ug of proteins were loaded per column for Western blotting. The quantification of protein bands was done using the Li-Cor Image Studio Acquisition Software. Statistical analysis could not be conducted due to a n value of 2.

3.3.6 TAZ and YAP translocate into the nucleus in BMDCs under mechanical stress

To identify potential mechanisms mediating DC mechanosensing, RNA sequencing was performed on BMDCs cultured on 2 and 50 kPa hydrogels **(Figure 4.2a)**. At the transcription level, the gene encoding for TAZ, *Wwrt1*, was one of the most significantly upregulated genes in BMDCs conditioned on 50 kPa gel. To expand on this, the expression of *Wwrt1* in splenic DCs on 2 kPa, 50 kPa, and plastic was examined with real-time PCR (**Figure 4.2b)**. Consistent with the RNA sequencing results, *Wwrt1* expression was positively affected by stiffness. Relative to 2 kPa, the expression of *Wwrt1* increased in BMDCs grown on stiffer substrates. Furthermore, our collaborators used integrated pathway analysis bioinformatics to examine potential genes controlled by TAZ. From this, the upregulated expression of TAZ is predicted to affect metabolic processes. Some notable metabolic genes regulated by TAZ included *Myc, Slc2a1,* and *Hk2*, which encodes for MYC, glucose transporter 1, and hexokinase 2, respectively (**Figure 4.2c)**. This upregulation of TAZ could possibly explain the distinct metabolic reprogramming we saw earlier in the Seahorse **(Figure 3.5)**.

The activity of YAP/TAZ are regulated by sequestration in the cytoplasm and initiate transcriptional programs via TEAD binding within the nucleus (**Figure 1.6)**. When cells are exposed to soft substrates, YAP/TAZ are cytoplasmic, but they translocate into the nucleus when under mechanical stress. To investigate YAP/TAZ activity at the protein level, ImageStream flow cytometry was performed to probe for the translocation of YAP/TAZ in BMDCs under 2 versus 50 kPa conditions (**Figure 4.3a)**. Comparison of protein localization of YAP/TAZ vs DAPI-stained nuclei shows a trend to increase in YAP and TAZ nuclear localization (**Figure 4.3b)**. Altogether, the results hint at the possibility that YAP/TAZ could be mediating the conversion of external mechanical cues to initiate downstream metabolic reprogramming.

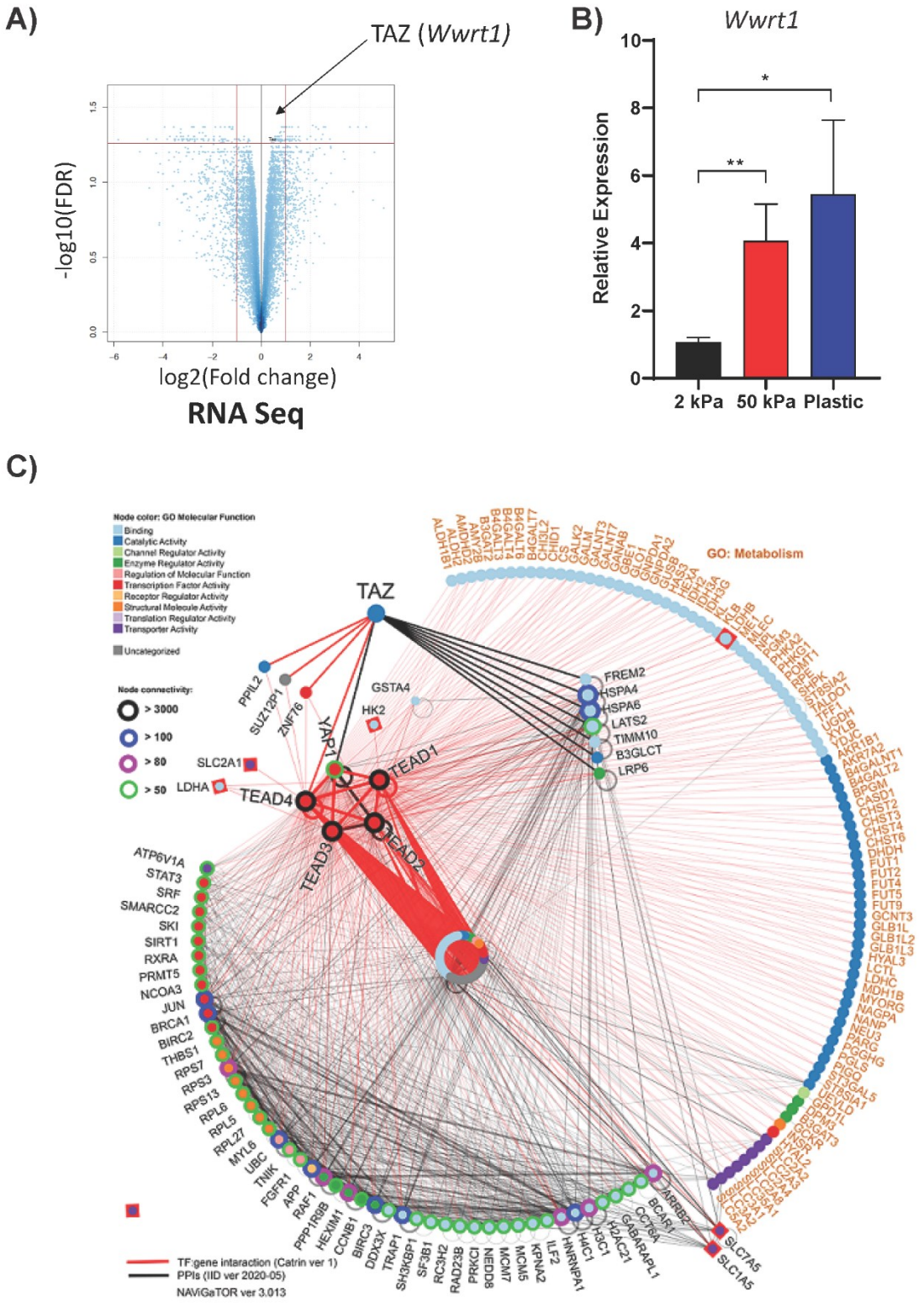
A)
TAZ (Wwrt1)
-log10(FDR)
log2(Fold change)
RNA Seq
B)
Wwrt1
Relative Expression
2 kPa
50 kPa
Plastic
C)
Node color: GO Molecular Function
Binding
Catalytic Activity
Channel Regulator Activity
Enzyme Regulator Activity
Regulation of Molecular Function
Transcription Factor Activity
Receptor Regulator Activity
Structural Molecule Activity
Translation Regulator Activity
Transporter Activity
Uncategorized
Node connectivity:
> 3000
> 100
> 80
> 50
GO: Metabolism
TAZ
YAP1
TEAD1
TEAD2
TEAD3
TEAD4
PPIL2
SUZ12P1
ZNF76
GSTA4
HK2
SLC2A1
LDHA
FREM2
HSPA4
HSPA6
LATS2
TIMM10
B3GLCT
LRP6
TF:gene interaction (Catrin ver 1)
PPIs (IID ver 2020-05)
NAViGaTOR ver 3.013

Figure 3.7. *Wwrt1* expression in BMDCs conditioned on varying substrate stiffness.

Expression of *Wwrt1*, encoding for TAZ is higher on stiffer substrates, as determined by RNA sequencing and real-time PCR. **(A)** Volcano plot showing TAZ is upregulated in BMDCs conditioned on 50 kPa (n=3). **(B)** Relative mRNA expression of *Wwrt1* in splenic DCs grown on hydrogels with stiffness of 2 and 50 kPa versus plastic (n=6-7). **(C)** TAZ interactome and transcription family network. Physical protein interactions from IID (black edges) and transcription regulatory network from Catrin (red edges) were combined in NAViGaTOR. Shown are direct TAZ interactors, highly connected nodes, and metabolism-related target genes, as per the legend. Details for transcriptomic analyses can be found at Chakraborty et al[107]. Data in (B) are presented as mean ± SEM. $*p < 0.05$, $**p < 0.01$ as determined by Mann-Whitney U test. Data generated in collaboration with Igor Jurisica (University Health Network).

A)

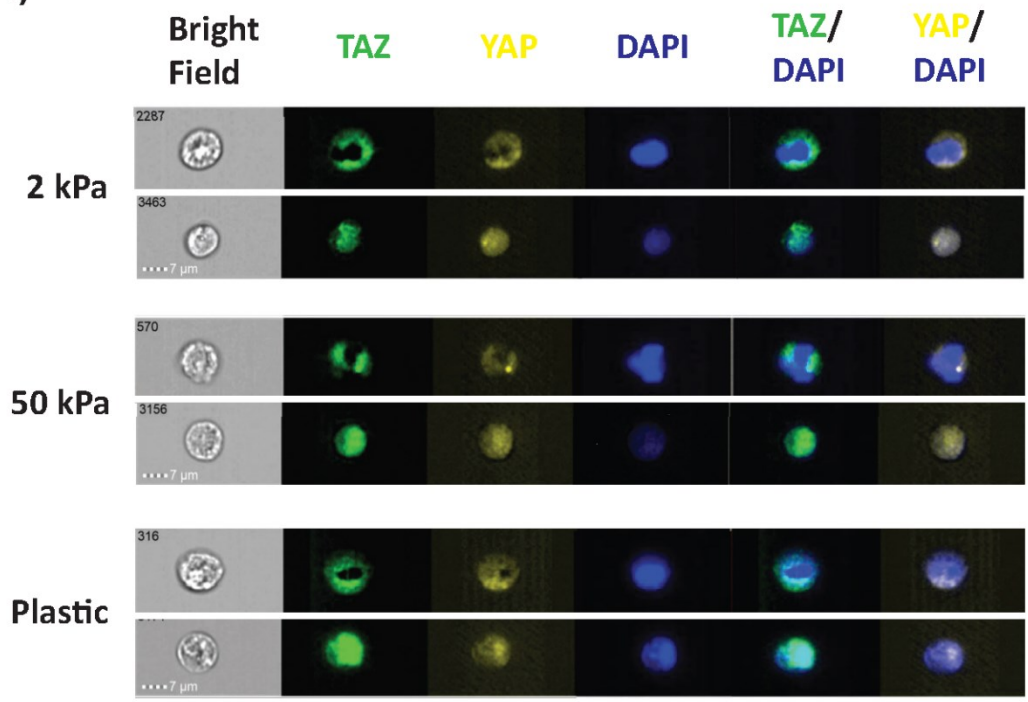
Bright Field
TAZ
YAP
DAPI
TAZ/ DAPI
YAP/ DAPI
2 kPa
50 kPa
Plastic

B)

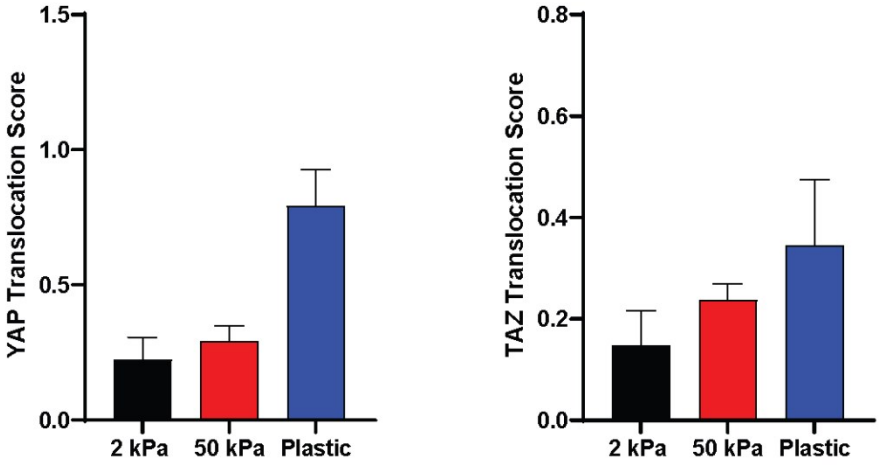
YAP Translocation Score
1.5
1.0
0.5
0.0
2 kPa
50 kPa
Plastic
TAZ Translocation Score
0.8
0.6
0.4
0.2
0.0
2 kPa
50 kPa
Plastic

Figure 3.8. YAP/TAZ in BMDCs translocate into the nucleus under mechanical stress. The localization of YAP/TAZ in purified BMDCs conditioned on 2 kPa, 50 kPa, and plastic were examined by ImageStream flow cytometry. **(A)** Representative images of anti-TAZ and anti-YAP immunofluorescent staining for each substrate condition. Green and yellow represent TAZ and YAP staining, respectively. The nuclei are stained blue with DAPI. **(B)** Quantified translocation of YAP (left) and TAZ (right) represented as translocation scores. The translocation scores were calculated via the IDEAS Workstation software nuclear localization algorithm, which compares staining signal distribution of DAPI (nuclear) vs those of YAP (n=5-6 experiments) or TAZ (n=6-7 experiments). Data are presented as mean +/- SEM.

3.4 Discussion

The effects of substrate stiffness on DC function have previously been examined by Mennens et al. using human moDCs derived from peripheral blood mononuclear cells. Substrate stiffness of 2 kPa, 12 kPa, and 50 kPa were used in their study. Among the three examined substrate stiffnesses, Mennens et al. reported human moDCs cultured on the physiologically relevant stiffness of 2 kPa acquired an immunologically active phenotype - displaying higher phagocytotic activity and expression of C-type lectin PRRs, when conditioned on the physiologically relevant stiffness of 2 kPa[106]. Overall, Mennens et al. saw the substrate stiffness of 12 kPa exerted weaker effects on DC maturation and function than 2 kPa, and the effects of 50 kPa was often ambiguous. Interestingly in their study, substrate stiffness had no effect on the expression of CD86 and MHC II on mature moDCs[106]. In contrast, we saw that 50 kPa conditioned BMDCs significantly upregulated the expression of co-stimulatory molecules than BMDCs of 2 kPa (**Figure 3.1**). We also found that substrate tension could modulate DC cytokine production, an aspect not examined by Mennens et al. (**Figure 3.2**).

When comparing 2 kPa versus 50 kPa in our study, the surface expression of co-stimulatory molecules CD80 and CD86 was significantly upregulated, and although insignificant, MHC II expression had a trending increase. Based on this active phenotype I hypothesized that BMDCs conditioned on high stiffness could potentially be more proficient activators of T cells. By using transgenic OT-I T cells, I was able to verify this hypothesis. Consistent with my hypothesis, OT-I T cells were more proliferative when activated by BMDCs from plastic than 2 kPa and 50 kPa, suggesting BMDCs conditioned on higher stiffness are better APCs (**Figure 3.3)**. Interestingly, this observation contrasts with Mennens et al. whom saw no difference in T cell proliferation when performing a mixed lymphocyte reaction by co-culturing

moDCs conditioned on 2 kPa, 12 kPa, or 50 kPa together with allogeneic peripheral blood lymphocytes[106]. This is perhaps due to intrinsic differences in the internalization of peptides. We previously showed that BMDCs grown at higher stiffness showed increased capacity for phagocytosis[107].

As DCs traverse microenvironments with different stiffnesses throughout their life cycle, an immediate question building from the work of my predecessors is whether the modulatory effect of substrate stiffness is reversible. By transferring BMDCs from supraphysiological stiffness onto pliant stiffness that is more akin to physiological tissues, I demonstrated that the influence of substrate tension is reversible by examining the surface expression of multiple co-stimulatory molecules in addition to MHC II using flow cytometry (**Figure 3.1d-g**). From my experiment, it seems BMDCs maintain a degree of plasticity after 7 days of development on a specific substrate tension. I did not look at conditioning DCs beyond the initial 7 days of culturing or for more than 2 days after transfer since DCs are remarkably short-lived and this would likely yield an abundance of dead cells[84]. An interesting future experiment would be to perform a proliferation assay to see if the ability to stimulate T cells is also correspondingly lower after transfer of BMDCs from a high to low stiffness.

A long-standing question of my work is to uncover and better understand the mechanism underpinning the connection between mechanical signaling and cellular function. As others have discovered, the metabolic profile of resting and activated DCs are unique[81,82,84]. Given that BMDCs grown on higher stiffness expressed higher levels of activation markers, I hypothesized substrate stiffness could modulate DC metabolism. Indeed, by using Seahorse assays, I found that higher stiffness conferred a more metabolically active state characterized by increased glycolysis and OXPHOS (**Figure 3.5)**. This coincided with the trending increase of AKT1 and

S6RP phosphorylation on higher stiffness (**Figure 3.6**). Importantly, this metabolic reprogramming was without PRR stimulation. Curiously, this phenotype is reminiscent of active immunogenic DCs. Normally, PRR-activated DCs undergo rapid upregulation of OXPHOS during early DC activation to support initial ATP demands. OXPHOS however cannot run indefinitely and is fated to decline as the mitochondria becomes increasingly damaged by nitric oxide production in response to activation[132]. As such, enhanced glycolysis is observed concurrently with the upregulation of OXPHOS to maintain cell survival by producing ATP as OXPHOS wanes in active DCs.

On the other hand, glycolysis is also upregulated independently of mitochondrial damage, in a process that is critical for maintaining function via conversion of pyruvate into citrate[84]. When DCs are activated by TLR ligation, glycolytic flux is achieved by the downstream activation of AKT1 which in turn promote the translocation of HK to the outer mitochondrial membrane. The translocation of HK allows direct access to newly generated ATP, which is required for the catalysis of glucose into G6P. Citrate is a critical metabolite that is not only used in the production of ATP, but also used to synthesize fatty acid to expand membrane organelles required to facilitate the synthesis and transport of effector proteins, including CD40, CD80, CD86, MHC II, and IL-6 and TNFα[84]. The observed enhanced glycolytic and OXPHOS flux (**Figure 3.5)** in BMDCs of higher stiffness is consistent with our early demonstration of heightened pro-inflammatory cytokine production (**Figure 3.2**) and co-stimulatory surface molecule expression (**Figure 3.1**) in response to tension. The capacity to activate T cells was impaired upon glycolysis inhibition with 2-DG but was not completely abrogated on higher stiffness (**Figure 3.3**). In healthy individuals, physiological stiffness beyond pliant stiffness is scarce, most commonly found in fibrotic diseases and cancer[2,93]. Therefore, it is plausible

substrate stiffness is acting as an activation stimulus or a bolstering signal to inform DCs of danger, whereby DC stimulatory abilities are altered in response to metabolic reprogramming. Credence to this notion is reinforced by my demonstration of the effects of substrate stiffness being partially reversible, a function that allow for regulation of DC activation (**Figure 3.1d-g)**.

As mentioned before, fatty acid synthesis is fueled by the influx of citrate produced via pyruvate. Since I did not explore if fatty acid metabolism could be modulated by substrate tension, it may be prudent to examine citrate flux due to the importance of the metabolite in maintaining DC function and survival. Methods to examine this could include colorimetric assays to quantify citrate synthase activity, or alternatively examine the expression of fatty acid metabolism enzymes, such as ATP citrate synthase and fatty acid transporters by real-time PCR.

In summary, I observed substrate stiffness could modulate DC biology. Specifically, under 2 versus 50 kPa conditions in the presence of LPS, BMDCs that were conditioned on 50 kPa were more pro-inflammatory and expressed higher activation markers. BMDCs grown on 50 kPa had a significantly higher production of IL-6 and TNFα and expression of CD80/86, and a trending increase in MHC II expression. The effects of substrate stiffness are a reversible process that may be linked with metabolic reprogramming. My examination of BMDC metabolism demonstrated BMDCs grown on higher stiffness were more glycolytic and respiratory, suggesting BMDCs are more metabolically active when conditioned on stiff substrates. To further understand the mechano-metabolism relationship, I also investigated the involvement AKT/mTOR signaling, a conserved pathway regulating metabolism. Here, consistent with increased metabolism, I saw an increasing trend of AKT and S6RP activation in BMDCs as substrate stiffness increased. Unexpectedly, substrate stiffness also induced a greater expression of total S6RP. Given that our TAZ interactome and transcriptome analysis revealed the

association of TAZ with several metabolic genes, and a key function of YAP/TAZ is the regulation of cellular metabolism, this observation is potentially related to YAP/TAZ signaling that requires further investigation (**Figure 3.7)**. By ImageStream flow cytometry, increased nuclear translocation of YAP/TAZ was observed in BMDCs under mechanical stress. Taken together, the modulation of BMDC metabolism by substrate stiffness is hinted to be mediated by YAP/TAZ signaling.

Chapter 4: TAZ/YAP signaling in DCs in steady state and during influenza infection

4.1 Contributions

RNA sequencing and bioinformatic data identifying the upregulation of TAZ expression in BMDCs cultured on stiff substrates were performed by our collaborators. The characterization of basal cDC numbers in our YAP/TAZ KO animals are work of my own. Antigen presentation assays were performed to better understand the role of YAP/TAZ deficiency on DC mechanosensing. Another undergraduate student, Camille Huang aided with assay preparation. To translate our *in vitro* findings to a physiologically relevant context, an influenza mouse model was used. The PR8 virus was generously provided by Dr. Kevin Kane, while the intranasal immunization protocol was demonstrated by Gang Zhou of the Kane lab – whom without their support, this influenza model would not be possible. The processing of influenza infected mouse tissues was expedited with the help from the members of the Tsai-Clemente lab.

4.2 Introduction

Notable consequences of immune cell mechanotransduction include regulation of lymphocyte extravasation, macrophage polarization, and T cell activation[6,121,133]. Generally, mechanical forces are sensed via cell adhesion molecules, such as integrins, selectins, and cadherins[133]. In addition, immunoreceptors are shown to exhibit mechanosensory properties. The TCR for instance, is an anisotropic mechanosensor activated by direction-specific physical forces[104]. Two landmark studies by Piccolo et al. and Sasaki et al. discovered a novel mechanism non-immune cells employ to modulate transcriptional programs in response to external mechanical cues[134,135]. These studies demonstrated YAP and TAZ, two downstream effectors of

Hippo signaling, relay cytoskeletal tension to the nuclei. YAP/TAZ shares 46% amino acid identity, and most data suggest YAP/TAZ as functionally interchangeable[108]. It is important to mention that while YAP/TAZ is best characterized in the context of Hippo signaling, other signaling pathways can also regulate YAP/TAZ activity. Such pathways include Rho-GTPases and Wnt signaling[108]. Regardless of upstream signal transduction pathways, YAP/TAZ activity are strictly inhibited by phosphorylation.

Expression of YAP/TAZ and components of the core Hippo signaling pathway has been identified in B and T cells, macrophages, and DC with regulatory roles. In macrophages, YAP mediated mechanotransduction is critical for directing inflammation *in vitro*[8]. Consistent with this, YAP/TAZ double knockdown mice have improved cardiac healing post myocardial infarction associated with increased reparative macrophage polarization[121]. For T cells, YAP activity and localization into the nucleus is upregulated after activation, but the consequences are inhibitory[6,124]. On high stiffness conditions, YAP-mediated inhibition of transcription factors impairs T cell proliferation. In addition, YAP activity suppresses T cell metabolism and function[6,120,124]. The activation and function of T cells are improved by T-cell specific knockout of YAP[6,120]. While much is known about the mechanisms regulating DC response to biochemical cues, such as nutrients and cytokines, the signaling pathways by which DCs transduce mechanical cues from the environment is unknown.

To date, one publication has briefly examined the role of YAP/TAZ via CD11c-Cre mice on DC homeostasis[123]. The relevant studies instead focus on MST1/2, the upstream regulators of YAP/TAZ phosphorylation in Hippo signaling[122,123,136]. Early publications suggest MST1 regulates cell adhesion and motility. One group reports the migration of skin DCs to draining lymph node (DLN) is impaired in MST1 deficient mice[136]. This effect was associated with

reduced DC adherence to the ECM[136]. MST1 deficiency in DCs can also impair CCR7 signaling, contributing to impaired LN trafficking and leading to aberrant cytoskeletal architecture *in vitro*[137]. More recently, MST1/2 signaling has been identified to couple metabolic state and function of DCs. MST1/2 is an indispensable regulator of mouse $CD8^+$ cDC1s function by integrating oxidative metabolism[123]. On the contrary, another group found MST1 deficiency promoted hyperactivation associated with increased AKT phosphorylation in monocyte derived BMDCs, suggestive of an active metabolic state[122]. While these studies emphasize a regulatory role of MST1/2 in DCs, the matter of whether YAP/TAZ signaling is important for DC homeostasis and function is unclear. Furthermore, the main scope of the studies presented do not factor in the influence of mechanical stimuli.

In this chapter, I aimed to investigate the role of YAP/TAZ on DC biology via CD11c-Cre driven YAP/TAZ single or double gene deleted mice (**Figure 4.1)**. In this model, the genes encoding YAP and TAZ are flanked by loxP sites that are recognized by the protein Cre recombinase. LoxP flanked genes are excised upon Cre recognition. The expression of Cre protein is regulated by cell-type specific promoter to ensure cell-type specific excision, in this case CD11c. To study the role of YAP/TAZ in DCs, I tested whether CD11c-Cre YAP/TAZ mice had impaired cDC development. I saw no difference in the numbers of cDC in the lungs and spleen of CD11c-Cre YAP/TAZ mice. To translate our findings to an animal model, we investigated the anti-viral response of CD11c-Cre^+ $YAP^{fl/fl}$ and CD11c-Cre^+ $YAP^{fl/fl}$ $TAZ^{fl/fl}$ mice to intranasal PR8 influenza A virus (PR8 IAV) infection on day 9. For these experiments, I examined T cell production of potent anti-viral cytokines, TNFα and IFNγ. In addition, the populations of cDCs and the generation of viral-specific T cells in secondary lymphoid organs

were assessed. I saw mostly no difference in the anti-viral response between wildtype versus CD11c-Cre^{+} YAP$^{fl/fl}$ and CD11c-Cre^{+} YAP$^{fl/fl}$ TAZ$^{fl/fl}$ mice in this model.

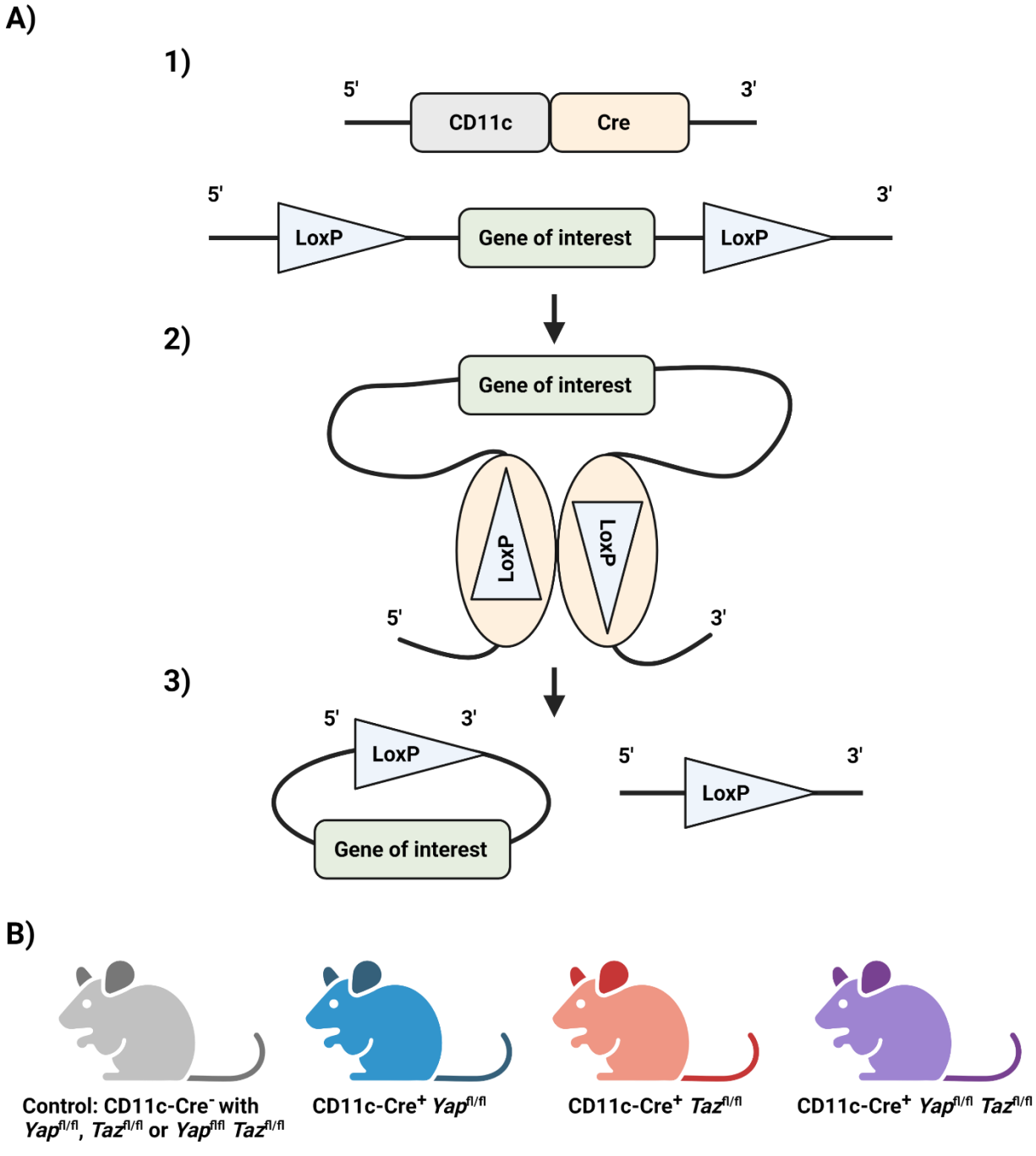
A)
1)
5'
CD11c
Cre
3'
5'
LoxP
Gene of interest
LoxP
3'
2)
Gene of interest
LoxP
LoxP
5'
3'
3)
5'
3'
LoxP
Gene of interest
5'
3'
LoxP
B)
Control: CD11c-Cre- with Yapfl/fl, Tazfl/fl or Yapfl/fl Tazfl/fl
CD11c-Cre+ Yapfl/fl
CD11c-Cre+ Tazfl/fl
CD11c-Cre+ Yapfl/fl Tazfl/fl

Figure 4.1. Cre-lox recombination and the generated mice used for experiments. The Cre-lox system is used to generate DC specific knockout of YAP and TAZ. (A) 1. The expression of the Cre recombinase protein is under control by the CD11c promoter. CD11c encodes an integrin expressed by DCs. The gene of interest is flanked by loxP sites that are recognized by Cre recombinase. 2. Recombination occurs when Cre recombinase binds to the loxP sites. 3. The outcome is a closed loop of excised genetic information containing the gene of interest that is eventually degraded. **(B)** Using the Cre-lox system, three strains of YAP/TAZ KO mice are generated. They are the single knockouts CD11c Cre^{+} $TAZ^{fl/fl}$, and CD11c Cre^{+} $YAP^{fl/fl}$, and the double knockout CD11c Cre^{+} $YAP^{fl/fl}$ $TAZ^{fl/fl}$ mice. Drawn on BioRender.com

4.3 Results

4.3.1 DC specific YAP and TAZ deletion does not affect cDC numbers at steady state

We previously saw TAZ was upregulated in BMDCs when under mechanical stress (**Figure 3.6)**. Increased nuclear translocation of YAP/TAZ was also observed when BMDCs were conditioned on higher stiffness (**Figure 3.7)**. These observations collectively hint that YAP/TAZ signaling may have a role in regulating DC biology as mediators of mechanosensing. However, our current understanding on the role of YAP and TAZ on DCs homeostasis and function is still largely unknown as this is an understudied field. To investigate the significance of YAP/TAZ on DC biology, I tested whether the loss of YAP/TAZ in DCs would impair cDC development as this is a cell type that would be affected in our YAP/TAZ KO mice. I examined the basal numbers of cDCs in the spleen and lungs of 6- to 8-week-old wildtype (WT) and single KO CD11c-Cre^{+} TAZ$^{fl/fl}$ and CD11c-Cre^{+} YAP$^{fl/fl}$ mice, and the double knockout CD11c-Cre^{+} TAZ$^{fl/fl}$ YAP$^{fl/fl}$ mice. Pre-cDCs during development egress from the BM to reach peripheral tissues such as the spleen and lungs to terminally differentiate into cDCs[41]. cDC1s are distinguished by the expression of CD11c^{hi} MHC II^{hi} CD103^{+} in the spleen and CD8^{+} in the lung. cDC2s are identified as CD11c^{hi} MHC II^{hi} CD11b^{+} cells in both the spleen and lungs.

Examination of cDCs from the whole spleen of CD11c-Cre^{+} TAZ$^{fl/fl}$, CD11c-Cre^{+} YAP$^{fl/fl}$ mice, and the double knockout CD11c-Cre^{+} TAZ$^{fl/fl}$ YAP$^{fl/fl}$ mice by flow cytometry revealed no difference in the absolute numbers of cDC1s and cDC2s **(Figure 4.2)**. Although, there is a trending increase of cDC2 in the spleen of YAP single KO mice (**Figure 4.2b)**. Analysis of basal cDC numbers in the lung were done by digesting one lobe for flow cytometry. The absolute numbers of cells were then normalized to the lobe weight. In a similar manner with splenic cDC numbers, there were no overall difference in the absolute numbers of cDC1s and cDC2s (**Figure**

4.2e & f). From this data, YAP and TAZ deficiency do not affect the basal numbers of cDCs in the spleen and lungs of mature mice.

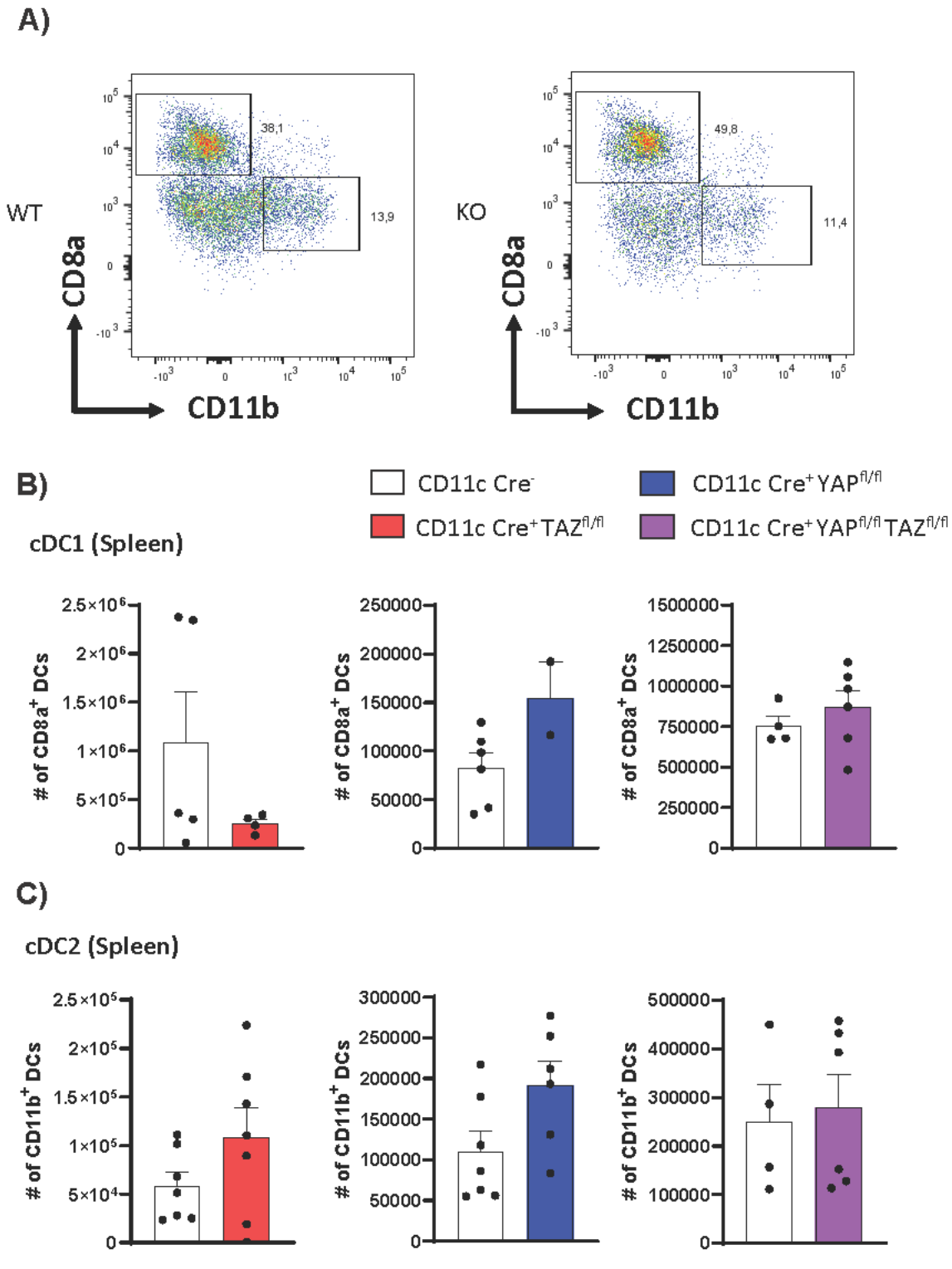
A)
WT
KO
CD8a
CD11b
38,1
13,9
49,8
11,4
B)
CD11c Cre-
CD11c Cre+YAPfl/fl
CD11c Cre+TAZfl/fl
CD11c Cre+YAPfl/flTAZfl/fl
cDC1 (Spleen)
# of CD8a+ DCs
C)
cDC2 (Spleen)
# of CD11b+ DCs

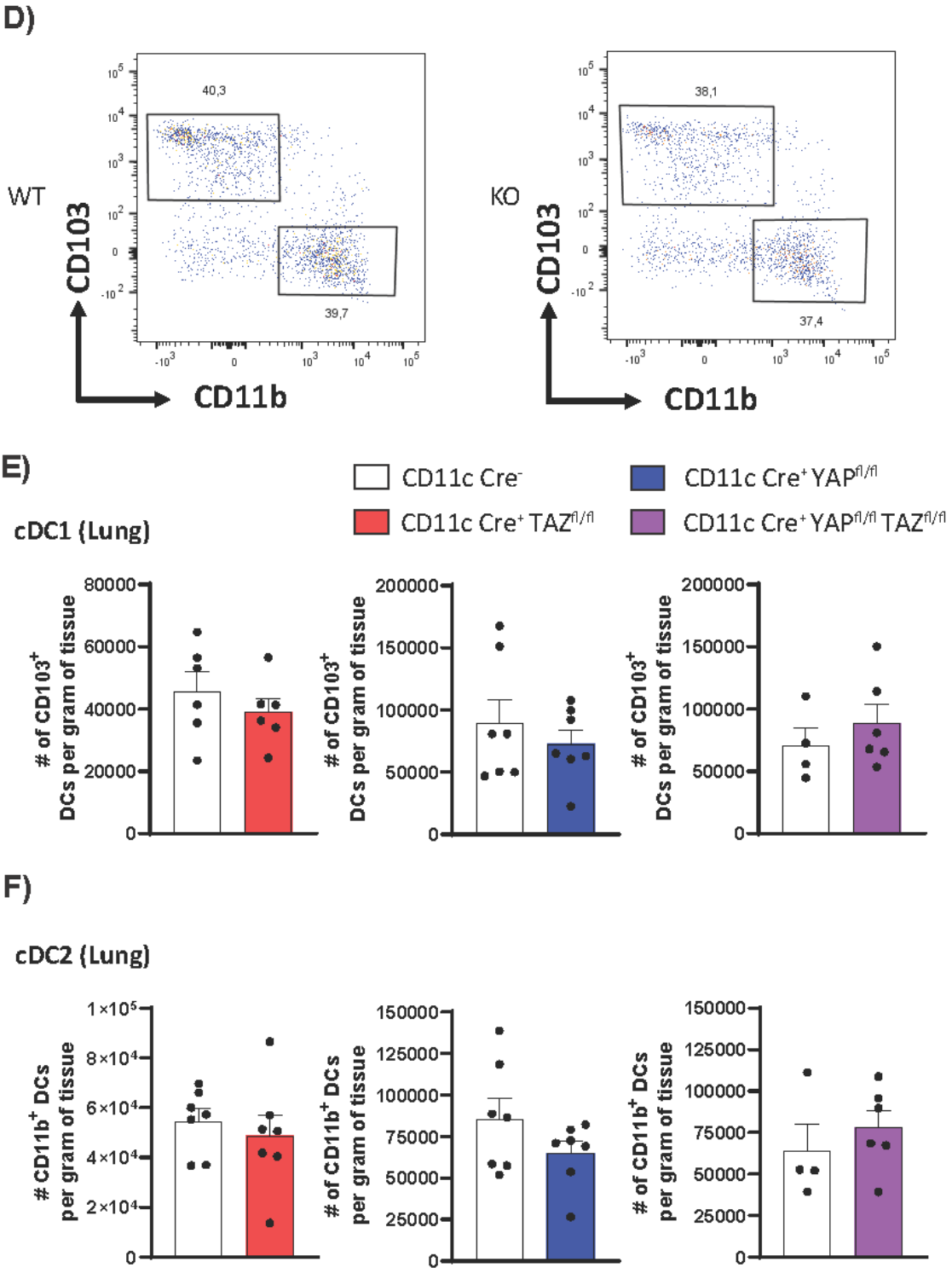
D)
WT
KO
CD103
CD11b
40,3
39,7
38,1
37,4
E)
CD11c Cre-
CD11c Cre+ YAPfl/fl
CD11c Cre+ TAZfl/fl
CD11c Cre+ YAPfl/fl TAZfl/fl
cDC1 (Lung)
# of CD103+ DCs per gram of tissue
F)
cDC2 (Lung)
CD11b+ DCs per gram of tissue
of CD11b+ DCs per gram of tissue

Figure 4.2. Single and double deletion of YAP/TAZ in CD11c^{+} cells do not affect basal cDC numbers in the spleen and lungs. Basal numbers of cDCs in spleen and lungs of 6-8 weeks old Cre^{+} TAZ$^{fl/fl}$, CD11c Cre^{+} YAP$^{fl/fl}$, and CD11c Cre^{+} YAP$^{fl/fl}$ TAZ$^{fl/fl}$ mice were tested by flow cytometry. All cDCs were gated from live and CD64^{-} CD11c^{hi} MHC II^{hi} – CD64 being a marker for monocytes and macrophages. **(A)** Representative flow plots of cDC gating in wildtype and TAZ KO spleen. **(B)** Bar graphs depicting the absolute numbers of CD8a expressing cDC1s in the spleen (n=2-6). **(C)** Bar graphs depicting the absolute numbers of expressing cDC2s in the spleen (n=4-6). **(D)** Representative flow plots of cDC gating in wildtype and YAP/TAZ double KO lung. **(E)** Bar graphs depicting the absolute numbers of CD103 expressing cDC1s in the lung (n=4-7). **(F)** Bar graphs depicting the absolute numbers of cDC2s in the lung (n=4-7). cDC absolute numbers from the lungs are normalized to the weight of digested lobe. The Mann-Whitney U test was used for statistical analysis. Data are presented as mean +/- SEM.

4.3.2 DC specific single deletion of YAP show trend of decreased OT-I T cell activation

Previously, we observed higher T cell proliferation when OT-I T cells were co-cultured with WT BMDCs conditioned on high stiffness. To investigate the involvement of YAP/TAZ mediated mechanosensing in DCs, I performed similar *in vitro* antigen presentation assays using BMDCs with YAP or YAP/TAZ deletion grown on different stiffness **(Figure 4.3)**. In doing so, I saw a trend wherein BMDCs with YAP deletion were associated with lower OT-I proliferation relative to WT BMDCs. BMDCs with YAP/TAZ deletion did not have an impaired capacity to activate OT-I T cells.

The antigen presentation assay was performed at two OVA peptide concentrations. Regardless of the peptide concentration, a trend of reduced T cell proliferation was seen when OT-I T cells were co-cultured with YAP deficient BMDCs compared to WT BMDCs across all three stiffness conditions (**Figure 4.3a & b)**. However, a greater degree of T cell proliferation is associated with YAP deficient BMDCs conditioned on plastic relative to 2 and 50 kPa **(Figure 4.3b)**. This suggests YAP may potentially have a role in regulating DC function and capacity to respond to substrate stiffness. Surprisingly, OT-I T cell proliferation when cultured with YAP/TAZ deficient BMDCs is comparable to WT samples **(Figure 4.3c)**. The capacity for YAP/TAZ BMDCs to activate OT-I T cells was also similar across different stiffness. In comparison, OT-I T cell proliferation moderately increases when cultured with WT BMDCs conditioned on stiff substrates **(Figure 4.3b & c)**. The differential impact on T cell activation due to YAP/TAZ double deletion or YAP single deletion could be suggestive of YAP and TAZ having non-redundant functions in DCs, such as YAP having an anti-inflammatory role whereas TAZ is pro-inflammatory.

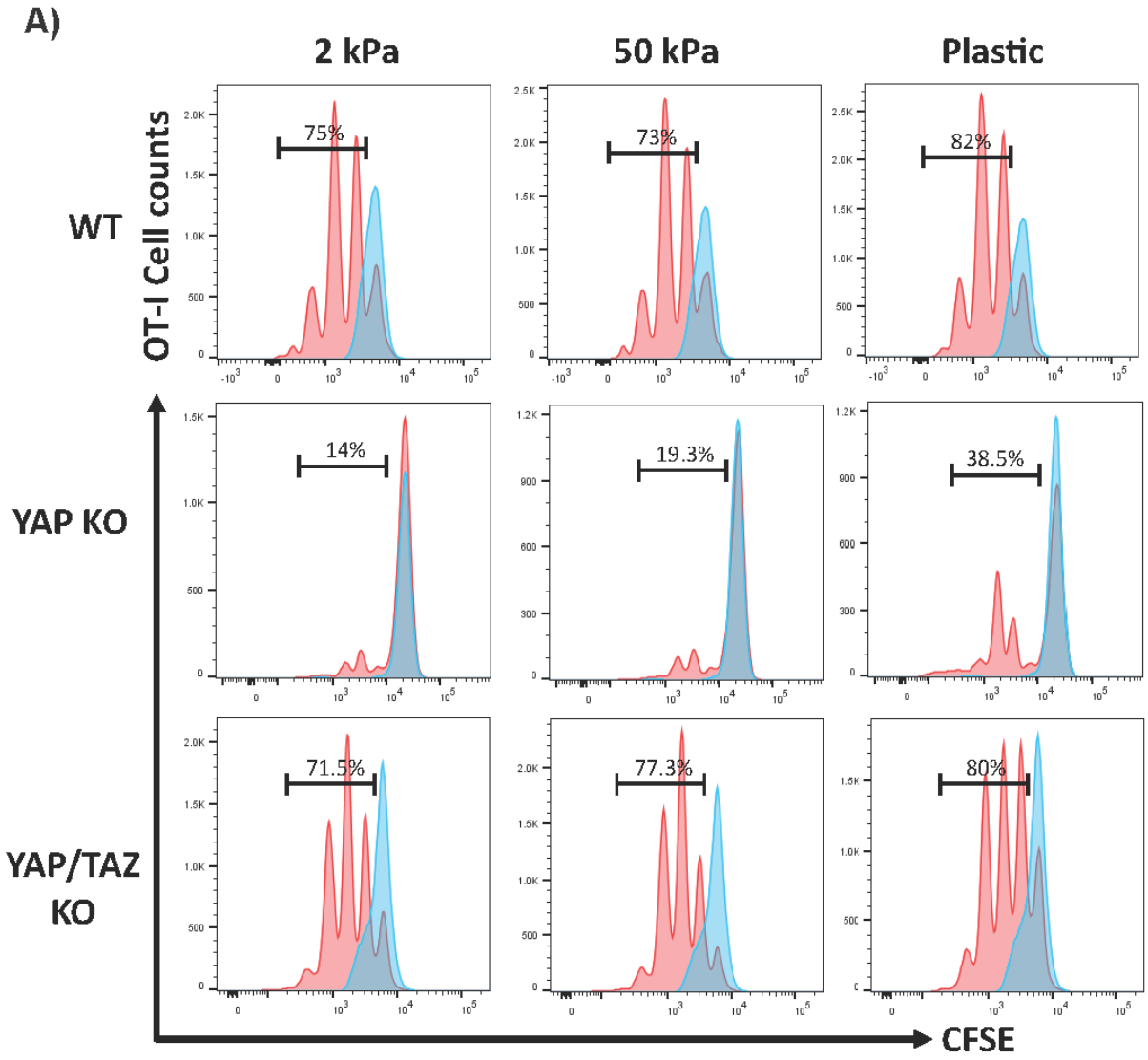

Figure 4.3. BMDCs with YAP single deletion show a trend of impaired capacity to activate OT-I T cells *in vitro*. Antigen presentation assay was performed by co-culturing CD11c-Cre^{+} YAP$^{fl/fl}$ or CD11c-Cre^{+} YAP$^{fl/fl}$ TAZ$^{fl/fl}$ BMDCs grown on 2 kPa, 50 kPa, and plastic with CFSE labelled OT-I T cells for 48 hrs. **(A)** Representative histogram of OT-I T cell proliferation co-cultured with: (Top) wildtype BMDCs (Middle) CD11c-Cre^{+} YAP$^{fl/fl}$ BMDCs (Bottom) CD11c-Cre^{+} YAP$^{fl/fl}$ TAZ$^{fl/fl}$ BMDCs.

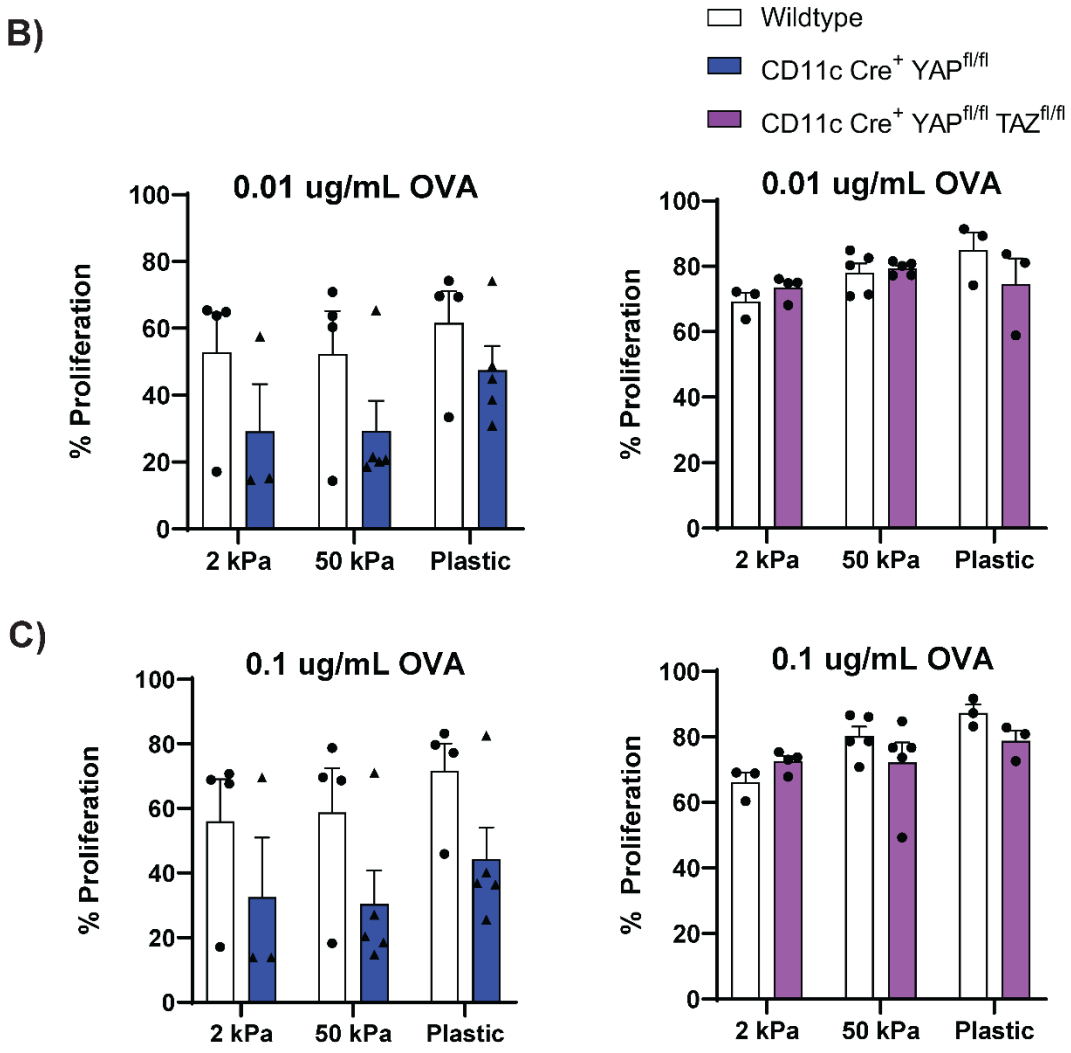

(B) OT-I T cell proliferation when co-cultured with BMDCs that are YAP deficient or YAP/TAZ deficient with 0.01 µg/mL of OVA peptide. **(C)** OT-I T cell proliferation when co-cultured with BMDCs that are YAP deficient or YAP/TAZ deficient with 0.1 µg/mL of OVA peptide.

4.3.3. PR8 influenza infection of CD11c YAP/TAZ$^{fl/fl}$ mice

Tissue dynamics are altered during disease and inflammation. In the case of pulmonary diseases such as influenza infection, the ECM of the lungs is modified[138]. Elastin and collagen are two prominent ECM proteins found in the lung parenchyma[138]. During a healthy state, the lung is under minimal stress and is relatively elastic, a characteristic attributed to elastin[138]. Collagen on the other hand is the major stress bearing component of the ECM found in the lung tissue[138]. At low pulmonary stress, collagen in the lung has a loose and wavy morphology but tightens when the lung parenchyma is distended[138]. This event stiffens the lung tissues. Besides the lung, the draining LNs enlarge and stiffen during inflammation due to the proliferation of lymphocytes. The mechanical cues exerted from tissues that have transitioned from physiological stiffness to a stiffer state therefore have the potential to direct the immune response by acting as an activating stimulus or a bolstering signal to inform DCs of danger[8].

So far, we have observed BMDCs conditioned on stiff substrates upregulate the expression of TAZ, and YAP/TAZ have increased nuclear translocation. These events suggest YAP/TAZ could be mediators of DC mechanosensing. Enrichment analysis of disease protein-protein interactions linked to tension in BMDCs strongly predicted respiratory diseases were associated with tension changes in BMDCs **(Figure 4.4)**. Therefore, we transitioned to an *in vivo* model using our CD11c-Cre^{+} YAP$^{fl/fl}$ and CD11c-Cre^{+} YAP$^{fl/fl}$ TAZ$^{fl/fl}$ mice. Using an intranasal influenza infection model, I sought to determine if the antiviral response of these KO mice is worsened due to the loss of YAP/TAZ dampening DC function or improved due to attenuated immune cell mediated tissue damage. In this animal model, mice are administered a sublethal dosage of Puerto Rico strain H1N1 influenza A virus (PR8 IAV). The infection is followed until peak infection at day 9. On the 9th day, the lungs, spleen, and mediastinal lymph node (MLN) –

the LN draining the lung - are harvested for analysis. The antiviral response was assessed by quantifying cDC subsets, T cell production of TNFα and IFNγ, and the identification of PR8 specific cytotoxic T cells by tetramer staining and flow cytometry.

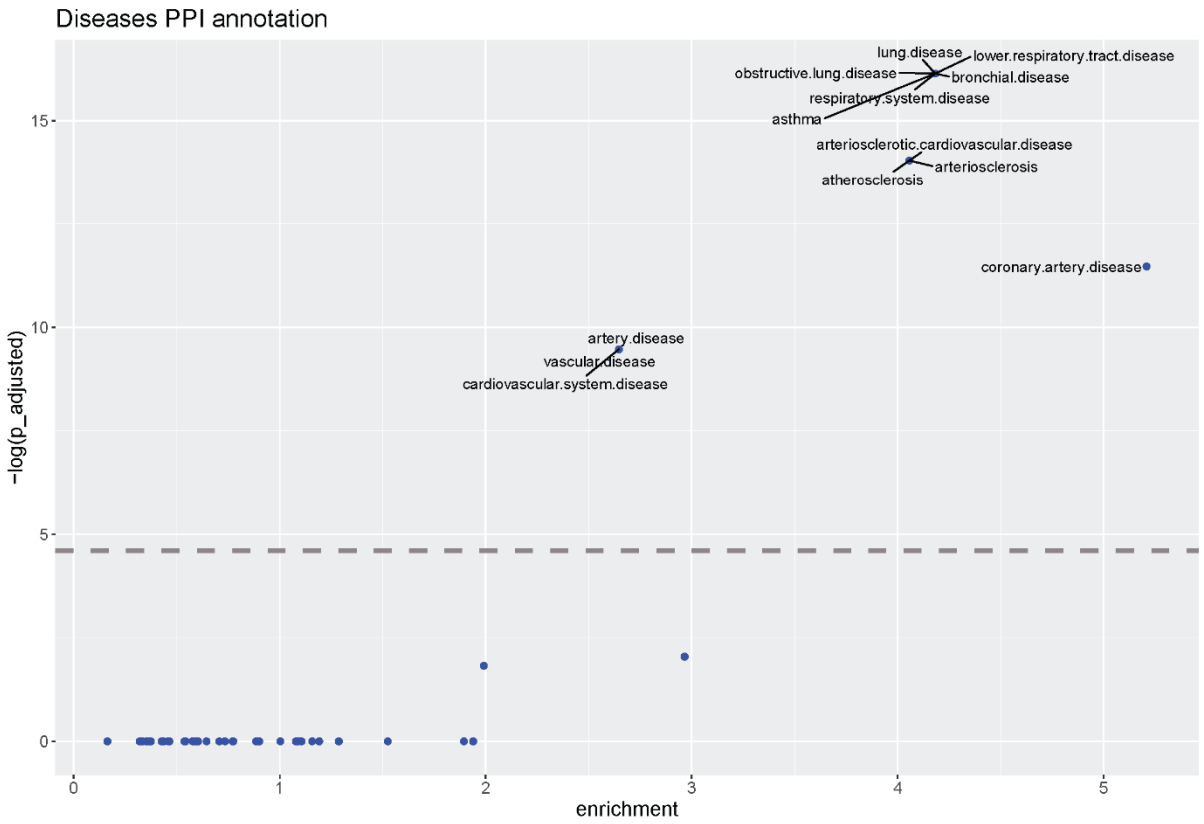

Figure 4.4. Respiratory diseases are predicted to be associated with tension-induced changes in BMDCs. (A) Mouse protein-protein interactions (PPI) were extracted from integrated interactions database v2020-05, and enrichment was performed on 91 disease PPI annotations using hypergeometric distribution to find diseases linked to tension in DCs. Detailed methodology can be found in Chakraborty et al.[107].

4.3.3.1. YAP deletion in CD11c$^+$ cells does not impair antiviral response at day 9

In my examination of CD11c Cre$^+$ YAP$^{fl/fl}$ mice response to PR8 infection, I saw both male and female CD11c Cre$^+$ YAP$^{fl/fl}$ mice displayed a trend of greater weight loss than CD11c Cre$^-$ YAP$^{fl/fl}$ mice. Weight loss typically began on the 3rd day post-infection, gradually declining until the endpoint at day 9 (**Figure 4.5)**. To characterize the antiviral response of YAP deficient DCs, I first examined whether cDC numbers in the lungs, spleen, and MLN of CD11c Cre$^+$ YAP$^{fl/fl+}$ were different at day 9 of PR8 infection (**Figure 4.6)**. In the lung, there were no difference in the population of CD103$^+$ cDC1s between CD11c Cre+ YAP$^{fl/fl+}$ and CD11c Cre$^-$ mice (**Figure 4.6a & b)**. There was also no difference in the population of CD11b$^+$ cDC2s in the MLN, lungs, and spleen of both CD11c Cre+ YAP$^{fl/fl+}$ and CD11c Cre$^-$ (**Figure 4.6 c, d & e)**.

During IAV, DCs may become infected with IAV and traffic from the lung to the MLN to present antigen to CD4$^+$ and CD8$^+$ T cells[139]. The arrival of IAV specific CD4$^+$ and CD8$^+$ T cells to the site of infection are critical for viral clearance. In the context of respiratory viral infection, DCs will migrate to the MLN after antigen acquisition, where they can present the antigen to prime naïve T cells[139]. In turn, activated T cells will migrate to the site of infection to mediate viral clearance. To determine whether YAP deficiency in DCs impaired the recruitment of antiviral T cell response, I quantified the numbers of CD4$^+$ and CD8$^+$ T cells in the lungs, spleen, and MLN. In doing so, I saw no difference in the populations of CD4$^+$ nor CD8$^+$ T cells within the corresponding tissues between infected CD11c Cre$^+$ YAP$^{fl/fl}$ mice and WT suggesting YAP deletion in DCs did not affect the recruitment of immune cells. **(Figure 4.7)**.

As part of the antiviral response, cytokines including TNFα and IFNγ are released by CD4$^+$ T cells and cytotoxic CD8$^+$ T cells to mediate the inflammatory response[140]. TNFα is a pleotropic cytokine with inflammatory and anti-inflammatory function[141]. In the context of

influenza infection, the production of TNFα is not essential for viral clearance[141,142]. Rather, TNFα is indispensable for mitigating lung tissue damage by acting as a negative regulator of $CD8^+$ T cells[142]. IFNγ on the other hand promotes viral clearance through modulating antigen presentation[143,144]. IFNγ acting on DCs upregulates the expression of MHC I molecules, thereby enhancing presentation of viral peptides to cognate cytotoxic T cells[143]. By using fluorophore conjugated MHC class I tetramers presenting a peptide from the PR8 virus ($NP_{366-374}/D^b$), $CD8^+$ T cells that are specific to a given antigen are detected and quantified *ex vivo*. In this segment, to investigate if YAP deficiency in $CD11c^+$ cells impair T cell antiviral responses, I examined $CD4^+$ and $CD8^+$ T cells production of TNFα and IFNγ by intracellular staining, and the presence of viral specific $CD8^+$ T cells by tetramer staining. My hypothesis for these experiments was that if the deletion of YAP in DCs impaired their capacity to activate T cells then there would be a reduction of TNFα and IFNγ producing $CD4^+$ and $CD8^+$ T cells and $NP_{366-374}/D^b$ positive $CD8^+$ T cells relative to the wildtype cohort.

Tetramer staining data suggest that there was no difference in the numbers of PR8 specific $CD8^+$ T cells in the examined tissues of WT and CD11c Cre^+ $YAP^{fl/fl}$ mice **(Figure 4.8)**. PMA/ionomycin-stimulated production of TNFα and IFNγ by $CD4^+$ and $CD8^+$ T cells were examined in infected lung, spleen, and MLN by intracellular staining **(Figure 4.9)**. A slight trending decrease in the numbers of TNFα and IFNγ positive $CD4^+$ is observed in most of the analysed tissues from CD11c Cre^+ $YAP^{fl/fl}$ mice **(Figure 4.9b & d)**. IFNγ production by $CD4^+$ T cells in the lung however was not impaired (**Figure 4.9d)**. No difference in cytokine production by $CD8^+$ T cells from tissues of CD11c Cre^+ $YAP^{fl/fl}$ versus WT mice is observed (**Figure 4.10)**.

In summary, the day 9 antiviral response of CD11c Cre^+ $YAP^{fl/fl}$ mice to PR8 IAV infection does not appear to be influenced by DC YAP deficiency, although CD11c Cre^+ $YAP^{fl/fl}$

mice did have an overall greater weight loss. No difference in the numbers of cDCs in PR8 IAV infected CD11c Cre^{+} $YAP^{fl/fl}$ versus WT mice is observed, suggesting DC YAP deficiency did not influence the recruitment of immune cells to the lung by day 9. The numbers of PR8 specific cytotoxic T cells were similar in CD11c Cre^{+} $YAP^{fl/fl}$ versus WT mice, suggesting that the T cell response is not impaired by YAP deletion in $CD11c^{+}$ cells. Consistent with this, there was no difference in T cell production of TNFα and IFNγ production from the lung, spleen, and MLN tissues of CD11c Cre^{+} $YAP^{fl/fl}$ versus WT mice.

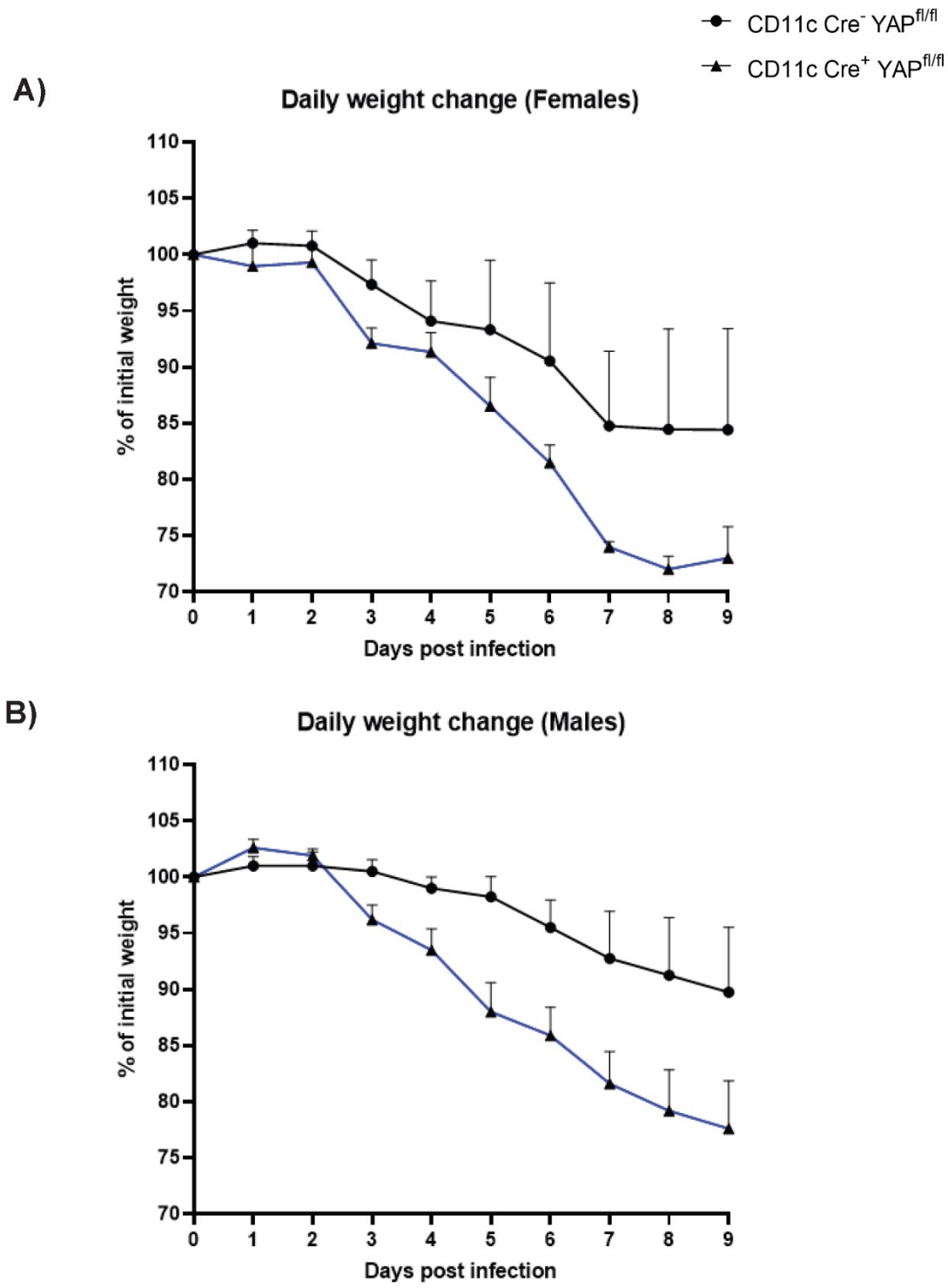
CD11c Cre- YAPfl/fl
CD11c Cre+ YAPfl/fl
A)
Daily weight change (Females)
% of initial weight
110
105
100
95
90
85
80
75
70
0
1
2
3
4
5
6
7
8
9
Days post infection
B)
Daily weight change (Males)
% of initial weight
110
105
100
95
90
85
80
75
70
0
1
2
3
4
5
6
7
8
9
Days post infection

Figure 4.5. Female and male CD11c-Cre^{+} YAP$^{fl/fl}$ mice have a trend of greater weight loss than WT mice during 9-day PR8 IAV infection. Weight was recorded daily at the same time post-infection for 9 days. Weight change is presented as a percentage of initial weight **(A)** Weight loss in female CD11c-Cre^{+} YAP$^{fl/fl}$ mice (n=3-4). **(B)** Weight loss in male CD11c-Cre^{+} YAP$^{fl/fl}$ mice (n =4-12). Data are presented as mean +/- SEM.

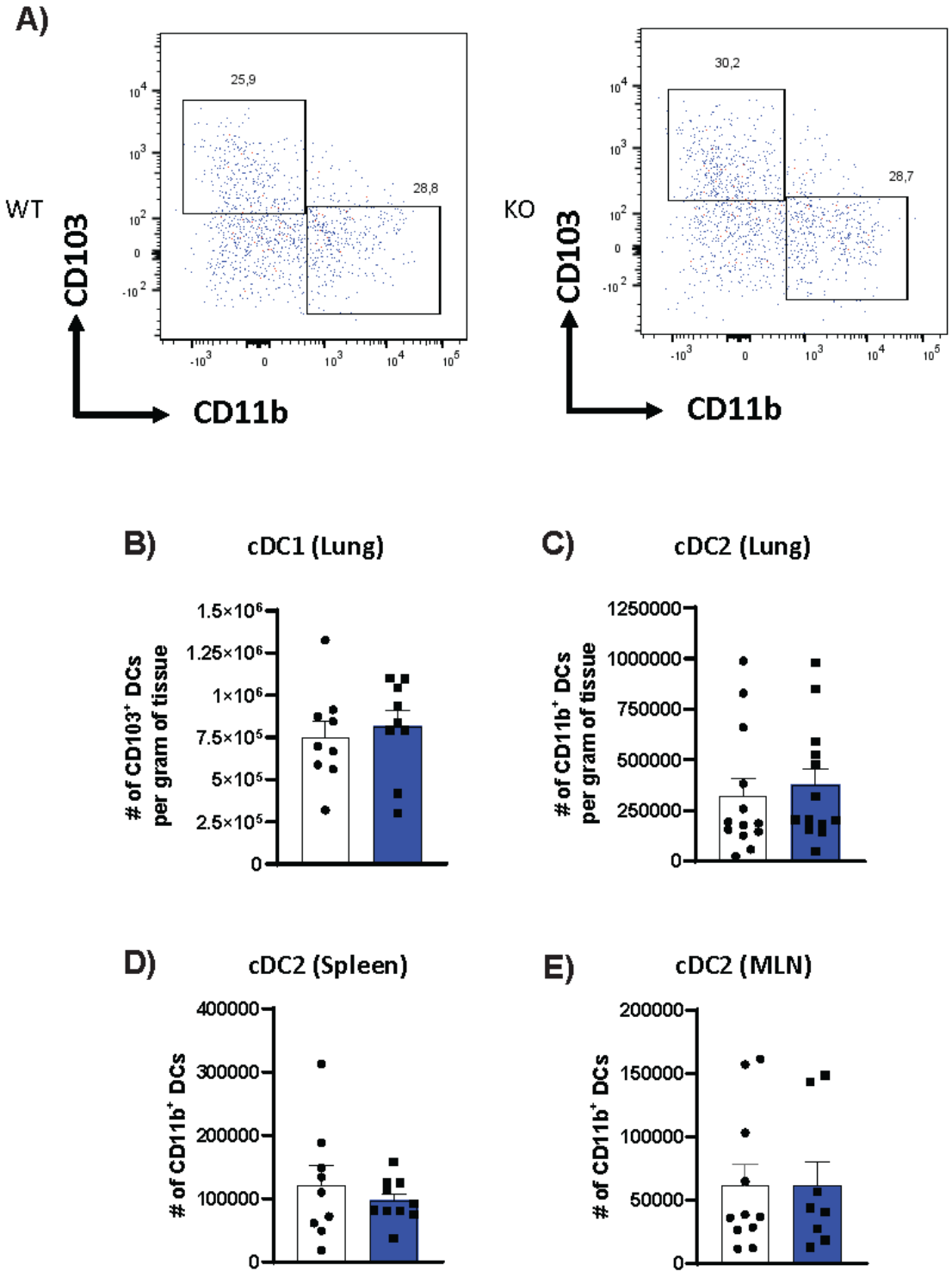
A)
WT
CD103
CD11b
25,9
28,8
KO
30,2
28,7
B)
cDC1 (Lung)
# of CD103+ DCs per gram of tissue
C)
cDC2 (Lung)
# of CD11b+ DCs per gram of tissue
D)
cDC2 (Spleen)
# of CD11b+ DCs
E)
cDC2 (MLN)
# of CD11b+ DCs

Figure 4.6. YAP deletion in CD11c^{+} cells does not modulate cDCs numbers at day 9 of PR8 infection. cDCs were quantified by flow cytometry from dissociated infected lungs, spleens, and MLNs. **(A)** Representative flow cytometry plot of cDCs in lung from CD11c-Cre^{-} YAP$^{fl/fl}$ mice (left) and CD11c-Cre^{+} YAP$^{fl/fl}$ mice (right). **(B)** Absolute numbers of CD103^{+} cDC1s in the lung (n=9). **(C)** Absolute numbers of CD11b^{+} cDC2s in the lung (n=9-15). **(D)** Absolute numbers of CD11b^{+} cDC2s in the spleen (n=9-10) **(E)** Absolute numbers of CD11b^{+} cDC2s in the MLN (n=8-11). The Mann-Whitney U test was used for statistical analysis. Data are presented as mean +/- SEM.

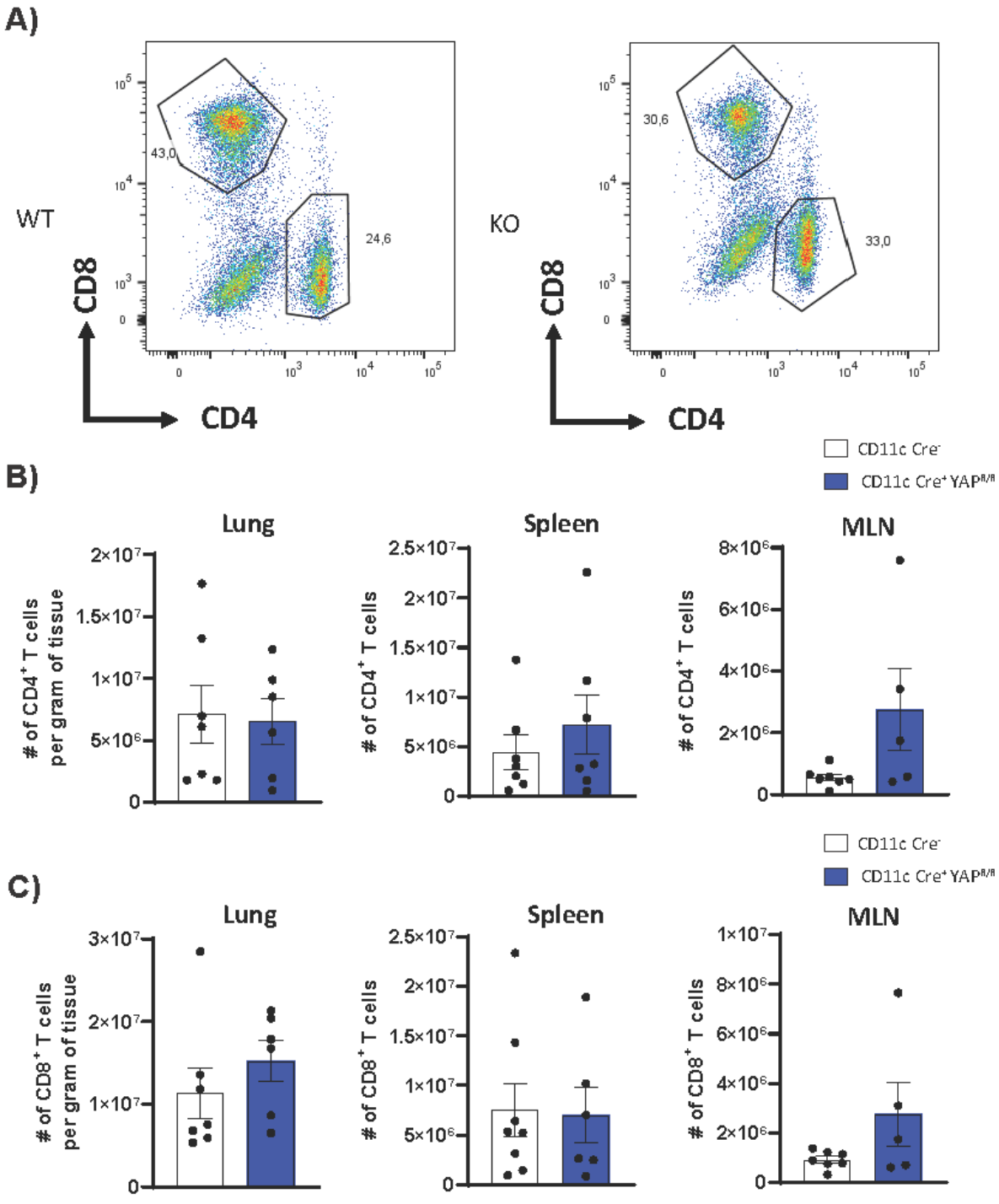
A)
WT
KO
CD8
CD4
43,0
24,6
30,6
33,0
B)
CD11c Cre-
CD11c Cre+YAPfl/fl
Lung
Spleen
MLN
# of CD4+ T cells per gram of tissue
# of CD4+ T cells
C)
# of CD8+ T cells per gram of tissue
# of CD8+ T cells

Figure 4.7. Female and male CD11c-Cre^{+} YAP$^{fl/fl}$ and WT mice have similar numbers of CD4^{+} and CD8^{+} T cells at day 9 of PR8 infection. Populations were quantified by flow cytometry from dissociated infected lungs, spleens, and MLNs. **(A)** Representative flow cytometry plots of CD4^{+} and CD8^{+} T cells from lungs of CD11c-Cre^{-} YAP$^{fl/fl}$ (left) and CD11c-Cre^{+} YAP$^{fl/fl}$ (right). **(B)** Absolute numbers of CD4^{+} T cells in the lung (left), spleen (middle), and MLN (right) (n=5-7). **(C)** Absolute numbers of CD8^{+} T cells in the lung (left), spleen (middle), and MLN (right) (n=6-8). The Mann-Whitney U test was used for statistical analysis. Data are presented as mean +/- SEM.

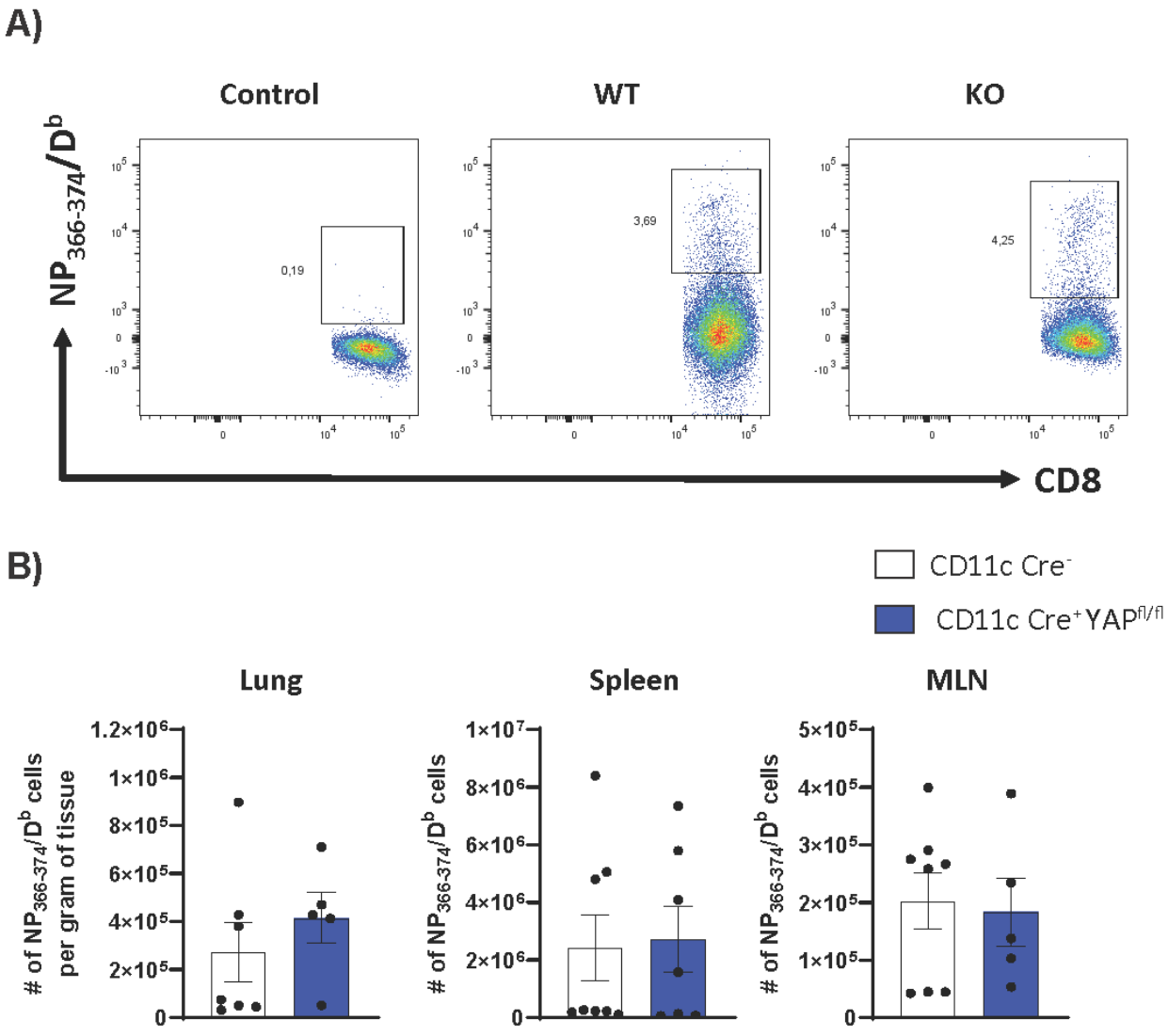

Figure 4.8. YAP single deletion in DCs do not modulate the numbers of PR8-specific CD8$^+$ T cells at day 9 of infection. Cells from dissociated lungs, spleens, and MLNs were stained with $NP_{366-374}/D^b$ tetramers. **(A)** Representative flow plot of $NP_{366-374}/D^b$ tetramers staining in lung. Shown are negative control (left), CD11c-Cre$^-$ YAP$^{fl/fl}$ (middle) and CD11c-Cre$^+$ YAP$^{fl/fl}$ (right) lung samples. **(B)** Absolute numbers of $NP_{366-374}/D^b$ tetramers positive CD8$^+$ T cells. The Mann-Whitney U test was used for statistical analysis (n=5-8). Data are presented as mean +/- SEM.

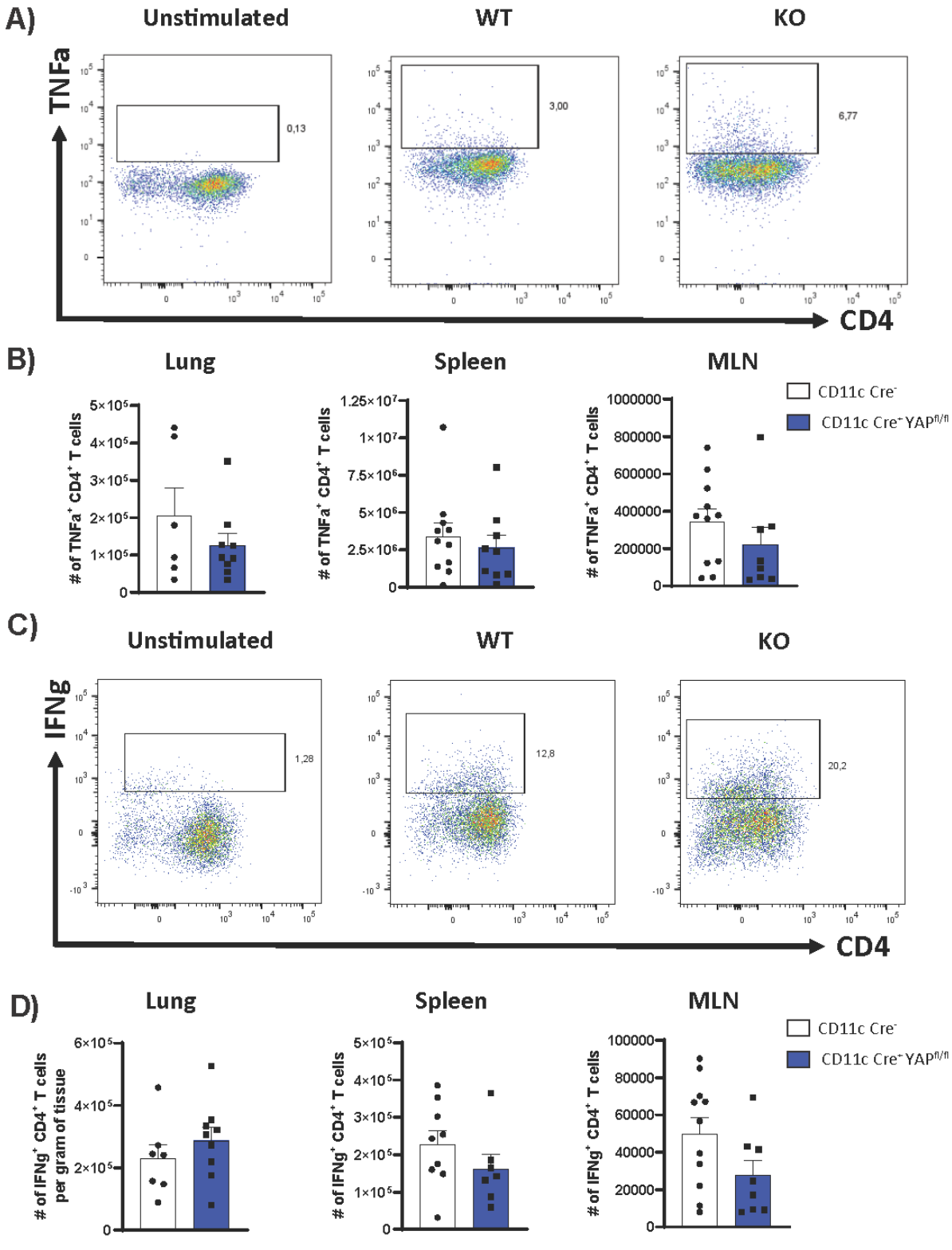
A)
Unstimulated
WT
KO
TNFa
CD4
0,13
3,00
6,77
B)
Lung
Spleen
MLN
CD11c Cre-
CD11c Cre+YAPfl/fl
# of TNFa+ CD4+ T cells
C)
Unstimulated
WT
KO
IFNg
CD4
1,28
12,8
20,2
D)
Lung
Spleen
MLN
CD11c Cre-
CD11c Cre+YAPfl/fl
# of IFNg+ CD4+ T cells per gram of tissue
# of IFNg+ CD4+ T cells

Figure 4.9. TNFα and IFNγ production by $CD4^+$ T cells of PR8 influenza infected female and male CD11c-Cre^+ $YAP^{fl/fl}$ mice at day 9. Cells from dissociated infected lung, spleen, and MLN tissues were stimulated with PMA/ionomycin with brefeldin A for 4hrs prior to intracellular staining of TNFα and IFNγ. **(A)** Representative flow plot of TNFα staining in $CD4^+$ T cells from unstimulated lungs (left) or stimulated CD11c-Cre^- $YAP^{fl/fl}$ (middle) and CD11c-Cre^+ $YAP^{fl/fl}$ (right) lung samples. **(B)** Absolute numbers of TNFα positive $CD4^+$ T cells (n=6-10). **(C)** Representative flow plot of IFNγ staining in $CD4^+$ T cells from unstimulated lungs (left) or stimulated CD11c-Cre^- $YAP^{fl/fl}$ (middle) and CD11c-Cre^+ $YAP^{fl/fl}$ (right) lung samples (n=7-11). **(D)** Absolute numbers of IFNγ positive $CD4^+$ T cells. The Mann-Whitney U test was used for statistical analysis. Data are presented as mean +/- SEM.

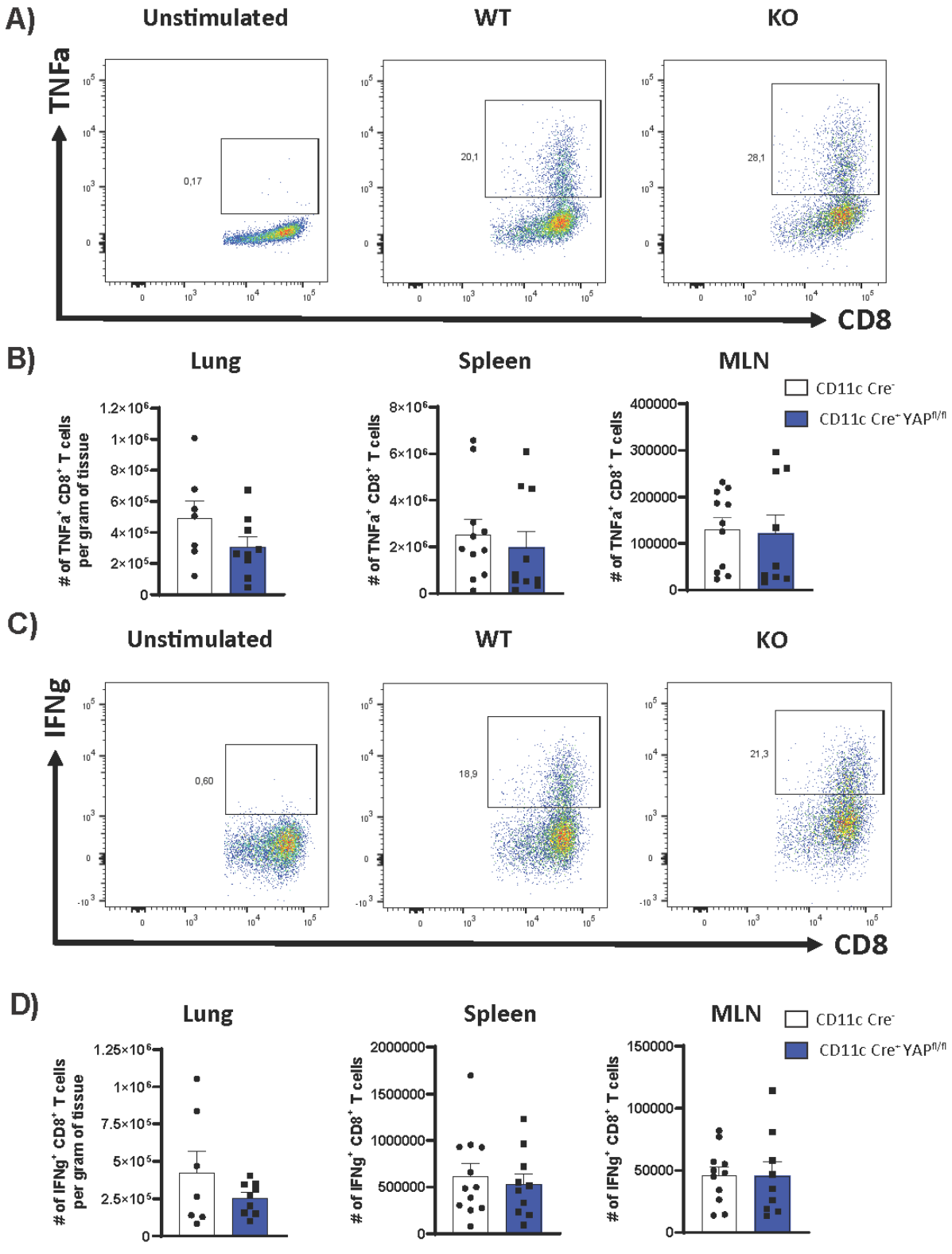
A)
Unstimulated
WT
KO
TNFa
CD8
0,17
20,1
28,1
B)
Lung
Spleen
MLN
CD11c Cre-
CD11c Cre+YAPfl/fl
# of TNFa+ CD8+ T cells per gram of tissue
# of TNFa+ CD8+ T cells
C)
Unstimulated
WT
KO
IFNg
CD8
0,60
18,9
21,3
D)
Lung
Spleen
MLN
CD11c Cre-
CD11c Cre+YAPfl/fl
# of IFNg+ CD8+ T cells per gram of tissue
# of IFNg+ CD8+ T cells

Figure 4.10. TNFα and IFNγ production by $CD8^+$ T cells the lungs, spleen, and MLN from both PR8 infected female and male CD11c-Cre^+ $YAP^{fl/fl}$ mice at day 9. Cells from dissociated infected lung, spleen, and MLN tissues were stimulated with PMA/ionomycin with brefeldin A for 4hrs prior to intracellular of TNFα and IFNγ. **(A)** Representative flow plot of TNFα staining in $CD8^+$ T cells from unstimulated lungs (left) or stimulated CD11c-Cre^- $YAP^{fl/fl}$ (middle) and CD11c-Cre^+ $YAP^{fl/fl}$ (right) lung samples. **(B)** Absolute numbers of TNFα positive $CD8^+$ T cells (n=7-9). **(C)** Representative flow plot of IFNγ staining in $CD8^+$ T cells from unstimulated lungs (left) or stimulated CD11c-Cre^- $YAP^{fl/fl}$ (middle) and CD11c-Cre^+ $YAP^{fl/fl}$ (right) lung samples. **(D)** Absolute numbers of IFNγ positive $CD8^+$ T cells (n=7-12). The Mann-Whitney U test was used for statistical analysis. Data are presented as mean +/- SEM.

4.3.3.2 YAP & TAZ double deletion in CD11c$^+$cells does not impair antiviral response at day 9

The nuclear localization of YAP/TAZ is an indicator of active YAP/TAZ[110]. In an earlier experiment, I saw increased nuclear translocation of both YAP/TAZ in BMDCs when under mechanical stress, hinting that DCs may have the ability for YAP/TAZ signaling (**Figure 3.8)**. As TAZ is a paralog of YAP with similar functionality[110], it is possible that TAZ is compensating for YAP deficiency in our CD11c-Cre$^+$ YAP$^{fl/fl}$ animals during influenza infection. To better characterize YAP/TAZ signaling in DCs biology, I infected CD11c-Cre$^+$ YAP$^{fl/fl}$ TAZ$^{fl/fl}$ mice, which have both YAP and YAZ deleted, with PR8 IAV as described previously. Using the same experimental approach as before, I investigated whether the double deletion of YAP/TAZ in CD11c$^+$ cells altered cDC numbers and T cell response in the lungs, spleen, and MLN during PR8 IAV infection.

CD11c-Cre$^+$ YAP$^{fl/fl}$ TAZ$^{fl/fl}$ mice did not lose more weight than WT mice during influenza disease progression (**Figure 4.11)**. The weight loss of PR8 IAV infected CD11c-Cre$^+$ YAP$^{fl/fl}$ TAZ$^{fl/fl}$ is comparable to WT mice. For both CD11c-Cre$^+$ YAP$^{fl/fl}$ TAZ$^{fl/fl}$ and WT mice, weight loss began on the 3rd day of infection, gradually declining over the course of 9 days. As cDCs are a cell-type directly impacted in our CD11c-Cre$^+$ YAP$^{fl/fl}$ TAZ$^{fl/fl}$ mice, I first investigated if CD11c-specific YAP/TAZ deficiency during influenza infection modulated the number of cDCs in the lung, spleen, and MLN. Analysis of cDC1s and cDC2s populations revealed no difference in numbers between CD11c-Cre$^+$ YAP$^{fl/fl}$ TAZ$^{fl/fl}$ versus WT mice (**Figure 4.12)**. The recruitment of T cells during influenza was also not impaired by YAP/TAZ double deletion in DCs, as the population of CD4$^+$ and CD8$^+$ T cells in the lung, spleen, and MLN of CD11c-Cre$^+$ YAP$^{fl/fl}$ TAZ$^{fl/fl}$ mice is similar to the WT cohort (**Figure 4.13)**.

To test whether YAP/TAZ double deletion in $CD11c^+$ cells altered T cell activation, I examined the production of TNFα and IFNγ in PMA/ionomycin stimulated T cells retrieved from PR8 IAV infected lung, spleen, and MLN tissues (**Figure 4.14 & 4.15)**. data revealed no difference in TNFα and IFNγ positive T cells regardless of mice genotype. Furthermore, the numbers of PR8 IAV specific $CD8^+$ T cells (measured by staining with $NP_{366\text{-}374}/D^b$ tetramers), were similar in infected tissues from Cre^+ $YAP^{fl/fl}$ $TAZ^{fl/fl}$ and WT mice (**Figure 4.16)**. Collectively, these data show that YAP/TAZ double deletion in $CD11c^+$ cells do not impair day 9 T cell-mediated antiviral response.

A)

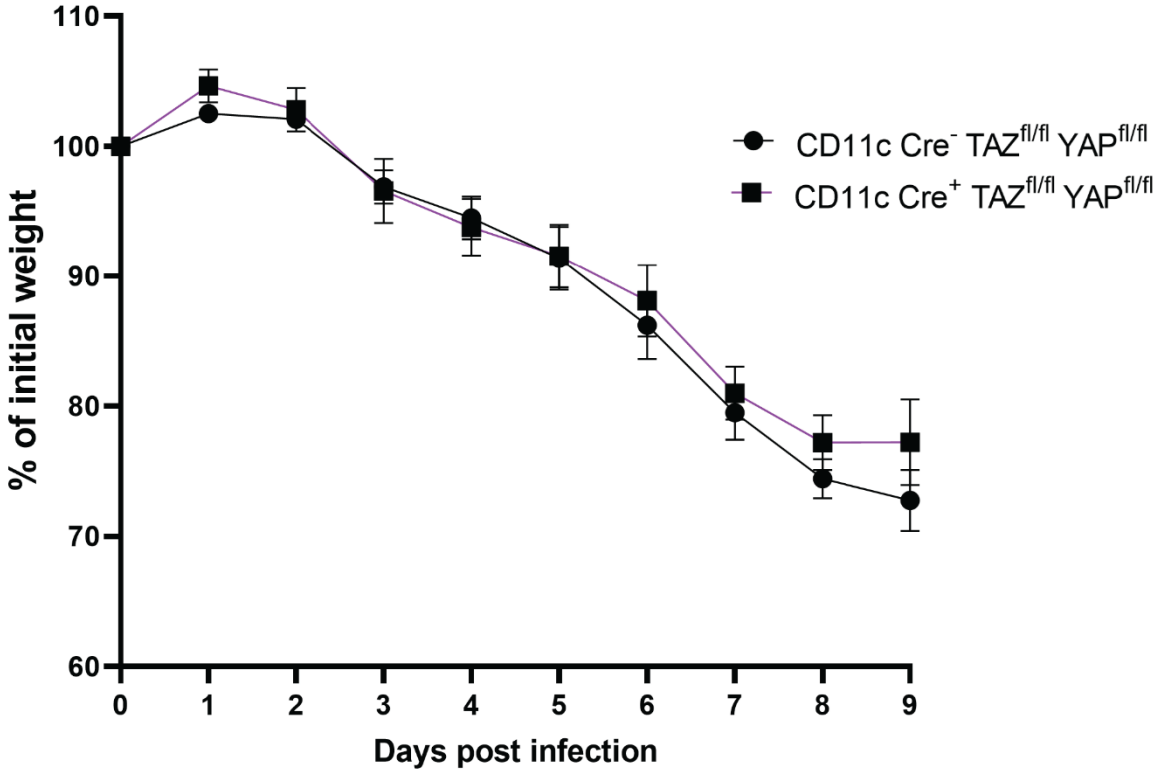

Figure 4.11. CD11c-Cre^{+} YAP$^{fl/fl}$ TAZ$^{fl/fl+}$ mice do not lose more weight than WT mice during 9-day PR8 IAV infection. Mice were weighed at the same time daily. **(A)** Daily weight loss in female CD11c-Cre^{+} YAP$^{fl/fl}$ TAZ$^{fl/fl}$ mice (n=8-10). Data are presented as mean +/- SEM.

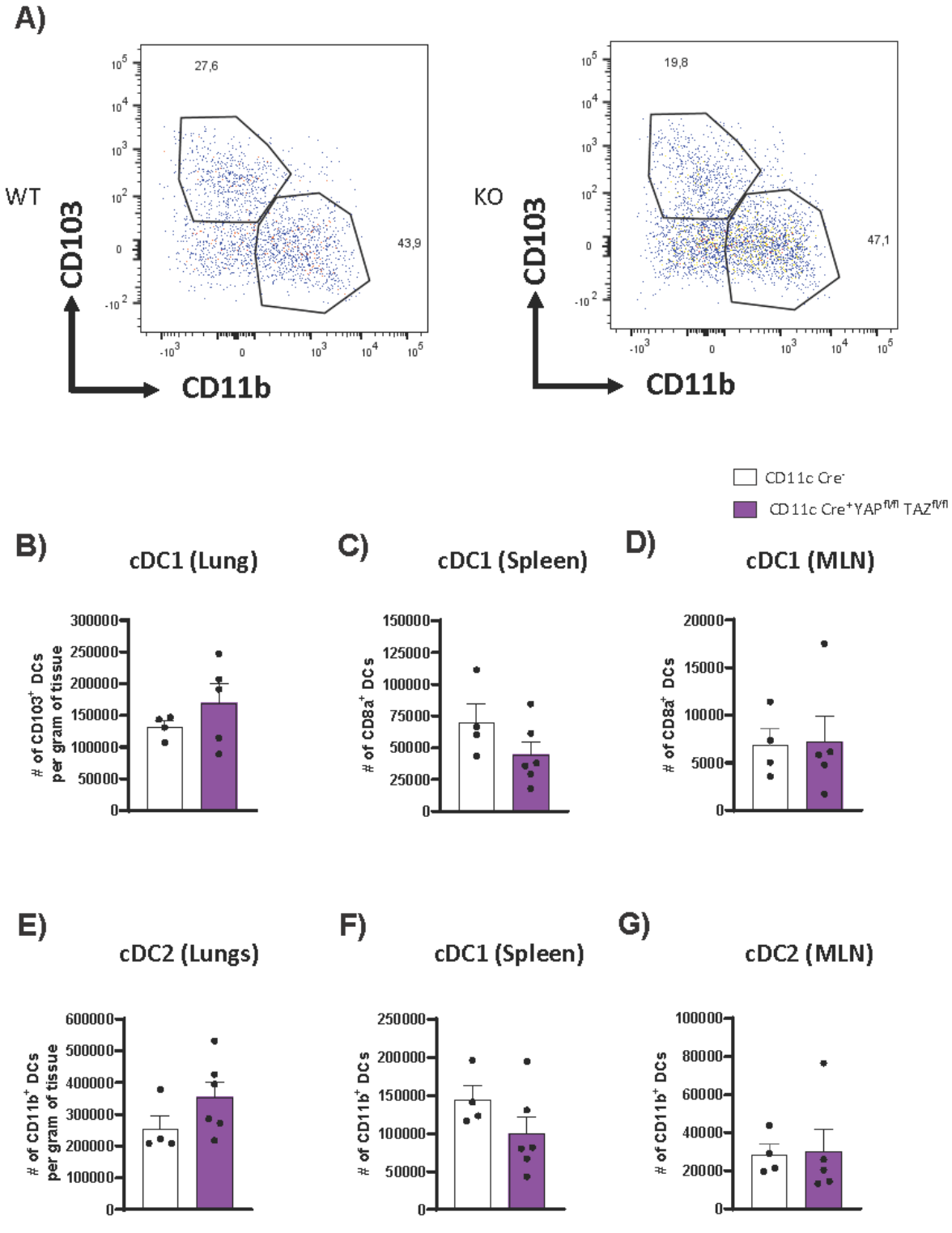
A)
WT
KO
CD103
CD11b
27,6
43,9
19,8
47,1
CD11c Cre-
CD11c Cre+YAPfl/fl TAZfl/fl
B)
cDC1 (Lung)
# of CD103+ DCs per gram of tissue
C)
cDC1 (Spleen)
# of CD8a+ DCs
D)
cDC1 (MLN)
# of CD8a+ DCs
E)
cDC2 (Lungs)
# of CD11b+ DCs per gram of tissue
F)
cDC1 (Spleen)
# of CD11b+ DCs
G)
cDC2 (MLN)
# of CD11b+ DCs

Figure 4.12. CD11c-Cre^{+} YAP$^{fl/fl}$ TAZ$^{fl/fl}$ mice do not have fewer cDC numbers at day 9 of PR8 IAV infection. cDCs were quantified in the lung, spleen, and MLN by flow cytometry after tissue digestion and processing. **(A)** Representative flow cytometry plot of cDCs in lung from WT (left) and CD11c Cre^{+} YAP$^{fl/fl}$ TAZ$^{fl/fl}$ mice (right). **(B)** Absolute numbers of CD103^{+} cDC1s in lungs (n=4-5). **(C)** Absolute numbers of CD8α^{+} cDC1s in spleens (n=4-6). **(D)** Absolute numbers of CD8α^{+} cDC1s in MLNs (n=4-5). **(E)** Absolute numbers of CD11b^{+} cDC2s in lungs (n=4-6). **(F)** Absolute numbers of CD11b^{+} cDC2s in spleens (n=4-6). **(G)** Absolute numbers of CD11b^{+} cDC2s in MLNs (n=4-5). The Mann-Whitney U test was used for statistical analysis. Data are presented as mean +/- SEM.

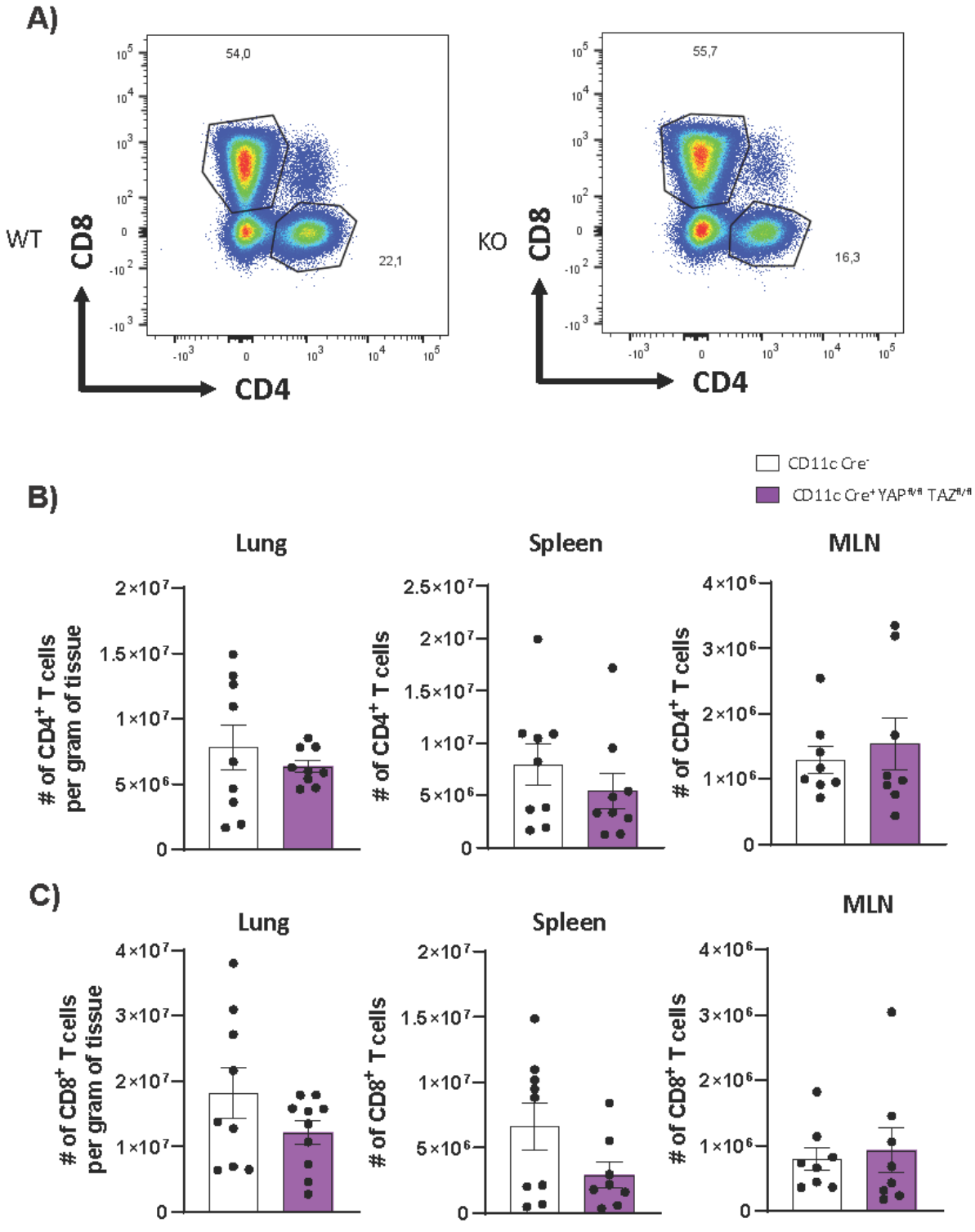
A)
WT
CD8
CD4
54,0
22,1
KO
55,7
16,3
B)
CD11c Cre-
CD11c Cre+ YAPfl/fl TAZfl/fl
Lung
Spleen
MLN
# of CD4+ T cells per gram of tissue
C)
# of CD8+ T cells per gram of tissue

Figure 4.13. CD11c-Cre^{+} YAP$^{fl/fl}$ TAZ$^{fl/fl}$ mice have similar numbers of CD4^{+} and CD8^{+} T cells at day 9 of PR8 IAV infection compared to CD11c-Cre^{-} YAP$^{fl/fl}$ TAZ$^{fl/fl}$ mice.

Populations in the lung, spleen, and MLN were quantified by flow cytometry after tissue digestion and processing. **(A)** Representative flow cytometry plots of CD4+ and CD8+ T cells from lungs of WT (left) and CD11c-Cre+ YAPfl/fl TAZfl/fl (right) mice. **(B)** Absolute numbers of CD4+ T cells in the lung (left), spleen (middle), and MLN (right) (n=9). **(C)** Absolute numbers of CD8+ T cells in the lung (left), spleen (middle), and MLN (right) (n=8-9). The Mann-Whitney U test was used for statistical analysis. Data are presented as mean +/- SEM.

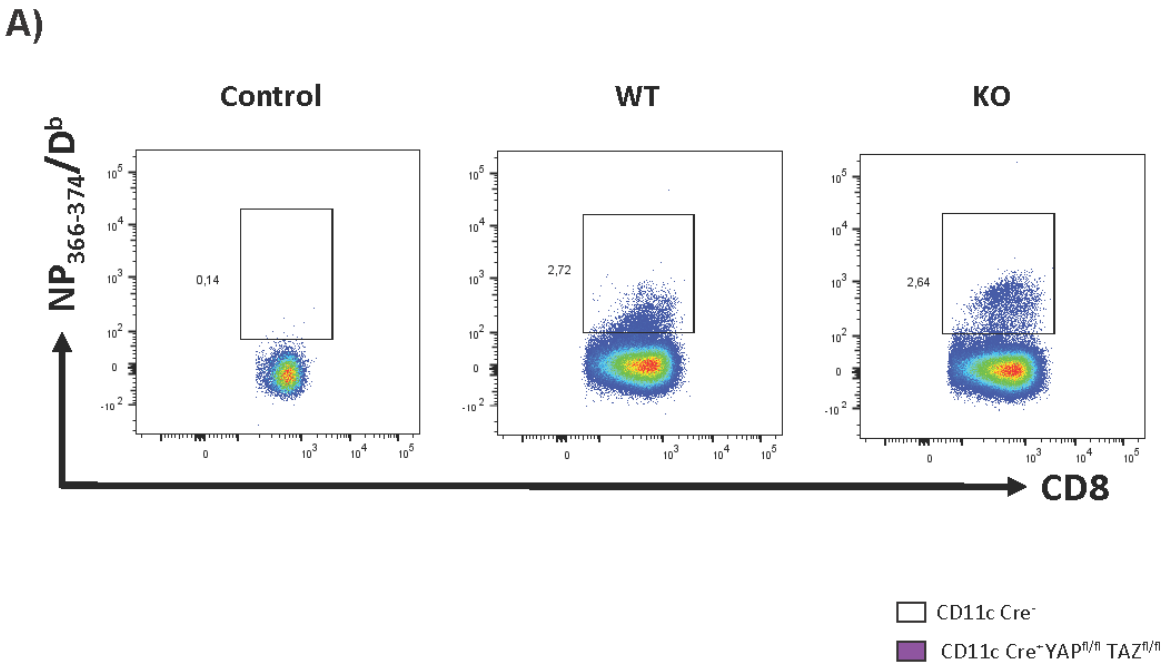
A)
Control
WT
KO
NP366-374/Db
0,14
2,72
2,64
CD8
CD11c Cre-
CD11c Cre-YAPfl/fl TAZfl/fl
B)
Lung
Spleen
MLN
# of NP366-374/Db+CD8+ T cells per gram of tissue
# of NP366-374/Db+CD8+ T cells
2×10^6
1.5×10^6
1×10^6
5×10^5
0
150000
100000
50000
25000
20000
15000
10000
5000

Figure 4.14. YAP/TAZ double deletion in DCs do not affect the numbers of PR8-specific $CD8^+$ T cells at day 9 of infection. Cells from dissociated lung, spleen, and MLN tissues were stained with $NP_{366-374}/D^b$ tetramers. **(A)** Representative flow plot of $NP_{366-374}/D^b$ tetramers staining in lung. Shown are negative control (left), WT (middle) and CD11c-Cre^+ $YAP^{fl/fl}$ $TAZ^{fl/fl}$ (right) lung samples. **(B)** Absolute numbers of $NP_{366-374}/D^b$ tetramers positive $CD8^+$ T cells (n=7-10). The Mann-Whitney U test was used for statistical analysis. Data are presented as mean +/- SEM.

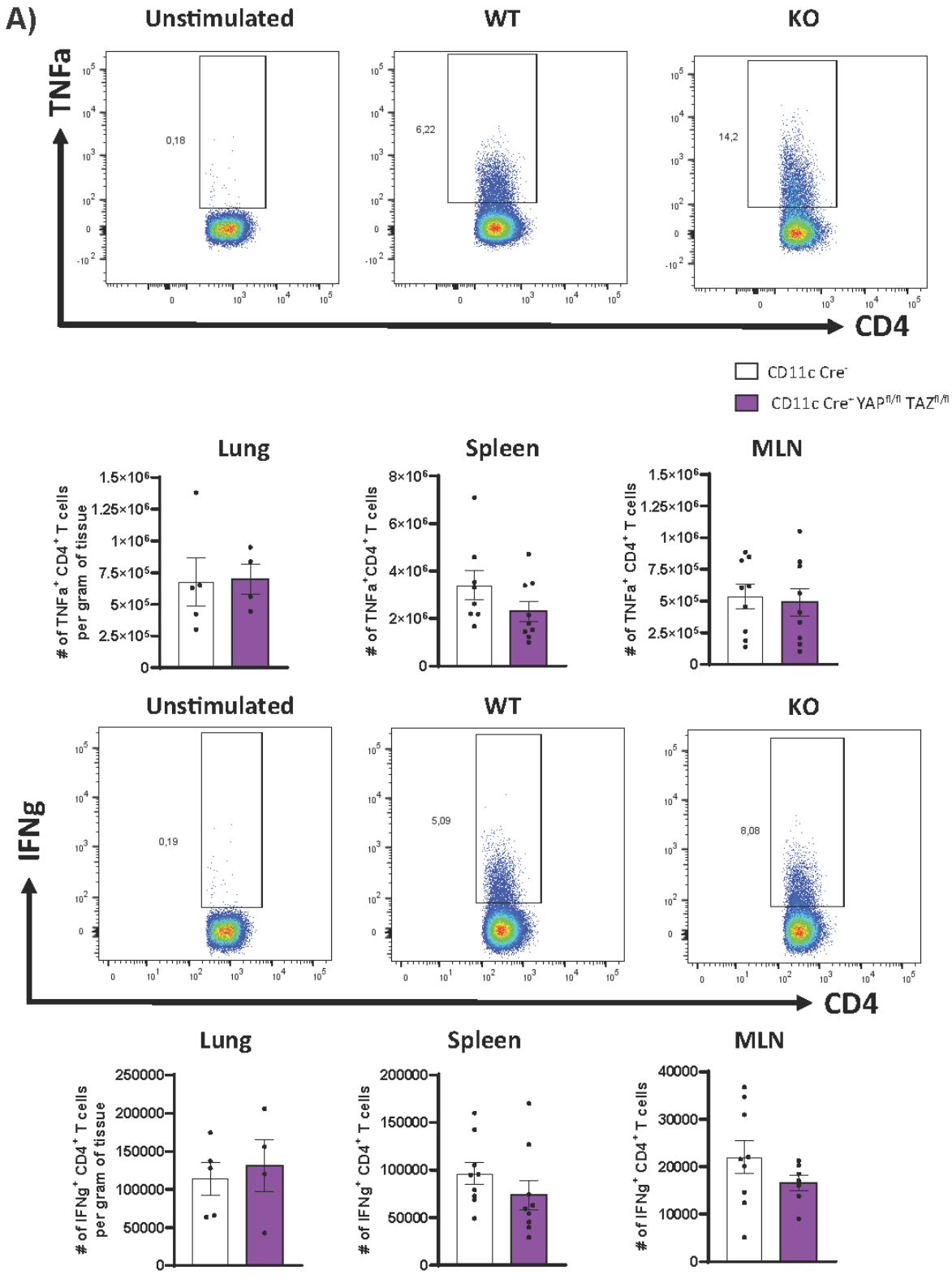
A)
Unstimulated
WT
KO
TNFa
CD4
0,18
6,22
14,2
CD11c Cre-
CD11c Cre+ YAPfl/fl TAZfl/fl
Lung
Spleen
MLN
# of TNFa+ CD4+ T cells per gram of tissue
# of TNFa+ CD4+ T cells
Unstimulated
WT
KO
IFNg
CD4
0,19
5,09
8,08
Lung
Spleen
MLN
# of IFNg+ CD4+ T cells per gram of tissue
# of IFNg+ CD4+ T cells

Figure 4.15. YAP/TAZ double deletion in DCs does not impair $CD4^+$ T cell production of TNFα and IFNγ at day 9 of PR8 IAV infection. Dissociated lung, spleen, and MLN tissues were stimulated with PMA/ionomycin with Brefeldin A for 4 hours prior to intracellular cytokine staining. **(A)** Representative flow plot of TNFα staining in $CD4^+$ T cells from unstimulated lungs (left) or stimulated WT (middle) and CD11c-Cre^+ $YAP^{fl/fl}$ $TAZ^{fl/fl}$ (right) lung samples. **(B)** Absolute numbers of TNFα positive $CD4^+$ T cells (lungs n=4-5; spleens & MLNs n=8-9). **(C)** Representative flow plot of IFNγ staining in $CD4^+$ T cells from unstimulated lungs (left) or stimulated WT (middle) and CD11c-Cre^+ $YAP^{fl/fl}$ $TAZ^{fl/fl}$ (right) lung samples. **(D)** Absolute numbers of IFNγ positive $CD4^+$ T cells (lungs n=4-5; spleens & MLNs n=8-9). The Mann-Whitney U test was used for statistical analysis. Data are presented as mean +/- SEM.

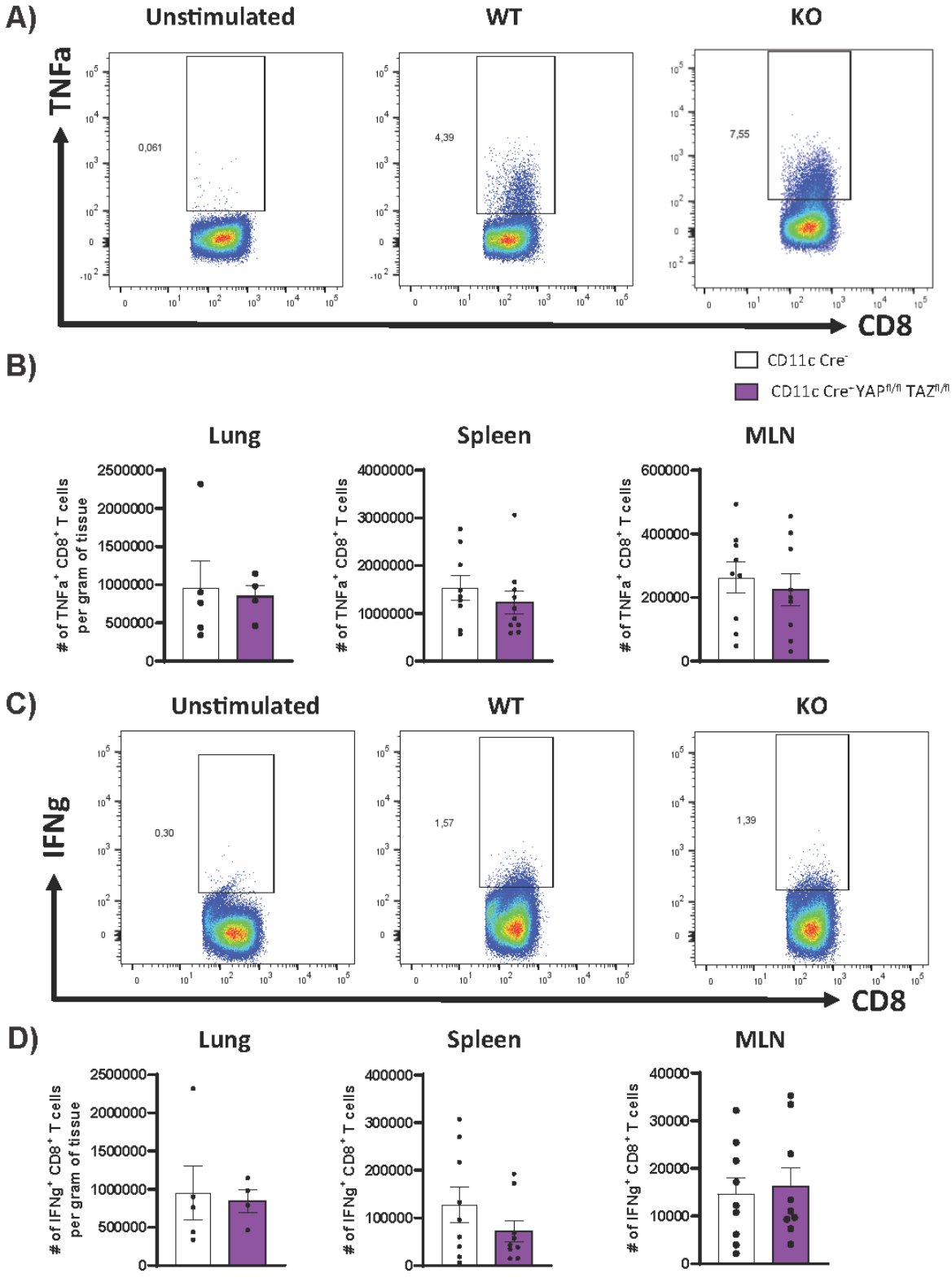
A)
Unstimulated
WT
KO
TNFa
CD8
0,061
4,39
7,55
B)
CD11c Cre-
CD11c Cre-YAPfl/fl TAZfl/fl
Lung
Spleen
MLN
# of TNFa+ CD8+ T cells per gram of tissue
# of TNFa+ CD8+ T cells
C)
Unstimulated
WT
KO
IFNg
CD8
0,30
1,57
1,39
D)
Lung
Spleen
MLN
# of IFNg+ CD8+ T cells per gram of tissue
# of IFNg+ CD8+ T cells

Figure 4.16. YAP/TAZ double deletion in DCs does not impair $CD8^+$ T cell production of TNFα and IFNγ at day 9 of PR8 IAV infection. Dissociated lung, spleen, and MLN tissues were stimulated with PMA/ionomycin with Brefeldin A for 4 hours prior to intracellular cytokine staining. **(A)** Representative flow plot of TNFα staining in $CD8^+$ T cells from unstimulated lungs (left) or stimulated WT (middle) and CD11c-Cre^+ $YAP^{fl/fl}$ $TAZ^{fl/fl}$ (right) lung samples. **(B)** Absolute numbers of TNFα positive $CD8^+$ T cells (lungs n=4-5; spleens & MLNs n=8-9). **(C)** Representative flow plot of IFNγ staining in $CD8^+$ T cells from unstimulated lungs (left) or stimulated WT (middle) and CD11c-Cre^+ $YAP^{fl/fl}$ $TAZ^{fl/fl}$ (right) lung samples. **(D)** Absolute numbers of IFNγ positive $CD8^+$ T cells (lungs n=4-5; spleens & MLNs n=8-9). The Mann-Whitney U test was used for statistical analysis. Data are presented as mean +/- SEM.

4.4 Discussion

In this chapter I investigated the role of YAP/TAZ in DCs using mice with CD11c specific deletion of YAP/TAZ. In our mouse model, a cell type directly affected by CD11c-specific YAP/TAZ deletion are cDCs. Pre-cDCs leave the BM during development, entering circulation to reach peripheral tissues such as the spleen and lungs to terminally differentiate into cDCs[41]. At a steady state, I found the tissue resident cDC1 and cDC2 population in the lung and spleen of CD11c-Cre^{+} YAP$^{fl/fl}$, CD11c-Cre^{+} TAZ$^{fl/fl}$, and CD11c-Cre^{+} YAP$^{fl/fl}$ TAZ$^{fl/fl}$ mice did not differ from the WT cohort **(section 4.3.1)**. This observation was unexpected as a major function of YAP/TAZ signaling in non-immune cell types is the regulation of genes involved in the cell cycle, such as cyclins and mitotic kinases[145]. As I did not directly examine the effects of CD11c-YAP/TAZ deletion on DC development in my study, I cannot conclude whether YAP/TAZ signaling is necessary for development. However, I would like to speculate a reason that the deletion of YAP/TAZ in DCs did not affect basal cDC numbers. It is possible that DC development is independent of YAP/TAZ signaling. In the case of CD8^{+} T cells, it has been reported that YAP deletion improved anti-tumor response without impairing CD8^{+} T cell proliferation[120]. Unfortunately, our current understanding of the transcriptional binding partners of YAP/TAZ in immune cells is highly limited given the novelty. For instance, no studies have examined whether expression of key DC differentiation transcription factors such as IRF8 and BATF3 are regulated by TEAD, the nuclear protein YAP/TAZ interacts with to induce transcription of target genes[11].

Our transition to an influenza model is prompted by our discovery that tensional changes to BMDCs were predicted to be strongly associated with respiratory diseases (**Figure 4.4**). In this chapter, I demonstrated that single deletion of YAP and double deletion of YAP/TAZ in

$CD11c^+$ cells did not impair day 9 T cell-mediated antiviral response to PR8 IAV infection. cDCs are integral during respiratory viral infection since IAV does not freely flow from the lung to the MLN and is dependent on the activity of cDCs to reach the MLN[139]. Therefore, the capture of viral antigens by cDC1s in the lung for presentation in the MLN to $CD8^+$ T cells during early infection is important in determining disease outcome[139]. At day 9 of PR8 IAV infection, I saw there were no difference in cDC numbers in the lungs, spleen, and MLN of CD11c-Cre^+ $YAP^{fl/fl}$ and CD11c-Cre^+ $YAP^{fl/fl}$ $TAZ^{fl/fl}$ versus WT mice (**Figure 4.5** and **Figure 4.11)**. Furthermore, single deletion of YAP and double deletion of YAP/TAZ in $CD11c^+$ cells did not impair the activation of T cells and expansion of PR8 IAV specific $CD8^+$ T cells as seen by intracellular TNFα and IFNγ staining and tetramer staining (**Figure 4.8**, **Figure 4.9**, **Figure 4.10**, **Figure 4.14**, **Figure 4.15**, and **Figure 4.16)**. Although the treatment of T cells with PMA stimulates pre-activated T cells to secrete cytokines in a short time frame, PMA stimulation may potentially bypass the impact of mechanosignaling thereby masking subtle differences due to YAP/TAZ deficiency in DCs. Since CD11c-Cre^+ $YAP^{fl/fl}$ and CD11c-Cre^+ $YAP^{fl/fl}$ $TAZ^{fl/fl}$ mice begin losing weight on the 3rd day post infection, and cDC migration is most critical during early infection, it is possible that the effects of YAP/TAZ deletion on cDCs is masked by day 9. Therefore, quantification at an earlier infection endpoint may reveal subtle differences. For instance, the trafficking of antigen bearing YAP/TAZ deficient cDCs to the MLN could potentially be impaired during early infection at day 1-3 but is allowed to catch up by day 9. During this early phase, other cell types such as natural killer cells may be compensating for this impairment by containing viral replication such that disease severity is kept in check[146]. Thus, the antiviral response of CD11c-Cre^+ $YAP^{fl/fl}$ and CD11c-Cre^+ $YAP^{fl/fl}$ $TAZ^{fl/fl}$ mice should be examined at an earlier time point, such as day 1-3.

A caveat in our mouse model is that I have not verified the efficiency of YAP/TAZ deletion from $CD11c^+$ cells. As the animals in our study are hemizygous for Cre recombinase, it is plausible that YAP/TAZ is not efficiently knocked out in our mice. Inefficient deletion of YAP/TAZ could therefore lead to no difference in the parameters I examined, relative to WT mice. However, the homozygous expression of Cre recombinase is not without issues, as the high expression of Cre recombinase has been reported to be toxic in mice[147]. Although lung tissue dynamics are reported to change during pulmonary infections[138], the degree lung tissues stiffen in our YAP/TAZ deletion animals is also unknown. Therefore, I speculate another reason that CD11c-Cre^+ $YAP^{fl/fl}$ and CD11c-Cre^+ $YAP^{fl/fl}$ $TAZ^{fl/fl}$ mice versus WT mice did not exhibit differences in day 9 antiviral response, is that perhaps the alterations to lung stiffness during IAV infection is insufficient to generate strong mechanical cues that could stimulate DCs. Additionally, within the microenvironment of infected mice are a milieu of stimuli that could potentially bypass the involvement of YAP/TAZ signaling. For instance, strong biochemical signaling through PRRs such as TLR3, TLR7, and TLR9 that recognize foreign genetic material may be compensating for subtle changes associated with YAP/TAZ deletion in DCs[146].

For future influenza experiments, pulmonary stiffness during IAV infection needs to be assessed. This can be done with a FlexiVent instrument, a machine that measures respiratory mechanics such as airway resistance and elasticity. Targeting an earlier disease endpoint may reveal consequences of YAP/TAZ deletion in $CD11c^+$ cells that are otherwise not seen on day 9. I believe 1-3 days post IAV infection would be a promising endpoint. In IAV infected mice, the migration of pulmonary DCs to the MLN peak around 18 hours post-infection, and a substantially higher number of cDCs is seen in the MLN on day 2[148,149]. Moreover, a recent study revealed increased DC motility after IAV infection coincided with metabolic reprogramming

favoring glycolysis and OXPHOS as early as 17 hours *in vivo*[150]. Since YAP/TAZ are involved in metabolism regulation, perhaps the impact of YAP/TAZ deletion in DC is better discerned *in vivo* on day 1-3 of IAV infection[151]. Alternatively, we can perform transwell migration assays with BMDCs from our CD11c-YAP/TAZ KO mice to examine migration patterns associated with YAP/TAZ deletion in DCs.

Overall, this chapter demonstrates that the deletion of YAP/TAZ in DCs did not affect the day 9 antiviral response of CD11c-Cre^{+} YAP$^{fl/fl}$ and CD11c-Cre^{+} YAP$^{fl/fl}$ TAZ$^{fl/fl}$ mice. This was demonstrated by following disease severity and by flow cytometric analysis of infected lungs, spleen, and MLN. In my examination, I saw no difference in cDC and T cell numbers when comparing YAP/TAZ KO mice with WT mice. Similarly, YAP/TAZ deletion in CD11c^{+} cells did not impair the generation of PR8 IAV specific CD8^{+} T cells and T cell production of TNFα and IFNγ. An earlier endpoint may be a more suitable endpoint to discern the impact of YAP/TAZ deletion on DCs.

Chapter 5: General Discussion

5.1. Conclusion

5.1.1 Substrate stiffness modulates DC inflammatory function and metabolism.

DCs live an inherently physical life. During circulation, DCs encounter a diverse landscape of biochemical and physical cues within the traversed microenvironment. Much like biochemical signals, physical forces are present in different types and forms. External physical forces that are naturally encountered by cells include sheer, compression, swelling, and tensional forces[2,152]. These external physical cues are commonly integrated with the intracellular cytoskeletal network via adhesion molecules and ion channels found on the plasma membrane[153]. For non-immune cell types, mechanotransduction regulates function and development in a manner associated with metabolic and transcriptional programming[110,154,155]. Unfortunately, the significance of mechanical forces on immune cells is a largely understudied field, but recent studies have shown macrophages and T cells are sensitive to substrate stiffness[6,8]. Taken into consideration the discoveries of mechanosensing in other cell types and the constant exposure of DCs to physical cues within their microenvironment, this prompted our investigation on whether physical forces may contribute to the regulation of DC biology and function. By culturing BMDCs on PDMS coated culturing plates that are engineered to have a stiffness of 2 and 50 kPa, I endeavored to show substrate stiffness as a modulator of DC biology.

I provided additional data supporting mechanical stiffness as a novel regulator of DC biology. We first established that BMDCs conditioned on 50 kPa expressed higher levels of activation markers and were more pro-inflammatory than BMDCs conditioned on 2 kPa (**Figure 3.1 & 3.2)**. *In vitro*, BMDCs from 50 kPa had a higher expression of co-stimulatory receptors CD80 and CD86, and MHC II molecule after LPS stimulation. BMDCs of 50 kPa also secreted a

higher concentration of pro-inflammatory cytokines, including TNFα and IL-6, as determined by multiplex and ELISA assays (**Figure 3.2)**. Strikingly, the enhanced production of TNFα and IL-6 was observed in the absence of LPS stimulation, suggesting that substrate stiffness alone may be able to stimulate DCs. Since tissue stiffness is not uniform and is generally within the range of 2-15 kPa depending on the tissue and organ, it is intuitive to think that the effects of substrate stiffness on DCs is reversible[2,93]. To test this, I stimulated with LPS, plastic grown BMDCs that had been transferred to 2 kPa for an additional two days after the initial 7 days growth period. In this experiment, plastic conditioned BMDCs that were transferred to 2 kPa had a lower expression of MHC II and co-stimulatory receptors than BMDCs that were kept on plastic (**Figure 3.1D-G)**. My preliminary experiment suggests that substrate stiffness induced DC maturation is perhaps reversible, but whether pro-inflammatory cytokine production also decreased in BMDCs that were transferred from plastic to 2 kPa is unknown since I did not examine this. Future work on the reversibility of substrate stiffness on DCs biology should thus examine the cytokine production of transferred BMDCs via intracellular staining and by analytic biochemical assays. Based on our observations and the relatively short half-life of cytokines[156], I speculate that if the effects of substrate stiffness on DCs is reversible, then the sustained production of cytokines should decline in BMDCs that were transferred from plastic to 2 kPa after LPS stimulation, relative to BMDCs conditioned on plastic only. Determining the reversibility on the effects of substrate stiffness on DCs has important implications for the treatment or prevention of pathologies associated with tissue stiffness.

Interestingly our observations on substrate stiffness induced DC maturation is contrary to the results of Mennens et al[106]. In their study using human derived moDCs, Mennens et al. report human moDCs conditioned on 2 kPa or 50 kPa did not influence DC maturation[106]. Specifically,

Mennens et al. saw no difference in the expression of CD86 and MHC II in response to substrate stiffness[106]. The differences between studies might be attributed interspecies differences since our DCs were of murine origin whereas Mennens et al. were from humans. However, the physical properties of the polymers used to make the substrates may also be a confounding factor. In our study we used the hydrophobic polymer PDMS, whereas Mennens et al. used substrates made from polyacrylamide which is a more hydrophilic polymer[156]. Polymer hydrophobicity can influence the adsorption of fibronectin to the polymer surface, as fibronectin poorly binds hydrophilic surfaces at low concentration[157]. Poor surface coating of with fibronectin would inaccurately portray the effects of substrate stiffness on DC maturation by hindering DC adhesion to the substrate. Since PDMS becomes hydrophilic when treated by plasma oxidation, it would be interesting to see if we could recapitulate our findings using hydrophilic PDMS gels[158]. The usage of synthetic polymer in our study however is a caveat as these compounds are not representative of an *in vivo* setting since they are not naturally encountered by DCs. Therefore, it may be prudent to transition our study to use biomaterials such as collagen and hyaluronic acid that better mimic an *in vivo* environment.

We saw the upregulated expression of *Wwrt1* in BMDCs conditioned on stiffer substrates (**Figure 3.7)**, suggesting YAP/TAZ as a potential mediator of DC mechanosensing. In non-immune cell types, the transcription co-factors YAP/TAZ are integrators of mechanical stimulation, and their activation promotes cellular growth and metabolic reprogramming through modulating transcriptional programs[108–110,134]. Using imaging flow cytometry, I observed elevated nuclear translocation of YAP/TAZ from BMDCs conditioned on stiffer substrates - again hinting at the involvement of YAP/TAZ in DC mechanosensing. Generally, DCs will upregulate glycolysis, OXPHOS, and lipid metabolism after activation to support their growth

and function[82]. By using Seahorse assays I found substrate stiffness also controlled DC metabolism. BMDCs cultivated on 50 kPa or plastic substrate had increased glycolysis and OXPHOS (**Figure 3.5)**. This observed elevation of glycolysis and OXPHOS in DCs conditioned on stiffer substrates is consistent with DCs having a more activated phenotype and secretion of pro-inflammatory cytokines in response to stiff substrates, as these cellular processes would require more metabolites and energy to sustain[84]. For activated DCs to prime T cells, in addition to upregulating the expression of co-stimulatory molecules, DCs also undergo actin cytoskeletal remodeling to support their migration, transport of internal cargo, and formation of immunological synapse with T cells[159,160]. These physiological processes all require ATP, however, actin polymerization is a particularly more energy demanding process due to the constant hydrolysis of ATP required to sustain actin elongation and stability[161,162]. Thus, I speculate that enhanced metabolism in response to stiff substrates is a potential novel mechanism to fine tune DC effector function. This accords with the observation of BMDCs conditioned on high stiffness being better activators of T cells and having upregulated expression of co-stimulatory receptors and metabolism. Furthermore, we previously saw BMDCs conditioned on 50 kPa were more immunogenic relative to 2 kPa when adoptively transferred in two autologous vaccination models[107].

Lipid metabolism in DCs is an important metabolic pathway that I did not investigate to see if substrate stiffness could also modulate. This pathway is indispensable for DCs as it supports cellular growth, and the synthesis and secretion of effector proteins such as CD40, CD80, CD86, MHC II, and IL-6 and TNFα[84]. Since YAP/TAZ activity is also associated with energy levels and is inhibited by low energy levels in non-immune cell types[151], it is tempting to speculate that the upregulation of glycolysis and OXPHOS in DCs conditioned on stiffer

substrates is associated with the earlier observation of increased YAP/TAZ nuclear translocation in BMDCs of higher stiffness (**Figure 3.8**). This notion, however, requires further testing since how substrate stiffness can modulate DC maturation and function is not well understood.

5.1.2 CD11c specific YAP/TAZ deletion does not impair day 9 DC anti-viral response.

Enrichment for diseases associated with tension-induced changes in BMDCs predicted respiratory diseases to be strongly associated (**Figure 4.4)**. As such, I characterized the role of YAP/TAZ deletion in DCs using an influenza infection model. I investigated the day 9 antiviral response of mice with CD11c-specific YAP single deletion or YAP/TAZ double deletion to PR8 IAV infection. Interestingly, disease progression was more severe in CD11c-Cre^{+} YAP$^{fl/fl}$ mice but not in CD11c-Cre^{+} YAP$^{fl/fl}$ TAZ$^{fl/fl}$ mice, relative to WT mice (**Figure 4.5 & 4.11)**. However overall, there were no difference in the day 9 antiviral response of CD11c-Cre^{+} YAP$^{fl/fl}$ and CD11c-Cre^{+} YAP$^{fl/fl}$ TAZ$^{fl/fl}$ mice versus WT mice despite earlier experiments hinting at the involvement of YAP/TAZ in DC mechanosensing (**see section 4.3.3.1 & 4.3.3.2)**. Specifically, there were no difference in cDC and T cell numbers in dissociated lung, spleen, and MLN tissues from PR8 infected WT versus CD11c-Cre^{+} YAP$^{fl/fl}$ and CD11c-Cre^{+} YAP$^{fl/fl}$ TAZ$^{fl/fl}$ mice at day 9. Furthermore, there was no difference in the generation of the immunodominant PR8 IAV specific CD8^{+} T cells and TNFα and IFNγ production by T cells, suggesting YAP/TAZ deletion in CD11c^{+} cells did not impair day 9 T cell-mediated antiviral response.

Currently, no definitive conclusion can be drawn on the significance of YAP/TAZ in DCs. It is possible that the early antiviral response is impaired in CD11c-Cre^{+} YAP$^{fl/fl}$ and CD11c-Cre^{+} YAP$^{fl/fl}$ TAZ$^{fl/fl}$ mice but the effects are missed by day 9. Other cell types such as natural killer cells that are essential for the early antiviral response may be compensating for the impaired function of YAP/TAZ deficient DCs during the early phase of infection. Since our mice

started losing weight on day 3 post-IAV infection, pivoting our investigation to an endpoint of day 3-5 may better reveal subtle changes associated with YAP/TAZ deletion in DCs. The migration of pulmonary DCs to MLN is reported to peak by 18 hours post IAV infection, which coincides with the period DCs undergo metabolic reprogramming favoring glycolysis and OXPHOS[148,149150]. By day 2, a substantial increase in cDC numbers is present in the MLN[148,149]. As such, an earlier endpoint may be more informative in our infection model to discern the impact of YAP/TAZ deletion in $CD11c^+$ cells.

Since the degree lung tissues stiffen during IAV infection was not tested, it is possible that alterations to lung stiffness during IAV is insufficient to generate strong mechanical cues that could stimulate DCs. Additionally, DCs encounter a milieu of stimuli in a physiological setting that may bypass YAP/TAZ signaling. Therefore, unknown stimuli within the microenvironment may be compensating for YAP/TAZ deficiency in DCs or take precedent over tensional forces acting on DCs. For instance, other mechanical signals such as cyclical hydrostatic pressure, a type of pressure arising from fluids, can potentially dominate over YAP/TAZ signaling through Piezo1, a mechanically sensitive ion channel with preference for calcium[163]. Calcium homeostasis may exert confounding effects in a physiological setting that are otherwise not seen *in vitro* where the environmental conditions are more controlled. Calcium plays a crucial role in translating external mechanical forces into biochemical signals to regulate biological processes[164]. This response mainly involves increasing intracellular calcium levels when mechanosensitive calcium ion channels on the cell surface are opened in response to mechanical forces[165]. The influx of intracellular calcium activate calcium dependent pathways such as NFAT and mitogen-activated protein kinase, both having a role in regulating DC

biology[166–168]. Thus, calcium dependent pathways could be contributing to the lack of difference observed in our animal model.

It is unclear if mechanical forces acting on the periphery of DCs is transmitted to YAP/TAZ or directly act on the nucleus. For non-immune cell types, YAP/TAZ is one pathway external physical forces are sensed. In the latter case, this mechanism could be YAP/TAZ independent. Recently cells were demonstrated to respond to external mechanical forces via nuclear mechanotransduction in a phospholipid dependent manner[169,170]. In this process, external forces acting on the cell promotes the stretching of the nuclear membrane and an influx of calcium into the nucleus. In turn, this induces the activation of cytosolic phospholipase A_2 within the nucleus, an enzyme involved in the cleavage of phospholipids into metabolites[169–171]. These metabolites have autocrine or paracrine effects that contribute to cell locomotion, survival, and differentiation, and is hinted to involve RhoA signaling but requires further investigation[170]. RhoA is known to mediate cytoskeletal reorganization which can induce the activation of LATS1/2, the regulators of YAP/TAZ activation[108]. However, RhoA can also induce activation of other mechanosignaling pathways such as the Rho kinase pathway, which has been implicated in the regulation of metabolism and cellular proliferation[172,173]. It is also possible that the impact of YAP/TAZ deficiency in DCs is shadowed by direct IAV infection of DCs and the activation of PRRs that are involved in recognition of viruses, including TLR3, TLR7, and TLR9. The activation of Myc, a regulator of numerous metabolic enzymes, can occur independently of YAP/TAZ signaling by TLR stimulation[82,151]. Studies comparing the metabolic profile of IAV infected BMDCs versus TLR3 or TLR7 agonist activated BMDCs report distinct metabolic profiles[174]. Both glycolysis and OXPHOS is upregulated after IAV infection or TLR activation, although IAV infected BMDCs were significantly more glycolytic which corresponded with an

overall higher ATP production[174]. In conclusion, there are various signaling pathways in DCs with the potential to compensate for YAP/TAZ deletion in DCs.

5.2. Future work

Early studies of YAP/TAZ in non-immune cell types often reported YAP/TAZ with redundant functions, but recently this thought has been challenged by the mapped crystal structure of YAP/TAZ and the identification of different YAP/TAZ isoforms[115–118,175]. Collectively, these contemporary studies report YAP/TAZ have overlapping and different functions. As I saw YAP deletion in DCs exhibited trends of dampened immune response – OT-I T cell proliferation was lower when cultured with YAP deficient BMDCs and CD11c-Cre^{+} YAP$^{fl/fl}$ mice lost more weight compared to WT cohorts – this is perhaps indicative of YAP & TAZ having different functions in DCs. Therefore, the expression of YAP/TAZ isoforms in DCs at the mRNA and protein level should be characterized in the future to delineate the importance of YAP/TAZ signaling in DCs.

Much of our experiments on the effects of substrate stiffness on DC biology was performed *in vitro* due to the difficulty of isolating large quantities of DCs from tissues[107]. These experiments are ultimately not representative of a physiological setting, which is further deviated by the usage of synthetic polymers as substrates. While technically challenging, it may be worthwhile to perform *ex vivo* experiments using a fibrotic model to further investigate the significance of substrate stiffness on DC biology. In the envisioned experiments, DCs would be conditioned to a known tissue stiffness under physiological conditions. DC maturation and cytokine production would then be quantified by comparing DCs isolated from fibrotic versus healthy tissues. As mechanical changes in tissues and cells are disease specific, adopting a fibrosis animal model would also provide juxtaposition to our preliminary influenza model[129].

Mice in our model are infected with a sublethal dosage of IAV and it is possible that the dosage is insufficient to induce significant mechanical changes to the lung, or perhaps stiffness is not a major stimulus for DCs during IAV infection. Fibrotic tissues undergo extensive ECM remodeling and may be a better model to tease the significance of YAP/TAZ mechanosensing in DCs[129]. Alternatively, transitioning from substrates made of synthetic polymers to substrates made from biocompatible materials that better mimic tissues can help test whether the effects of substrate stiffness on DC biology we observed hold true.

As I did not examine the metabolism of YAP/TAZ deficient DCs, it is still unclear if YAP/TAZ signaling are involved or necessary for the regulation of DC metabolism. To test this the Seahorse assays I employed should be performed with YAP/TAZ deficient DCs conditioned on 2 kPa, 50 kPa, and plastic substrates. Given that WT BMDCs upregulated glycolysis and OXPHOS on higher stiffness, if YAP/TAZ deficient DCs have impaired mechanosensing then YAP/TAZ deficient DCs may have less pronounced metabolic reprogramming in response to stiffness. Lipid metabolism should also be investigated as it is a key pathway supporting DC function and development – this can be done by quantifying citrate flux[82,84,91]. Methods to examine this include colorimetric assays to quantify citrate synthase activity, or alternatively quantify the expression of fatty acid metabolism enzymes, such as ATP citrate synthase and fatty acid transporters by real-time PCR. The impact of substrate stiffness on DC fatty acid metabolism can also be examined using a palmitate oxidation stress test kit available from Seahorse. This assay inhibits the oxidation of palmitate; as metabolites from palmitate oxidation can be used to fuel OXPHOS, significance of fatty acid oxidation can be quantified via changes to oxygen consumption after pharmacologic inhibition of palmitate oxidation. Lastly, to test for the involvement of calcium dependent pathways potentially compensating for YAP/TAZ

deficiency in DCs, intracellular calcium level should be examined. For instance, imaging intracellular calcium in WT or YAP/TAZ deficient DCs when conditioned on 2 kPa, 50 kPa, and plastic substrates.

Through my study, I expanded on the impact of substrate stiffness on DC biology. Specifically, I found metabolism is a physiological process linking DC function with mechanosensing. I discovered BMDCs conditioned on stiffer substrate were more proficient at presenting antigen and activating T cells in a tension dependent manner. Building from this, I found tension could induce metabolic changes in BMDCs. Using Seahorse assays, I observed increased glycolysis and OXPHOS in BMDCs that were grown on 50 kPa and plastic relative to 2 kPa. The metabolic profile of BMDCs from higher stiffness were reminiscent to immunologically activated DCs[82]. Consistent with elevated metabolism in response to tension, I found a trending increase in the phosphorylation of AKT and S6RP, two key nutrient sensors involved in the coordination of anabolic and catabolic processes[130,131]. Our collaborators previously identified YAP/TAZ as a potential mediator of DC mechanosensing and predicted that tension induced effects on DCs is strongly associated with respiratory diseases. By image flow cytometry, I saw a trending increase in the nuclear translocation of YAP/TAZ in BMDCs conditioned on stiff substrates, hinting at the possible involvement of YAP/TAZ in DC mechanosensing. When I transitioned to studying the role of YAP/TAZ in DCs using a 9-day influenza model, I found that mice with DC specific YAP deletion was associated with greater weight loss that is not seen in the double KO animals. However, mice with DC specific YAP single deletion or double deletion of YAP/TAZ did not impair day 9 antiviral response. Given that DCs are activated early during influenza infection, it may be more informative to examine

the antiviral response at an earlier timepoint. Lastly, as I never examined the effects of YAP/TAZ deletion on the metabolism of DCs, this should be tested in the future.

There are immense therapeutic applications as our understanding of DC mechanosensing improves. As initiators of the adaptive immune response, DCs have an important role in determining the course of an immune response. DC secreted cytokines can promote their activation alongside PRR ligation and skew T cell responses. The manipulation of DCs from a mechanical angle therefore constitutes one avenue for attenuating or enhancing immune responses. For instance, implants could be improved by engineering implants with tunable or specific stiffness that favor tolerance vs immunogenicity. Since we saw that DCs are more pro-inflammatory when conditioned on 50 kPa and plastic substrates, identification of the mechanism behind this phenomenon could enable the manipulation of DCs such that they undergo signaling as if they are constitutively exposed to high stiffness. In turn, this can be exploited for DC-based vaccines directed at priming T cell responses.

References

1. Martinez, V. G. *et al.* Fibroblastic Reticular Cells Control Conduit Matrix Deposition during Lymph Node Expansion. *Cell Rep.* **29**, (2019).

2. Wells, R. G. Tissue mechanics and fibrosis. *Biochimica et Biophysica Acta - Molecular Basis of Disease* vol. 1832 (2013).

3. Martinez-Vidal, L. *et al.* Causal contributors to tissue stiffness and clinical relevance in urology. *Communications Biology* vol. 4 (2021).

4. Thomas, S. N., Rohner, N. A. & Edwards, E. E. Implications of Lymphatic Transport to Lymph Nodes in Immunity and Immunotherapy. *Annual Review of Biomedical Engineering* vol. 18 (2016).

5. Natkanski, E. *et al.* B cells use mechanical energy to discriminate antigen affinities. *Science (80-.).* **340**, (2013).

6. Meng, K. P., Majedi, F. S., Thauland, T. J. & Butte, M. J. Mechanosensing through YAP controls T cell activation and metabolism. *J. Exp. Med.* **217**, (2020).

7. Dustin, M. L. *et al.* Different TCR-induced T lymphocyte responses are potentiated by stiffness with variable sensitivity. *Elife* **6**, (2017).

8. Meli, V. S. *et al.* YAP-mediated mechanotransduction tunes the macrophage inflammatory response. *Sci. Adv.* **6**, (2020).

9. Wu, L. *et al.* Development of thymic and splenic dendritic cell populations from different hemopoietic precursors. *Blood* **98**, (2001).

10. Guilliams, M. *et al.* Unsupervised High-Dimensional Analysis Aligns Dendritic Cells

across Tissues and Species. *Immunity* **45**, (2016).

11. Bosteels, C. & Scott, C. L. Transcriptional regulation of DC fate specification. *Molecular Immunology* vol. 121 (2020).

12. Ghosh, H. S., Cisse, B., Bunin, A., Lewis, K. L. & Reizis, B. Continuous Expression of the Transcription Factor E2-2 Maintains the Cell Fate of Mature Plasmacytoid Dendritic Cells. *Immunity* **33**, (2010).

13. Wu, L. & Liu, Y. J. Development of Dendritic-Cell Lineages. *Immunity* vol. 26 (2007).

14. Karsunky, H., Merad, M., Cozzio, A., Weissman, I. L. & Manz, M. G. Flt3 ligand regulates dendritic cell development from Flt3+ lymphoid and myeloid-committed progenitors to Flt3+ dendritic cells in vivo. *J. Exp. Med.* **198**, (2003).

15. Cueto, F. J. & Sancho, D. The flt3l/flt3 axis in dendritic cell biology and cancer immunotherapy. *Cancers* vol. 13 (2021).

16. Watowich, S. S. & Liu, Y. J. Mechanisms regulating dendritic cell specification and development. *Immunol. Rev.* **238**, (2010).

17. Kingston, D. *et al.* The concerted action of GM-CSF and Flt3-ligand on in vivo dendritic cell homeostasis. *Blood* **114**, (2009).

18. Sathaliyawala, T. *et al.* Mammalian target of rapamycin controls dendritic cell development downstream of Flt3 ligand signaling. *Immunity* **33**, (2010).

19. Del Rio, M. L., Bernhardt, G., Rodriguez-Barbosa, J. I. & Förster, R. Development and functional specialization of CD103+ dendritic cells. *Immunological Reviews* vol. 234 (2010).

20. Onai, N., Obata-Onai, A., Tussiwand, R., Lanzavecchia, A. & Manz, M. G. Activation of the Flt3 signal transduction cascade rescues and enhances type I interferon-producing and dendritic cell development. *J. Exp. Med.* **203**, (2006).

21. Laouar, Y., Welte, T., Fu, X. Y. & Flavell, R. A. STAT3 Is Required for Flt3L-Dependent Dendritic Cell Differentiation. *Immunity* **19**, (2003).

22. Inba, K. *et al.* Generation of large numbers of dendritic cells from mouse bone marrow cultures supplemented with granulocyte/macrophage colony-stimulating factor. *J. Exp. Med.* **176**, (1992).

23. Lutz, M. B. *et al.* An advanced culture method for generating large quantities of highly pure dendritic cells from mouse bone marrow. *J. Immunol. Methods* **223**, (1999).

24. Cousins, D. J., Staynov, D. Z. & Lee, T. H. Regulation of interleukin-5 and granulocyte-macrophage colony-stimulating factor expression. in *American Journal of Respiratory and Critical Care Medicine* vol. 150 (1994).

25. Nimer, S. D. & Uchida, H. Regulation of granulocyte-macrophage colony-stimulating factor and interleukin 3 expression. *Stem Cells* **13**, (1995).

26. Serbina, N. V., Salazar-Mather, T. P., Biron, C. A., Kuziel, W. A. & Pamer, E. G. TNF/iNOS-producing dendritic cells mediate innate immune defense against bacterial infection. *Immunity* **19**, (2003).

27. Shin, K. S. *et al.* Monocyte-derived dendritic cells dictate the memory differentiation of CD8+ T cells during acute infection. *Front. Immunol.* **10**, (2019).

28. Vremec, D. *et al.* The influence of granulocyte/macrophage colony-stimulating factor on

dendritic cell levels in mouse lymphoid organs. *Eur. J. Immunol.* **27**, (1997).

29. Gilliet, M. *et al.* The development of murine plasmacytoid dendritic cell precursors is differentially regulated by FLT3-ligand and granulocyte/macrophage colony-stimulating factor. *J. Exp. Med.* **195**, (2002).

30. Van De Laar, L., Coffer, P. J. & Woltman, A. M. Regulation of dendritic cell development by GM-CSF: Molecular control and implications for immune homeostasis and therapy. *Blood* vol. 119 (2012).

31. Dorner, B. G. *et al.* Selective Expression of the Chemokine Receptor XCR1 on Cross-presenting Dendritic Cells Determines Cooperation with CD8+ T Cells. *Immunity* **31**, (2009).

32. Reizis, B., Bunin, A., Ghosh, H. S., Lewis, K. L. & Sisirak, V. Plasmacytoid dendritic cells: Recent progress and open questions. *Annu. Rev. Immunol.* **29**, (2011).

33. Grajales-Reyes, G. E. *et al.* Batf3 maintains autoactivation of Irf8 for commitment of a CD8α + conventional DC clonogenic progenitor. *Nat. Immunol.* **16**, (2015).

34. Hildner, K. *et al.* Batf3 deficiency reveals a critical role for CD8α+ dendritic cells in cytotoxic T cell immunity. *Science (80-.).* **322**, (2008).

35. Ginhoux, F. *et al.* The origin and development of nonlymphoid tissue CD103+ DCs. *J. Exp. Med.* **206**, (2009).

36. Sung, S.-S. J. *et al.* A major lung CD103 (α E)-β 7 integrin-positive epithelial dendritic cell population expressing Langerin and tight junction proteins . *J. Immunol.* **176**, (2006).

37. Mildner, A. & Jung, S. Development and function of dendritic cell subsets. *Immunity* vol.

40 (2014).

38. Förster, R. *et al.* CCR7 coordinates the primary immune response by establishing functional microenvironments in secondary lymphoid organs. *Cell* **99**, (1999).

39. Riol-Blanco, L. *et al.* The Chemokine Receptor CCR7 Activates in Dendritic Cells Two Signaling Modules That Independently Regulate Chemotaxis and Migratory Speed. *J. Immunol.* **174**, (2005).

40. Steinman, R. M. & Witmer, M. D. Lymphoid dendritic cells are potent stimulators of the primary mixed leukocyte reaction in mice. *Proc. Natl. Acad. Sci. U. S. A.* **75**, (1978).

41. Sichien, D., Lambrecht, B. N., Guilliams, M. & Scott, C. L. Development of conventional dendritic cells: From common bone marrow progenitors to multiple subsets in peripheral tissues. *Mucosal Immunology* vol. 10 (2017).

42. Ho, A. W. S. *et al.* Lung CD103 + Dendritic Cells Efficiently Transport Influenza Virus to the Lymph Node and Load Viral Antigen onto MHC Class I for Presentation to CD8 T Cells . *J. Immunol.* **187**, (2011).

43. Hargadon, K. M. *et al.* Major Histocompatibility Complex Class II Expression and Hemagglutinin Subtype Influence the Infectivity of Type A Influenza Virus for Respiratory Dendritic Cells. *J. Virol.* **85**, (2011).

44. Helft, J. *et al.* Cross-presenting CD103+ dendritic cells are protected from influenza virus infection. in *Journal of Clinical Investigation* vol. 122 (2012).

45. Henry, C. J., Ornelles, D. A., Mitchell, L. M., Brzoza-Lewis, K. L. & Hiltbold, E. M. IL-12 Produced by Dendritic Cells Augments CD8 + T Cell Activation through the

Production of the Chemokines CCL1 and CCL17 . *J. Immunol.* **181**, (2008).

46. GeurtsvanKessel, C. H. *et al.* Clearance of influenza virus from the lung depends on migratory langerin+CD11b- but not plasmacytoid dendritic cells. *J. Exp. Med.* **205**, (2008).

47. Merad, M., Sathe, P., Helft, J., Miller, J. & Mortha, A. The dendritic cell lineage: Ontogeny and function of dendritic cells and their subsets in the steady state and the inflamed setting. *Annual Review of Immunology* vol. 31 (2013).

48. Miller, J. C. *et al.* Deciphering the transcriptional network of the dendritic cell lineage. *Nat. Immunol.* **13**, (2012).

49. Bajaña, S., Roach, K., Turner, S., Paul, J. & Kovats, S. IRF4 Promotes Cutaneous Dendritic Cell Migration to Lymph Nodes during Homeostasis and Inflammation. *J. Immunol.* **189**, (2012).

50. Dudziak, D. *et al.* Differential antigen processing by dendritic cell subsets in vivo. *Science (80-.).* **315**, (2007).

51. Vander Lugt, B. *et al.* Transcriptional programming of dendritic cells for enhanced MHC class II antigen presentation. *Nat. Immunol.* **15**, (2014).

52. Kim, T. S., Gorski, S. A., Hahn, S., Murphy, K. M. & Braciale, T. J. Distinct dendritic cell subsets dictate the fate decision between effector and memory CD8+ T cell differentiation by a CD24-dependent mechanism. *Immunity* **40**, (2014).

53. Belz, G. T. *et al.* Distinct migrating and nonmigrating dendritic cell population are involved in MHC class I-restricted antigen presentation after lung infection with virus.

Proc. Natl. Acad. Sci. U. S. A. **101**, (2004).

54. Gurevich, I. *et al.* Active dissemination of cellular antigens by DCs facilitates CD8+ T-cell priming in lymph nodes. *Eur. J. Immunol.* **47**, (2017).

55. Ballesteros-Tato, A., León, B., Lund, F. E. & Randall, T. D. Temporal changes in dendritic cell subsets, cross-priming and costimulation via CD70 control CD8+T cell responses to influenza. *Nat. Immunol.* **11**, (2010).

56. Keller, A. M., Xiao, Y., Peperzak, V., Naik, S. H. & Borst, J. Costimulatory ligand CD70 allows induction of CD8+ T-cell immunity by immature dendritic cells in a vaccination setting. *Blood* **113**, (2009).

57. Plantinga, M., Hammad, H. & Lambrecht, B. N. Origin and functional specializations of DC subsets in the lung. *European Journal of Immunology* vol. 40 (2010).

58. Desch, A. N. *et al.* CD103+ pulmonary dendritic cells preferentially acquire and present apoptotic cell-associated antigen. *J. Exp. Med.* **208**, (2011).

59. De Heer, H. J., Hammad, H., Kool, M. & Lambrecht, B. N. Dendritic cell subsets and immune regulation in the lung. *Semin. Immunol.* **17**, (2005).

60. Honda, K. *et al.* IRF-7 is the master regulator of type-I interferon-dependent immune responses. *Nature* **434**, (2005).

61. Cella, M., Facchetti, F., Lanzavecchia, A. & Colonna, M. Plasmacytoid dendritic cells activated by influenza virus and CD40L drive a potent TH1 polarization. *Nat. Immunol.* **1**, (2000).

62. Fonteneau, J. F. *et al.* Activation of influenza virus-specific CD4+ and CD8+ T cells: A

new role for plasmacytoid dendritic cells in adaptive immunity. *Blood* **101**, (2003).

63. Cella, M. *et al.* Plasmacytoid monocytes migrate to inflamed lymph nodes and produce large amounts of type I interferon. *Nat. Med.* **5**, (1999).

64. McNab, F., Mayer-Barber, K., Sher, A., Wack, A. & O'Garra, A. Type I interferons in infectious disease. *Nature Reviews Immunology* vol. 15 (2015).

65. Wolf, A. I. *et al.* Plasmacytoid Dendritic Cells Are Dispensable during Primary Influenza Virus Infection. *J. Immunol.* **182**, (2009).

66. Smit, J. J., Rudd, B. D. & Lukacs, N. W. Plasmacytoid dendritic cells inhibit pulmonary immunopathology and promote clearance of respiratory syncytial virus. *J. Exp. Med.* **203**, (2006).

67. Naik, S. H. *et al.* Cutting Edge: Generation of Splenic CD8 + and CD8 − Dendritic Cell Equivalents in Fms-Like Tyrosine Kinase 3 Ligand Bone Marrow Cultures . *J. Immunol.* **174**, (2005).

68. Helft, J. *et al.* GM-CSF Mouse Bone Marrow Cultures Comprise a Heterogeneous Population of CD11c+MHCII+ Macrophages and Dendritic Cells. *Immunity* **42**, (2015).

69. Shortman, K. & Naik, S. H. Steady-state and inflammatory dendritic-cell development. *Nature Reviews Immunology* vol. 7 (2007).

70. Xu, Y., Zhan, Y., Lew, A. M., Naik, S. H. & Kershaw, M. H. Differential Development of Murine Dendritic Cells by GM-CSF versus Flt3 Ligand Has Implications for Inflammation and Trafficking. *J. Immunol.* **179**, (2007).

71. Naik, S. H. *et al.* Intrasplenic steady-state dendritic cell precursors that are distinct from

monocytes. *Nat. Immunol.* **7**, (2006).

72. Zmora, N., Bashiardes, S., Levy, M. & Elinav, E. The Role of the Immune System in Metabolic Health and Disease. *Cell Metabolism* vol. 25 (2017).

73. Ganeshan, K. & Chawla, A. Metabolic Regulation of Immune Responses. *Annu. Rev. Immunol.* **32**, 609 (2014).

74. Buck, M. D., O'Sullivan, D. & Pearce, E. L. T cell metabolism drives immunity. *J. Exp. Med.* **212**, 1345–60 (2015).

75. Wang, R. *et al.* The Transcription Factor Myc Controls Metabolic Reprogramming upon T Lymphocyte Activation. *Immunity* **35**, 871–882 (2011).

76. Loftus, R. M. & Finlay, D. K. Immunometabolism: Cellular Metabolism Turns Immune Regulator. *J. Biol. Chem.* **291**, 1–10 (2016).

77. Kessler, G. & Friedman, J. Metabolism of fatty acids and glucose. *Circulation* **98**, 1350a – 1353 (1998).

78. O'Neill, L. A. J., Kishton, R. J. & Rathmell, J. A guide to immunometabolism for immunologists. *Nat. Rev. Immunol.* **16**, 553–565 (2016).

79. Pfeiffer, T., Schuster, S. & Bonhoeffer, S. Cooperation and competition in the evolution of ATP-producing pathways. *Science (80-.).* **292**, (2001).

80. HIF-1alpha is essential for myeloid cell-mediated inflammation. *Nature* (2003) doi:10.1038/news030303-8.

81. Wculek, S. K., Khouili, S. C., Priego, E., Heras-Murillo, I. & Sancho, D. Metabolic Control of Dendritic Cell Functions: Digesting Information. *Frontiers in immunology* vol.

10 (2019).

82. Pearce, E. J. & Everts, B. Dendritic cell metabolism. *Nature Reviews Immunology* (2015) doi:10.1038/nri3771.

83. Köhler, T., Reizis, B., Johnson, R. S., Weighardt, H. & Förster, I. Influence of hypoxia-inducible factor 1α on dendritic cell differentiation and migration. *Eur. J. Immunol.* **42**, (2012).

84. Everts, B. *et al.* TLR-driven early glycolytic reprogramming via the kinases TBK1-IKKε supports the anabolic demands of dendritic cell activation. *Nat. Immunol.* **15**, (2014).

85. Szatmari, I. *et al.* PPARγ regulates the function of human dendritic cells primarily by altering lipid metabolism. *Blood* **110**, (2007).

86. Wumesh, K. C. *et al.* L-Myc expression by dendritic cells is required for optimal T-cell priming. *Nature* **507**, (2014).

87. Wang, Y. *et al.* Tuberous sclerosis 1 (Tsc1)-dependent metabolic checkpoint controls development of dendritic cells. *Proc. Natl. Acad. Sci. U. S. A.* **110**, (2013).

88. Pan, H. *et al.* Critical Role of the Tumor Suppressor Tuberous Sclerosis Complex 1 in Dendritic Cell Activation of CD4 T Cells by Promoting MHC Class II Expression via IRF4 and CIITA. *J. Immunol.* **191**, (2013).

89. Liberti, M. V. & Locasale, J. W. The Warburg Effect: How Does it Benefit Cancer Cells? *Trends in Biochemical Sciences* vol. 41 (2016).

90. Shi, L. & Tu, B. P. Acetyl-CoA and the regulation of metabolism: Mechanisms and consequences. *Current Opinion in Cell Biology* vol. 33 (2015).

91. Williams, N. C. & O'Neill, L. A. J. A role for the krebs cycle intermediate citrate in metabolic reprogramming in innate immunity and inflammation. *Frontiers in Immunology* vol. 9 (2018).

92. Zhang, D. *et al.* 2-Deoxyglucose reverses the promoting effect of insulin on colorectal cancer cells in vitro. *PLoS One* **11**, (2016).

93. Janmey, P. A. & Miller, R. T. Mechanisms of mechanical signaling in development and disease. *Journal of Cell Science* vol. 124 (2011).

94. Jansen, L. E., Birch, N. P., Schiffman, J. D., Crosby, A. J. & Peyton, S. R. Mechanics of intact bone marrow. *J. Mech. Behav. Biomed. Mater.* **50**, (2015).

95. Arda, K., Ciledag, N., Aktas, E., Aribas, B. K. & Köse, K. Quantitative assessment of normal soft-tissue elasticity using shear-wave ultrasound elastography. *Am. J. Roentgenol.* **197**, (2011).

96. Choi, Y. J., Lee, J. H. & Baek, J. H. Ultrasound elastography for evaluation of cervical lymph nodes. *Ultrasonography* vol. 34 (2015).

97. Acton, S. E. *et al.* Dendritic cells control fibroblastic reticular network tension and lymph node expansion. *Nature* **514**, (2014).

98. Asano, S. *et al.* Matrix stiffness regulates migration of human lung fibroblasts. *Physiol. Rep.* **5**, (2017).

99. Woolf, E. *et al.* Lymph node chemokines promote sustained T lymphocyte motility without triggering stable integrin adhesiveness in the absence of shear forces. *Nat. Immunol.* **8**, (2007).

100. Alon, R. & Dustin, M. L. Force as a Facilitator of Integrin Conformational Changes during Leukocyte Arrest on Blood Vessels and Antigen-Presenting Cells. *Immunity* vol. 26 (2007).

101. Marshall, B. T. *et al.* Direct observation of catch bonds involving cell-adhesion molecules. *Nature* **423**, (2003).

102. Kumari, S. *et al.* Cytoskeletal tension actively sustains the migratory T-cell synaptic contact. *EMBO J.* **39**, (2020).

103. Matalon, O., Reicher, B. & Barda-Saad, M. Wiskott-Aldrich syndrome protein - Dynamic regulation of actin homeostasis: From activation through function and signal termination in T lymphocytes. *Immunol. Rev.* **256**, (2013).

104. Kim, S. T. *et al.* The αβ T cell receptor is an anisotropic mechanosensor. *J. Biol. Chem.* **284**, (2009).

105. Spillane, K. M. & Tolar, P. B cell antigen extraction is regulated by physical properties of antigen-presenting cells. *J. Cell Biol.* **216**, (2017).

106. Mennens, S. F. B. *et al.* Substrate stiffness influences phenotype and function of human antigen-presenting dendritic cells. *Sci. Rep.* **7**, (2017).

107. Chakraborty, M. *et al.* Mechanical Stiffness Controls Dendritic Cell Metabolism and Function. *Cell Rep.* **34**, (2021).

108. Piccolo, S., Dupont, S. & Cordenonsi, M. The biology of YAP/TAZ: Hippo signaling and beyond. *Physiol. Rev.* **94**, (2014).

109. Heng, B. C. *et al.* Role of YAP/TAZ in Cell Lineage Fate Determination and Related

Signaling Pathways. *Frontiers in Cell and Developmental Biology* vol. 8 (2020).

110. Pocaterra, A., Romani, P. & Dupont, S. YAP/TAZ functions and their regulation at a glance. *J. Cell Sci.* **133**, (2020).

111. White, S. M., Murakami, S. & Yi, C. The complex entanglement of Hippo-Yap/Taz signaling in tumor immunity. *Oncogene* vol. 38 (2019).

112. Ma, S., Meng, Z., Chen, R. & Guan, K. L. The hippo pathway: Biology and pathophysiology. *Annual Review of Biochemistry* vol. 88 (2019).

113. Meng, Z., Moroishi, T. & Guan, K. L. Mechanisms of Hippo pathway regulation. *Genes and Development* vol. 30 (2016).

114. Lin, K. C., Park, H. W. & Guan, K. L. Regulation of the Hippo Pathway Transcription Factor TEAD. *Trends in Biochemical Sciences* vol. 42 (2017).

115. Finch-Edmondson, M. L. *et al.* TAZ protein accumulation is negatively regulated by YAP abundance in mammalian cells. *J. Biol. Chem.* **290**, (2015).

116. Wang, X. *et al.* Expression levels and activation status of Yap splicing isoforms determine self-renewal and differentiation potential of embryonic stem cells. *Stem Cells* **39**, (2021).

117. Gaffney, C. J. *et al.* Identification, basic characterization and evolutionary analysis of differentially spliced mRNA isoforms of human YAP1 gene. *Gene* **509**, (2012).

118. Xu, Y. *et al.* Identification of novel Taz isoforms and functional comparison in pluripotency maintenance of mouse embryonic stem cells. *Gene* **773**, (2021).

119. Vigneron, A. M., Ludwig, R. L. & Vousden, K. H. Cytoplasmic ASPP1 inhibits apoptosis through the control of YAP. *Genes Dev.* **24**, (2010).

120. Lebid, A., Chung, L., Pardoll, D. M. & Pan, F. YAP Attenuates CD8 T Cell-Mediated Anti-tumor Response. *Front. Immunol.* **11**, (2020).

121. Mia, M. M. *et al.* YAP/TAZ deficiency reprograms macrophage phenotype and improves infarct healing and cardiac function after myocardial infarction. *PLoS Biol.* **18**, (2020).

122. Cho, K. M., Kim, M. S., Jung, H. J., Choi, E. J. & Kim, T. S. Mst1-Deficiency Induces Hyperactivation of Monocyte-Derived Dendritic Cells via Akt1/c-myc Pathway. *Front. Immunol.* **10**, (2019).

123. Du, X. *et al.* Hippo/Mst signalling couples metabolic state and immune function of CD8α+ dendritic cells. *Nature* **558**, (2018).

124. Stampouloglou, E. *et al.* Yap suppresses T-cell function and infiltration in the tumor microenvironment. *PLoS Biol.* **18**, (2020).

125. Wynn, T. A., Chawla, A. & Pollard, J. W. Macrophage biology in development, homeostasis and disease. *Nature* vol. 496 (2013).

126. Zhang, N. *et al.* The Merlin/NF2 Tumor Suppressor Functions through the YAP Oncoprotein to Regulate Tissue Homeostasis in Mammals. *Dev. Cell* **19**, (2010).

127. Caton, M. L., Smith-Raska, M. R. & Reizis, B. Notch-RBP-J signaling controls the homeostasis of CD8- dendritic cells in the spleen. *J. Exp. Med.* **204**, (2007).

128. Reginensi, A. *et al.* Yap- and Cdc42-Dependent Nephrogenesis and Morphogenesis during Mouse Kidney Development. *PLoS Genet.* **9**, (2013).

129. Martinez-Vidal, L. *et al.* Causal contributors to tissue stiffness and clinical relevance in urology. *Communications Biology* vol. 4 (2021).

130. Saxton, R. A. & Sabatini, D. M. mTOR Signaling in Growth, Metabolism, and Disease. *Cell* vol. 168 (2017).

131. Weichhart, T., Hengstschläger, M. & Linke, M. Regulation of innate immune cell function by mTOR. *Nature Reviews Immunology* vol. 15 (2015).

132. Everts, B. *et al.* Commitment to glycolysis sustains survival of NO-producing inflammatory dendritic cells. *Blood* **120**, (2012).

133. Engler, A. J., Sen, S., Sweeney, H. L. & Discher, D. E. Matrix Elasticity Directs Stem Cell Lineage Specification. *Cell* **126**, (2006).

134. Dupont, S. *et al.* Role of YAP/TAZ in mechanotransduction. *Nature* **474**, (2011).

135. Wada, K. I., Itoga, K., Okano, T., Yonemura, S. & Sasaki, H. Hippo pathway regulation by cell morphology and stress fibers. *Development* **138**, (2011).

136. Katagiri, K. *et al.* Mst1 controls lymphocyte trafficking and interstitial motility within lymph nodes. *EMBO J.* **28**, (2009).

137. Torres-Bacete, J., Delgado-Martín, C., Gómez-Moreira, C., Simizu, S. & Rodríguez-Fernández, J. L. The Mammalian Sterile 20–like 1 Kinase Controls Selective CCR7-Dependent Functions in Human Dendritic Cells. *J. Immunol.* **195**, (2015).

138. Faffe, D. S. & Zin, W. A. Lung parenchymal mechanics in health and disease. *Physiological Reviews* vol. 89 (2009).

139. Guilliams, M., Lambrecht, B. N. & Hammad, H. Division of labor between lung dendritic cells and macrophages in the defense against pulmonary infections. *Mucosal Immunology* vol. 6 (2013).

140. Hufford, M. M., Kim, T. S., Sun, J. & Braciale, T. J. The effector t cell response to influenza infection. *Curr. Top. Microbiol. Immunol.* **386**, (2015).

141. DeBerge, M. P., Ely, K. H. & Enelow, R. I. Soluble, but Not Transmembrane, TNF-α Is Required during Influenza Infection To Limit the Magnitude of Immune Responses and the Extent of Immunopathology. *J. Immunol.* **192**, (2014).

142. Damjanovic, D. *et al.* Negative regulation of lung inflammation and immunopathology by TNF-α during acute influenza infection. *Am. J. Pathol.* **179**, (2011).

143. Lee, A. J. & Ashkar, A. A. The dual nature of type I and type II interferons. *Frontiers in Immunology* vol. 9 (2018).

144. Jorgovanovic, D., Song, M., Wang, L. & Zhang, Y. Roles of IFN-γin tumor progression and regression: A review. *Biomarker Research* vol. 8 (2020).

145. Kim, W. *et al.* Hippo signaling is intrinsically regulated during cell cycle progression by APC/CCdh1. *Proc. Natl. Acad. Sci. U. S. A.* **116**, (2019).

146. Schultz-Cherry, S. Role of nk cells in influenza infection. *Curr. Top. Microbiol. Immunol.* **386**, (2015).

147. Pomplun, D., Florian, S., Schulz, T., Pfeiffer, A. F. H. & Ristow, M. Alterations of pancreatic beta-cell mass and islet number due to Ins2-controlled expression of Cre recombinase: RIP-Cre revisited; part 2. *Horm. Metab. Res.* **39**, (2007).

148. Legge, K. L. & Braciale, T. J. Accelerated migration of respiratory dendritic cells to the regional lymph nodes is limited to the early phase of pulmonary infection. *Immunity* **18**, (2003).

149. Kandasamy, M. *et al.* Complement Mediated Signaling on Pulmonary CD103+ Dendritic Cells Is Critical for Their Migratory Function in Response to Influenza Infection. *PLoS Pathog.* **9**, (2013).

150. Rezinciuc, S. *et al.* Dynamic metabolic reprogramming in dendritic cells: An early response to influenza infection that is essential for effector function. *PLoS Pathog.* **16**, (2020).

151. Koo, J. H. & Guan, K. L. Interplay between YAP/TAZ and Metabolism. *Cell Metabolism* vol. 28 (2018).

152. Wells, R. G. The role of matrix stiffness in regulating cell behavior. *Hepatology* vol. 47 (2008).

153. Martino, F., Perestrelo, A. R., Vinarský, V., Pagliari, S. & Forte, G. Cellular mechanotransduction: From tension to function. *Frontiers in Physiology* vol. 9 (2018).

154. Romani, P., Valcarcel-Jimenez, L., Frezza, C. & Dupont, S. Crosstalk between mechanotransduction and metabolism. *Nature Reviews Molecular Cell Biology* vol. 22 (2021).

155. Boulter, E. *et al.* Cell metabolism regulates integrin mechanosensing via an SLC3A2-dependent sphingolipid biosynthesis pathway. *Nat. Commun.* **9**, (2018).

156. Aziz, N. *et al.* Stability of cytokines, chemokines and soluble activation markers in unprocessed blood stored under different conditions. *Cytokine* **84**, (2016).

157. Grinnell, F. & Feld, M. K. Fibronectin adsorption on hydrophilic and hydrophobic surfaces detected by antibody binding and analyzed during cell adhesion in serum-

containing medium. *J. Biol. Chem.* **257**, (1982).

158. Kim, B., Peterson, E. T. K. & Papautsky, I. Long-term stability of plasma oxidized PDMS surfaces. in *Annual International Conference of the IEEE Engineering in Medicine and Biology - Proceedings* vol. 26 VII (2004).

159. Konietzny, A., Bär, J. & Mikhaylova, M. Dendritic actin cytoskeleton: Structure, functions, and regulations. *Frontiers in Cellular Neuroscience* vol. 11 (2017).

160. Rodríguez-Fernández, J. L. & Criado-García, O. The Actin Cytoskeleton at the Immunological Synapse of Dendritic Cells. *Frontiers in Cell and Developmental Biology* vol. 9 (2021).

161. Korn, E. D., Carlier, M. F. & Pantaloni, D. Actin polymerization and ATP hydrolysis. *Science (80-.).* **238**, (1987).

162. Ranjith, P., Mallick, K., Joanny, J. F. & Lacoste, D. Role of ATP-hydrolysis in the dynamics of a single actin filament. *Biophys. J.* **98**, (2010).

163. Solis, A. G. *et al.* Mechanosensation of cyclical force by PIEZO1 is essential for innate immunity. *Nature* **573**, (2019).

164. Benavides Damm, T. & Egli, M. Calcium's role in mechanotransduction during muscle development. *Cellular Physiology and Biochemistry* vol. 33 (2014).

165. Agarwal, P. *et al.* A dysfunctional TRPV4–GSK3β pathway prevents osteoarthritic chondrocytes from sensing changes in extracellular matrix viscoelasticity. *Nat. Biomed. Eng.* (2021) doi:10.1038/s41551-021-00691-3.

166. Fric, J. *et al.* NFAT control of innate immunity. *Blood* vol. 120 (2012).

167. Nakahara, T., Moroi, Y., Uchi, H. & Furue, M. Differential role of MAPK signaling in human dendritic cell maturation and Th1/Th2 engagement. *Journal of Dermatological Science* vol. 42 (2006).

168. Hogan, P. G., Chen, L., Nardone, J. & Rao, A. Transcriptional regulation by calcium, calcineurin, and NFAT. *Genes and Development* vol. 17 (2003).

169. Lomakin, A. J. *et al.* The nucleus acts as a ruler tailoring cell responses to spatial constraints. *Science (80-.).* **370**, (2020).

170. Venturini, V. *et al.* The nucleus measures shape changes for cellular proprioception to control dynamic cell behavior. *Science (80-.).* **370**, (2020).

171. Enyedi, B., Jelcic, M. & Niethammer, P. The Cell Nucleus Serves as a Mechanotransducer of Tissue Damage-Induced Inflammation. *Cell* **165**, (2016).

172. Huang, H., Lee, D. H., Zabolotny, J. M. & Kim, Y. B. Metabolic actions of Rho-kinase in periphery and brain. *Trends in Endocrinology and Metabolism* vol. 24 (2013).

173. Hartmann, S., Ridley, A. J. & Lutz, S. The function of rho-associated kinases ROCK1 and ROCK2 in the pathogenesis of cardiovascular disease. *Frontiers in Pharmacology* vol. 6 (2015).

174. Bahadoran, A., Bezavada, L. & Smallwood, H. S. Fueling influenza and the immune response: Implications for metabolic reprogramming during influenza infection and immunometabolism. *Immunological Reviews* vol. 295 (2020).

175. Kristal Kaan, H. Y. *et al.* Crystal structure of TAZ-TEAD complex reveals a distinct interaction mode from that of YAP-TEAD complex. *Sci. Rep.* **7**, (2017).